



<https://theses.gla.ac.uk/>

Theses Digitisation:

<https://www.gla.ac.uk/myglasgow/research/enlighten/theses/digitisation/>

This is a digitised version of the original print thesis.

Copyright and moral rights for this work are retained by the author

A copy can be downloaded for personal non-commercial research or study, without prior permission or charge

This work cannot be reproduced or quoted extensively from without first obtaining permission in writing from the author

The content must not be changed in any way or sold commercially in any format or medium without the formal permission of the author

When referring to this work, full bibliographic details including the author, title, awarding institution and date of the thesis must be given

Enlighten: Theses

<https://theses.gla.ac.uk/>
research-enlighten@glasgow.ac.uk

SENSOR SYSTEMS FOR AUTOMATIC CONTROL OF ABDOMINAL
STIMULATION FOR RESPIRATORY SUPPORT IN TETRAPLEGIA

A THESIS

SUBMITTED TO THE DEPARTMENT OF MECHANICAL ENGINEERING

FACULTY OF ENGINEERING

UNIVERSITY OF GLASGOW

IN FULFILLMENT OF THE REQUIREMENTS

FOR THE DEGREE OF

MASTER OF SCIENCE BY RESEARCH

By

Wei Chen

July 2007

© Copyright 2007 by Wei Chen

All Rights Reserved

ProQuest Number: 10390709

All rights reserved

INFORMATION TO ALL USERS

The quality of this reproduction is dependent upon the quality of the copy submitted.

In the unlikely event that the author did not send a complete manuscript and there are missing pages, these will be noted. Also, if material had to be removed, a note will indicate the deletion.



ProQuest 10390709

Published by ProQuest LLC (2017). Copyright of the Dissertation is held by the Author.

All rights reserved.

This work is protected against unauthorized copying under Title 17, United States Code
Microform Edition © ProQuest LLC.

ProQuest LLC.
789 East Eisenhower Parkway
P.O. Box 1346
Ann Arbor, MI 48106 – 1346

GLASGOW
UNIVERSITY
LIBRARY:

Abstract

This thesis describes the evaluation of using an inertial measurement unit (IMU) device to measure the movement of the abdomen with the aim to detect different breathing activities and to demonstrate the feasibility to use this technique for automatic control of Functional Electrical Stimulation of Abdominal Muscles (FESAM). People with high-level spinal cord injury (SCI) have difficulties on voluntary breathings, as well as forced respiration, such as cough. The method of FESAM can improve respiratory function.

Respiratory activity can be obtained directly by measuring the airflow at the mouth and nose, using a face mask connected to a spirometer. While this approach is suitable in a laboratory environment, the face mask is inconvenient for long-term, every day use. An alternative way to detect respiratory activity is to measure the movement of the abdomen, which is less intrusive and more comfortable. Plethysmography is typically used to measure such movement in sleep studies. In this work, the suitability of an IMU sensor device attached to the abdomen is investigated.

Experiments were conducted with 5 neurologically intact subjects with both an IMU and spirometer device. Signals recorded from both sensors during different breathing tasks such as quiet breathing, cough, deep breathing and talking are compared. The phase-shifts between the signals from the two sensors are analysed and found to be within $\pm 1s$. Analysis of the magnitude of the IMU signals and their power spectrum confirm that it is possible to represent different breathing activities with these sensors.

A control system which can detect breathing activity in real-time, and controls a stimulator to generate appropriate electrical stimulations to the abdominal muscles, is also presented in this thesis. A multi-characteristic-analysis algorithm has been developed. This enhanced control system can analyse multiple characteristics of the breathing signal in real-time, and uses a flowchart structure to detect breathing activities. The results are used to control the stimulator which delivers suitable electrical stimulations during quiet breathing and coughing.

A graphical user interface (GUI) was implemented to interface with the sensor system, control system and stimulator system. This GUI was designed to graphically control the parameters of the entire system, and to show the system results visually. By using the GUI, the entire control system is more accessible to non-technical people. In addition, the control of the three systems becomes easier and is simplified. The possibility to save and load profiles for different patients also makes the configuration of the system more convenient.

Acknowledgements

I would like to thank Dr. Henrik Gollee for his constant support and professional supervision. He has taught me so much about basic research skills, MATLAB and Simulink knowledge and thesis writing rules. I am also very grateful for his tireless and helpful corrections on my informal and inappropriate English grammar and phrase usage. He has revised this thesis no less than 3 times going over every single word. Finally, I would like to thank him for his friendly way of supervision: totally unlike the relationship between a teacher and student in China, I felt it was very easy to communicate with him. By a regular weekly meeting, my problems always got a quick response.

I would like to thank Professor Ken Hunt and Mrs Elaine McNamara for their kind support to my application for the ORS scholarship (although failed). Elaine has also helped me a lot on arrangements for my demonstrating and tutoring work at the University of Glasgow.

At the Centre for Rehabilitation Engineering, University of Glasgow, I met a lot of lovely and friendly colleagues – Calum, Simon, Geraint, Ben, Emily, Helen, Sylvie, Lindsay, Andrew, Georg, Ingvild. . . . As my office roommate when I first came to Scotland, Calum told me a lot of stuff about the life in Scotland. I will never forget the “engineer” joke by Simon. Thanks to him and Geraint for being good neighbours when I moved to the office in the lab. Lindsay and Sylvie are always there to arrange meetings in the kitchen and out. Thanks for their arrangements which strengthen the team on and off duty. Also special thanks for the five brave subjects (Calum, Emily, Geraint, Simon, Ingvild) for the experiment for this study. Thanks for their tolerance with a face mask on for nearly half an hour, twice! Thanks for all my colleagues who are always there to give me a hand on study and life in Scotland.

Special thanks goes to my girlfriend, Xinran, who is always there when I need motivation and strength. She made my study life much easier and comfortable. I can always enjoy delicious Chinese food when I came home from school. I can always get encouragement when I felt depressed at work or study. Most important of all, she is always there when I need to talk to someone about everything.

Finally, I need to thank my parents for their support. I can never come to study at Glasgow University if it wasn't for their support. They have spent so much to raise me. There is no word to express my gratitude.

Thesis Outline

Chapter 1 This chapter introduces the physiological and technical background of this study. The necessary background in respiratory physiology, such as respiratory mechanics and muscles is introduced first. Spinal cord injury and its effect on the respiratory system are described as the motivation for this study. Methods to assist the respiratory function in tetraplegia are then reviewed. In particular, the method of functional electrical stimulation of abdominal muscle (FESAM) is described, including its principles and characteristics. Open issues of the automatic control system for functional electrical stimulation of abdominal muscle are identified at the end of this chapter, leading to the following chapters.

Chapter 2 The experiments with an inertial measurement unit (IMU) sensor and a spirometer sensor as reference in the automatic control system for FESAM are described in this chapter. Spirometer and IMU devices are reviewed first. By analysing the IMU signals and comparing them with the spirometer signals as reference, the possibility to use an IMU sensor to detect breathing signals is demonstrated. Five neurologically intact subjects were involved in experiments with a spirometer and IMU device to record respiratory activities. Signal characteristics such as the amplitudes and the phase-shift between the signals from the IMU and the spirometer are analysed. The results confirm that the IMU sensor system has the potential to detect respiratory activities. Issues with the IMU system in the experiments as well as further work are also discussed.

Chapter 3 This chapter discusses the algorithm of the automatic FESAM control system that detects respiratory activity and generates stimulation triggers for quiet breathing and coughing patterns. The basic structure of the system and its implementation in the Simulink environment are introduced. Analysis of the signal characteristics from different breathing patterns is discussed as background of the multi-characteristic control system which detects the different breathing patterns of quiet breathing, cough and others such as speaking.

Chapter 4 The stimulator which delivers the electrical stimulation is introduced in this chapter first. A user graphical interface is used to interface with the sensor system, control system and stimulator system. Through this interface, the parameters of the three systems can be set graphically. The results of the control system as well as the electrical stimulation can also be shown by the graphical viewer of the interface.

Chapter 5 A summary and further discussions about the entire automatic FESAM system, including the sensor system, control system and stimulator system, is presented in this chapter.

Chapter 6 This chapter summarises the contributions of this study, which include conducting the sensor experiment, developing the multi-characteristic control system and a graphical user interface for the control of the entire system, and draws conclusions. Further work for future development of the system is also discussed in this chapter.

Contributions

- Experiments with both the inertial measurement unit and a spirometer were carried out to evaluate the inertial measurement unit sensor system. Statistical analysis on the phase-shift and value difference between signals from the two sensor were carried out.
- The multi-characteristic-analysis algorithm to detect different breathing patterns (quiet breathing, cough, speaking) online was developed. Multiple characteristics of the breathing signal can be integrated in a flowchart structure to detect breathing activities in real-time.
- A graphical user interface was created to integrate the sensor system, control system and stimulator system into a control panel. All the system parameters can be set in the panel. System results can also be shown on the panel of the interface.

Publications

1. H. Gollé, W. Chen. Real-time measurement of respiratory activity using an inertial measurement unit. In *Proc. 29th IEEE EMBS Annual International Conference*, Lyon, France, August 2007.

Contents

Abstract	i
Acknowledgements	ii
Thesis Outline	iii
Contributions	v
Publications	vi
1 Introduction and Background	1
1.1 Relevant Respiratory Physiology	1
1.1.1 Respiratory Process	1
1.1.2 Respiratory Muscles and Mechanics	2
1.2 Spinal Cord Injury and Tetraplegia	4
1.2.1 Nervous System	4
1.2.2 Spinal Cord	4
1.2.3 Spinal Cord Injury and Tetraplegia	4
1.2.4 Functional Electrical Stimulation (FES)	6
1.3 Effect of Spinal Cord Injury and Tetraplegia on Respiratory Function	7
1.3.1 Main Respiratory Muscle Paralysis in Different Levels of Lesion	7
1.3.2 Effect of Spinal Cord Injury on Respiratory Phases	8
1.4 Respiratory Therapies	9
1.4.1 Mechanical Ventilation (MV)	10
1.4.2 Diaphragm Pacing (DP)	11
1.4.3 Stimulation of the Abdominal Muscles	12
1.4.4 Summary of the Respiratory Therapies	14
1.5 Open Issues in the Automatic Control System for FESAM	15
2 Experiments with an IMU Sensor System	17
2.1 Introduction and Background	17
2.1.1 The Role and Requirement of the Sensor in the Automatic FESAM System	17
2.1.2 Spirometer	19

2.1.3	Biopotentials	20
2.1.4	Respiratory Inductive Plethysmography (RIP)	22
2.1.5	Electroglottography (EGG)	22
2.1.6	Inertial Measurement Unit (IMU)	23
2.1.7	Summary of the Device and Experiment	24
2.2	Methods	25
2.2.1	Devices	25
2.2.2	Subjects	27
2.2.3	Experimental Protocol	27
2.2.4	Data Processing Overview	28
2.2.5	Data Processing of the IMU Signal	29
2.2.6	Data Processing of the Spirometer Signal	34
2.2.7	Methodology of Analysis	37
2.3	Results	40
2.3.1	Overview of the Experiments	40
2.3.2	Experimental Problems	40
2.3.3	Detection of Onset of Expiration and Inspiration	45
2.3.4	Differentiation Between Different Breathing Patterns	50
2.4	Discussion	55
2.4.1	Phase-shift between the Airflow at the Mouth and the Abdomen Movement	55
2.4.2	Detection of Different Breathing Patterns	60
2.5	Issues and Further Work	61
2.5.1	Attachment of the IMU to the Abdomen	61
2.5.2	Additional Sensor to Detect the Chest Movement	62
2.5.3	Additional Sensor to Eliminate Unwanted Body Movement	62
2.5.4	Different Situations with Tetraplegic People	62
2.6	Conclusions	63
3	The Algorithm of the FESAM Control System	64
3.1	Background and Introduction	64
3.1.1	The Basic Control System (BCS)	65
3.2	The Multi-characteristic Control System (MCCS)	66
3.2.1	Typical Breathing Signals of Different Patterns	67
3.2.2	The Analysis of the Characteristics of Breathing Signal for Detection	68
3.2.3	The Decision Flowchart Sub-system which Analyses the Outputs of the Sub-systems which Analyses the Signal Characteristics	79
3.2.4	Generation of the Stimulation Trigger	80
3.3	Testing the Multi-characteristic Control System (MCCS)	81

3.3.1	Improvement of the Detection of Speaking Patterns by the MCCS	81
3.3.2	Testing the MCCS with the IMU and Spirometer Signals	82
3.4	Results of the Tests Using MCCS to Analyse the Signals from both the IMU and Spirometer Device	85
3.4.1	System Parameters with All the Data Sets	85
3.4.2	Testing Results	86
3.5	Discussion	87
3.5.1	Improvement of the Detection of SP patterns	87
3.5.2	MCCS Results with QB, C and SP patterns with the IMU and Spirometer Signals	87
3.5.3	Result with DB and SC patterns with the Signals from the Sensor Experiment	87
3.6	Conclusion	89
4	Implementation of the Automatic Control System Using a Graphical User Interface	90
4.1	Structure of the Automatic Control System for FESAM	90
4.2	The Stimulator System	92
4.2.1	Hardware	92
4.2.2	Software	93
4.3	The Graphical User Interface (GUI) of the Automatic Control System	95
4.3.1	The Main Panel of the GUI	95
4.3.2	The Configuration Panel of the GUI	97
4.4	Integration of the GUI with the MCCS Simulink System	98
4.5	Conclusion and Further Work	100
5	Discussion	101
5.1	Further Physiological Discussion on the Movement of the Abdomen	101
5.2	Potential Modifications to the Multi-characteristic Control System (MCCS)	103
5.3	Integration of the Sensor System, MCCS and Stimulator with the Graphic User Interface (GUI)	103
6	Conclusion and Further Work	105
	Appendix	108
A	Original Data from the Experiments with IMU	109
A.1	Subject 01	109
A.2	Subject 02	113
A.3	Subject 03	116
A.4	Subject 04	119

A.5 Subject 05	122
B Abbreviations	125
Bibliography	126

List of Tables

1.1	Segmental spinal cord level and function.	5
1.2	Muscles of respiration and their innervation.	8
1.3	Summary of main characteristics of techniques of respiratory therapy	15
2.1	Summary of essential characteristics of candidate sensors mentioned in this study. . .	25
2.2	Subject information.	27
2.3	A sample data acquired by the IMU with the Euler angles convention.	31
2.4	The configuration for the highpass filter to remove the offset of the IMU raw signal. .	33
2.5	The configuration for the lowpass filter to remove the high frequency noises of the spirometer raw signal.	34
2.6	An overview of the experiment result.	41
2.7	A summary of the experimental problems of the recorded data.	44
2.8	Summary of the FFT frequency spectrum analysis of different breathing pattern samples.	53
3.1	Thresholds set for the test with both BCS and MCCS to improve the detection QB, C and SP patterns.	83
3.2	Summary of the thresholds of the six sub-systems for the tests of the MCCS with the data sets from the IMU and spirometer.	85
3.3	Results of the testing of the MCCS with the signals from the IMU and spirometer. . .	86

List of Figures

1.1	Simplified diagram of the respiratory process.	2
1.2	Main respiratory muscles.	3
1.3	Illustration of the volume and pressure change of the thorax during inspiration and expiration	3
1.4	Central nervous system (CNS) and the divisions of the spinal nerves.	5
1.5	A basic FES system.	6
1.6	FES applications in spinal cord dysfunction.	7
1.7	A sample endotracheal tube of a positive pressure ventilator.	11
1.8	Position of the electrode in Diaphragm Pacing.	12
1.9	The electrodes and the four stimulation channels in FESAM.	13
1.10	The automatic control structure of FESAM.	14
2.1	Sample data showing the difference between different respiratory patterns.	18
2.2	Sample respiratory data of quiet breathing acquired from a spirometer.	18
2.3	A portable spirometer	19
2.4	Electromyography (EMG) test with a needle electrode.	20
2.5	Electroneurography (ENG) in a closed-loop hand grasp neuroprosthesis system.	21
2.6	A Respiratory Inductive Plethysmograph (RIP) system.	22
2.7	A raw waveform of Electroglottography recorded during speaking.	23
2.8	A commercial IMU device developed to detect human motion.	24
2.9	The MT9-B IMU algorithm.	26
2.10	A subject during experiment wearing both face mask and the IMU device.	26
2.11	Protocol of the IMU sensor experiment.	28
2.12	The flowchart of data processing in the IMU sensor experiment.	29
2.13	A sample set of raw breathing signals from the spirometer and IMU.	29
2.14	Co-ordinate systems of the MT9-B IMU system.	30
2.15	Euler-angle systems in aeronautics.	31
2.16	A unit 3D movement projected on the YZ plane in the IMU system.	32
2.17	Figures showing how the high pass filter works to remove the zero-frequency offset of the raw IMU signal B_{raw}^{IMU}	33

2.18	The magnitude and phase response of the highpass filter used to remove the offset of the IMU signal.	34
2.19	Figures to show how the low pass filter worked to remove the high frequency noise of the raw spirometer signal B_{raw}^{spiro}	35
2.20	The magnitude and phase response of the lowpass filter used to remove noise of the spirometer signal.	35
2.21	This figure shows the maximum and minimum peaks used to normalise signals.	36
2.22	A sample IMU signal shows the normalisation process.	37
2.23	A sample series of QB data showing the detection of inspiratory and expiratory onsets.	38
2.24	An illustration showing the indicators in a notched box plot.	39
2.25	The peak points of a cough sample were detected.	40
2.26	Box plots of the phase-shifts during different breathing activities and respiratory phases with all the subjects.	45
2.27	Box plots of the phase-shifts during the inspiratory and expiratory phases of C and DB activities with subject 01.	47
2.28	Box plots of the phase-shifts during different breathing activities and respiratory phases with subject 02.	48
2.29	Box plots of the phase-shifts during different breathing activities and respiratory phases with subject 03.	48
2.30	Box plots of the phase-shifts during different breathing activities and respiratory phases with subject 05.	49
2.31	Box plots of the data sets of the peak values with the QB signals.	51
2.32	Box plots of the data sets of the peak values with the C signals.	51
2.33	Box plots of the data sets of the peak values with the DB signals.	52
2.34	Frequency spectra and areas of one series of the cough sample from subject 01.	53
2.35	Speaking signals from both sensors in both time and frequency domain. Left plots show the signal in time domain. Right plots show their frequency spectra. This is from the experiment part iii of subject 03.	54
2.36	A flowchart of the respiratory cycle of neurologically intact people.	56
2.37	The abnormal large phase-shift between the signals from the IMU and spirometer device with the data set i with subject 03.	58
2.38	The abnormal spread of phase-shift between the signals from the IMU and spirometer device with the DB signals with subject 03.	59
2.39	Signals from both devices during the DB activities with subject 05.	59
3.1	The overall structure of the control system for FESAM.	64
3.2	Illustration showing one detection cycle for the characteristic detection of the breathing signal.	65

3.3	A flow chart showing the algorithm of the basic control system (BCS).	66
3.4	A flowchart showing the structure of the multi-characteristic control system (MCCS).	67
3.5	Typical breathing signals of QB, DB, C and SP patterns.	68
3.6	The structure of the sub-system I which analyses the magnitude of inspiratory signal.	70
3.7	The structure of the sub-system which analyses the cross-correlation of the breathing signal with QB reference signal.	71
3.8	The structure of the sub-system which analyses the area of the FFT magnitude of the breathing signal over a certain period.	72
3.9	The sub-system which calculates FFT magnitude and its area of the breathing signal over a certain period.	73
3.10	The sub-system which analyses the magnitude of the previous expiratory signal.	74
3.11	The sub-system which counts the peak number of the previous expiratory signal.	75
3.12	Signals showing the process of the sub-system which counts the peak numbers of expiratory signal.	78
3.13	The sub-system which analyses the derivative of the breathing signals during inspiratory phase.	78
3.14	Illustrations showing the inputs and outputs of the decision flowchart sub-system of the MCCS.	79
3.15	The structure of the flowchart sub-system.	81
3.16	Detection results of the BCS and MCCS with a sample spirometer signal.	84
3.17	The results with data set ii-2 with subject 01.	88
4.1	Illustration showing the three sub-systems of the automatic control system for FE-SAM and a graphical user interface (GUI) which configures the system parameters and shows system results.	91
4.2	The electrical stimulation delivered by the stimulator at one channel.	92
4.3	The connection of the PC, stimulator and the DAQ card of the stimulator system.	93
4.4	The front and rear view of the stimulator (RehaStim, HASOMED GmbH, Germany).	93
4.5	Illustration showing the stimulation system which implements the DAQ control and the stimulator interface.	94
4.6	The Simulink interface of the stimulator.	95
4.7	The main panel of the GUI of the automatic control system.	96
4.8	The graphical viewer after an offline simulation using a local breathing signal file.	97
4.9	The configuration panel of the GUI.	98
4.10	Flowchart showing the work flow of S-function block which updates the scope on the main panel of the GUI in real-time.	99
A.1	Original and filtered signal of part i of the experiment with subject 01.	110
A.2	Original and filtered signal of part ii-1 of the experiment with subject 01.	110

A.3	Original and filtered signal of part ii-2 of the experiment with subject 01.	111
A.4	Original and filtered signal of part ii-3 of the experiment with subject 01.	111
A.5	Original and filtered signal of part iii of the experiment with subject 01.	112
A.6	Original and filtered signal of part i of the experiment with subject 02.	113
A.7	Original and filtered signal of part ii-1 of the experiment with subject 02.	113
A.8	Original and filtered signal of part ii-2 of the experiment with subject 02.	114
A.9	Original and filtered signal of part ii-3 of the experiment with subject 02.	114
A.10	Original and filtered signal of part iii of the experiment with subject 02.	115
A.11	Original and filtered signal of part i of the experiment with subject 03.	116
A.12	Original and filtered signal of part ii-1 of the experiment with subject 03.	116
A.13	Original and filtered signal of part ii-2 of the experiment with subject 03.	117
A.14	Original and filtered signal of part ii-3 of the experiment with subject 03.	117
A.15	Original and filtered signal of part iii of the experiment with subject 03.	118
A.16	Original and filtered signal of part i of the experiment with subject 04.	119
A.17	Original and filtered signal of part ii-1 of the experiment with subject 04.	119
A.18	Original and filtered signal of part ii-2 of the experiment with subject 04.	120
A.19	Original and filtered signal of part ii-3 of the experiment with subject 04.	120
A.20	Original and filtered signal of part iii of the experiment with subject 04.	121
A.21	Original and filtered signal of part i of the experiment with subject 05.	122
A.22	Original and filtered signal of part ii-1 of the experiment with subject 05.	122
A.23	Original and filtered signal of part ii-2 of the experiment with subject 05.	123
A.24	Original and filtered signal of part ii-3 of the experiment with subject 05.	123
A.25	Original and filtered signal of part iii of the experiment with subject 05.	124

1 Introduction and Background

Summary

Respiration is an essential part of human physiological function. Inspiration and expiration are activated by inspiratory and expiratory muscles, respectively. These respiratory muscles are innervated at different levels of the spinal cord. When the spinal cord is damaged, different respiratory muscles are partially or completely paralysed according to the damage level. Cervical spinal cord injury results in tetraplegia. In tetraplegic individuals, the respiratory function is compromised to different extents. Respiratory therapies are therefore needed. Available respiratory therapies include mechanical ventilation, diaphragm pacing for normal breathing, and functional magnetic stimulation for cough. The method of functional electrical stimulation can be an alternative to these methods. A novel control system to apply functional electrical stimulation to abdominal muscles to assist normal breathing and cough has been developed in a previous study. There are two open issues in this control system. They are the sensor system which acquires the breathing signal and the control system which detects different breathing activities.

In this chapter, basic respiratory physiology is introduced first. Spinal cord injury is then discussed. Finally, respiratory therapies including functional electrical stimulation are discussed.

1.1 Relevant Respiratory Physiology

As the functional electrical stimulation method activates abdominal muscles to assist respiration, the respiratory muscles and mechanics are reviewed.

1.1.1 Respiratory Process

Respiration is one of the most essential functions of human beings. Respiration integrates nervous control of breathing, the function of the lungs, the circulation of the blood and the metabolism of the tissues [1].

The word 'respiration' in this thesis only refers to the process of breathing. Therefore, the respiratory process in this thesis is the process of inhaling (inspiration) and exhaling (expiration) air into and from the lung. Other complicated physiological background such as the lung function and gas exchanges between organs and blood will not be discussed in this thesis. They can be found in many text books [2-4].

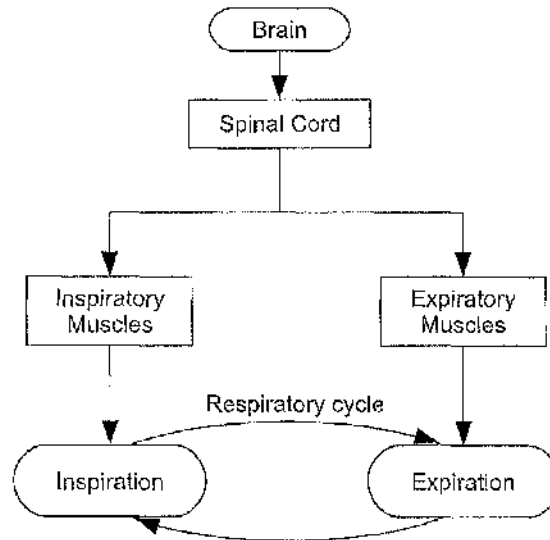


Figure 1.1: Simplified diagram of the respiratory process.

The process of respiration discussed in this thesis is illustrated by a simplified diagram, as shown in Figure 1.1. Inspiration and expiration are controlled by respiratory muscles. The respiratory muscles are innervated by the spinal cord, whose signal comes from the brain.

1.1.2 Respiratory Muscles and Mechanics

A. Inspiration

John B. West described basic algorithms of the inspiratory mechanism in [2]. The primary inspiratory muscle is the *diaphragm*, as shown in Figure 1.2. When forced inspiration takes place, accessory inspiratory muscles will be recruited as well. They include: the *external intercostal muscles* and *parasternal intercostal muscles*, as well as the *scalene* and *sternocleidomastoid muscles*. During inspiration, the diaphragm contracts from a flat sheet to a dome-shape sheet; while the accessory muscles pull the rib cage upwards and outwards. The main task of these inspiratory muscles is to increase the volume of the thorax. The inspiratory process is illustrated in Figure 1.3(a). The thorax volume increase will result in a pressure decrease (increase in negative pressure) in the thorax according to *Boyle's Law*¹. Air will be sucked into the lung due to the pressure difference between the alveolus and the atmosphere.

B. Expiration

Usually, quiet expiration by neurologically intact people doesn't involve any expiratory muscle – the expiration process is generally a passive process. Lung, diaphragm and thoracic cage have elasticity.

¹Boyle's law is one of the ideal gas law. It states that the product of the volume and pressure of a fixed quantity of ideal gas is constant, given constant temperature. The formula for Boyle's law is: $pV = k$ where V and p are volume and pressure of the gas respectively, and k is a constant.

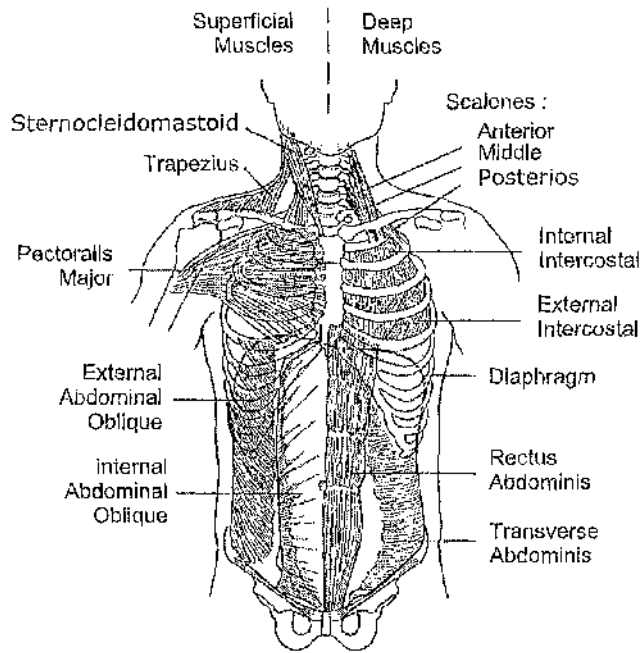


Figure 1.2: Main respiratory muscles. Adapted from [5].

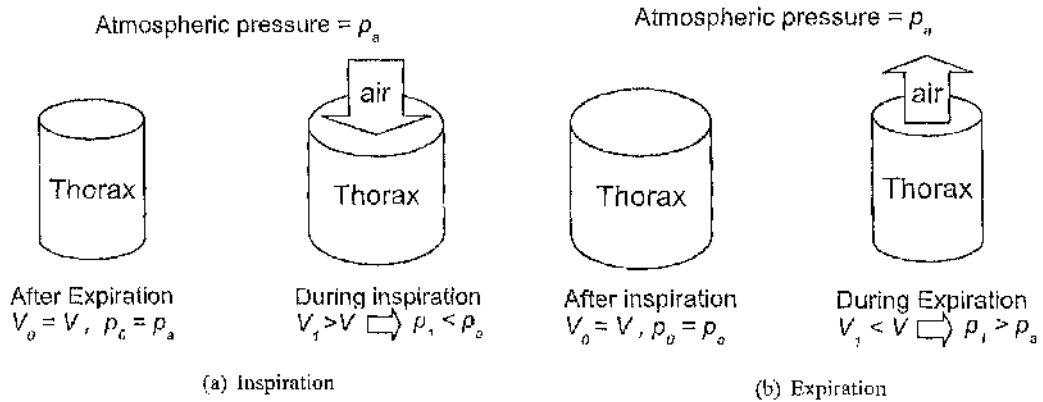


Figure 1.3: Illustration of the volume and pressure change of the thorax during inspiration and expiration. V_0 and p_0 denote the initial volume and pressure of the thorax, whilst V_1 and p_1 denote the volume and pressure during the phase of inspiration or expiration. p_a denotes the atmospheric pressure.

When the diaphragm is contracted during inspiration, a recoil force can be produced by elasticity to pull it back. When the force to contract diaphragm disappears (i.e. inspiration ends), the passive recoil of diaphragm and thoracic cage will pull back the diaphragm. The process of inspiration is reversed, as shown in Figure 1.3(b). The thorax volume decreases due to the recoil of diaphragm. According to Boyle's law, the volume decrease inside the thorax will generate an increasing intrathoracic pressure. Gas will flow out of the thorax due to the pressure difference between the intrathoracic pressure and

atmospheric pressure until they reach equilibrium.

In the case of forced expiration, such as cough and deep breathing, the expiratory muscles are recruited to assist expiration. The primary expiratory muscles are the abdominal muscles. The abdominal muscles include: *rectus abdominis*, *oblique abdominis* (external and internal) and *transverse abdominis*, as shown in Figure 1.2. The *intercostal internal muscles* and *triangularis sterni* are the accessory expiratory muscles. The primary expiratory muscles lower the bottom ribs, whilst the accessory muscles move the ribs upwards and outwards. The main task of the expiratory muscles is to pull back the diaphragm **actively**, rather than let it recoil **passively**.

1.2 Spinal Cord Injury and Tetraplegia

This study aims to benefit tetraplegic patients. In this section, some basic background about spinal cord injury and the effect of tetraplegia on the respiratory function are discussed. A general review of functional electrical stimulation (FES) is introduced at the end of this section.

1.2.1 Nervous System

Human body movement and feelings (respiratory muscle movement for instance) depend on natural electrical currents which flow through nerves in the human body. The natural electrical currents are transferred by specialised cells known as *neurons* from one part of the human body to another. All the neurons of an *organism*, together with their supporting cells, constitute a *nervous system* [6].

The *nervous system* includes the *Central Nervous System (CNS)* and *Peripheral Nervous System (PNS)*. The CNS (shown in Figure 1.4) consists the brain and the spinal cord. It controls major functions of the human body. The PNS provides nerves connecting the CNS and rest of the body.

1.2.2 Spinal Cord

The spinal cord is a *thin*, tubular structure that is an extension of the CNS from the brain and is enclosed in and protected by the bony vertebral column. The main function of the spinal cord is to transmit the neural inputs from the periphery to the brain and vice versa. It is a vital structure in our survival and functional capacity.

The spinal cord is divided into several segments by its location, as illustrated on the left side of Figure 1.4. The segmental nature of the spinal cord is reflected in a series of paired spinal nerves, each of which is attached to the cord by a dorsal sensory root and a ventral motor root [6].

1.2.3 Spinal Cord Injury and Tetraplegia

Spinal cord injury occurs when the function of the spinal cord is damaged. This damage could be trauma such as a car accident or disease such as spina bifida.

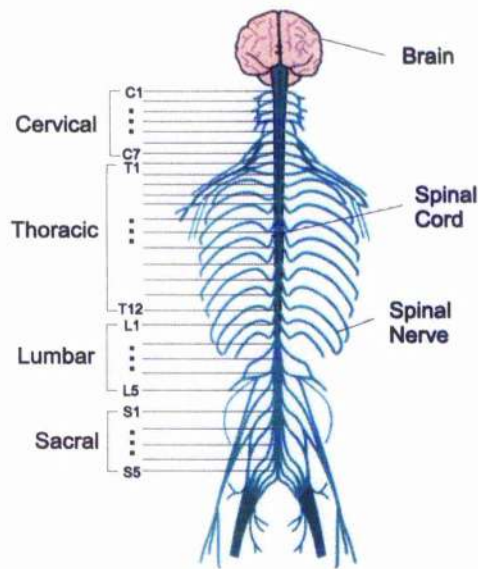


Figure 1.4: Illustration of the central nervous system and the divisions of the spinal nerves. Adapted from http://www.backrack.co.uk/nervous_index.shtml.

Level	Function
C3 – C5	Supply diaphragm (mostly C4)
C5 – C6	Shoulder movement, raise arm, flexion of elbow
C7 – C8, T1	Flexes wrist
T1 – T6	Intercostals and trunk above the waist
T6 – L1	Abdominal muscles
L1 – L4	Thigh flexion

Table 1.1: Segmental spinal cord level and function. Note that this table only shows the essential spinal cord levels and functions. This table is part of the table from <http://www.makoa.org/scimap.htm>.

Spinal cord injury can leave patients with different levels of dysfunction of the body. There can be incomplete or complete loss of motor or sensory functions in the arms, trunks, etc.. The level of the injury is usually defined in the UK by giving the most distal uninvolved segment of the cord [7], as discussed in Section 1.2.2. Some essential body functions of certain spinal cord levels are listed in Table 1.1. For instance, generally speaking, an individual with spinal cord injury at above C5 would have diaphragm dysfunction.

Spinal cord injury can lead to *tetraplegia* and *paraplegia*. These two terms are defined by the levels of the cord damage.

Tetraplegia (also known as quadriplegia) It refers to impairment or loss of motor and/or sensory function in the cervical segments of the spinal cord due to damage of neural elements within the spinal

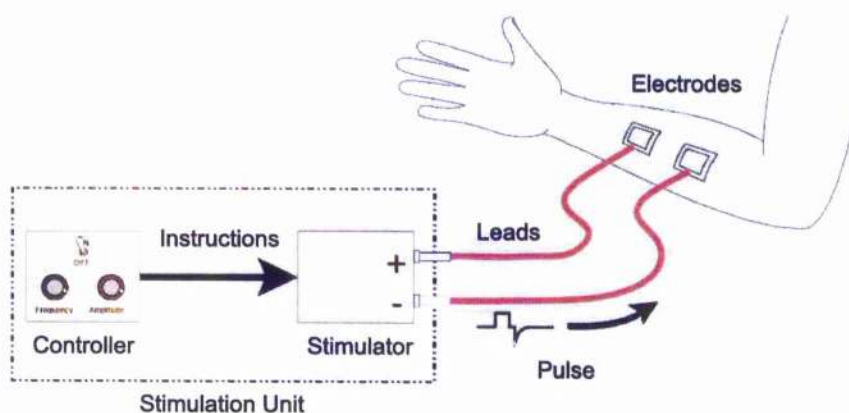


Figure 1.5: A basic FES system [10].

cord. Tetraplegia results in impairment of function in the arms as well as the trunk, legs and pelvic organs [7]. The level of the functional damage depends on the cervical level (from C1 to C7) of the injury. For instance, as Table 1.1 shows, a C3 – C5 level of injury will lead to partial paralysis of the diaphragm, as well as all the functions below it; whilst a C7 injury can leave some remaining control of the shoulder movement. To conclude, cervical injuries (tetraplegia) results in serious damage to activities of daily life, therefore requiring intensive help from others.

Paraplegia This term refers to impairment or loss of motor and/or sensory function in the thoracic, lumbar or sacral (but not cervical) segments of the spinal cord [7]. Arm function is spared in case of paraplegia, but the functions of trunk, legs and pelvic organs are impaired subject to the level of the injury.

1.2.4 Functional Electrical Stimulation (FES)

Functional electrical stimulation (FES) has become a fast developing technique to restore or improve body functions to individuals with spinal cord injury (SCI). This method has been developed for more than 20 years, and FES centers have been established around the world [8, 9].

FES works by applying low levels of pulsed electrical current to motor nerves, thus activating paralysed muscles. FES can work because when damage occurs only to the CNS, muscles and their peripheral nerves are intact. The muscles are paralysed because the biological signal generated from the brain cannot reach the nerves which activate the muscle. What FES does is to apply artificial electrical signals directly to the nerves. FES can also benefit Multiple Sclerosis patients as they also have problems in transmission of nerve signals [10].

A basic FES system is shown in Figure 1.5. The electrodes can be surface or implanted ones. Pulsed electrical signals go through the lead to the electrodes from the stimulator, whilst parameters such as pulse width and electrical amplitude can be configured by a controller connected to the stimulator.

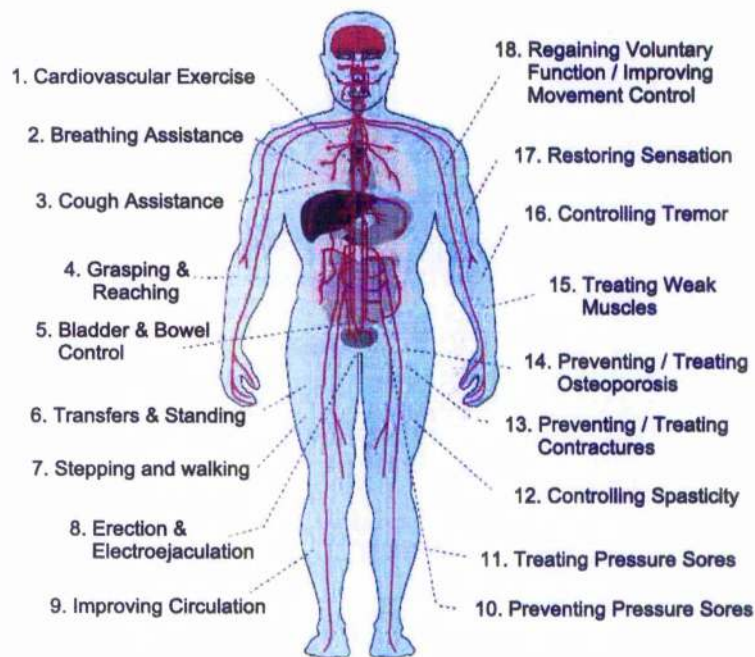


Figure 1.6: FES applications in spinal cord dysfunction [10].

FES has been applied in many spinal cord dysfunctions. Figure 1.6 shows 18 ways that FES can benefit individuals with SCI. Rehabilitation engineers have developed systems for FES technique in the following areas: paraplegic standing [11–17], lower-limb cycling [18–20], upper-limb exercise [21,22], bladder and bowel functions [23], respiratory function [24–30].

1.3 Effect of Spinal Cord Injury and Tetraplegia on Respiratory Function

1.3.1 Main Respiratory Muscle Paralysis in Different Levels of Lesion

When a spinal cord injury occurs, the respiratory muscles innervated below the level of the lesion will be impaired, leading to complete or partial paralysis. The respiratory muscles and their innervation are shown in Table 1.2. Patients with partial or complete paralysis of any of the muscles of respiration will need special care [7].

People with high cervical spinal cord injury (C1-C5) have the diaphragm completely or partially paralysed, leading to serious respiratory failure. The initial mortality of high cervical spinal cord injury is high due to the instant respiratory failure. Ventilators are mandatory to individuals with high cervical spinal cord injury.

Individuals with lower thoracic and lumbar lesions have little damage to the lung function due to the intact diaphragm and abdominal function. When the spinal cord is injured at T6-L1 (or above), the abdominal muscles are partially or completely paralysed. In this case, the ability of active (forced)

Muscle	Innervation
Inspiratory, primary	
Diaphragm	C3-C5
Intercostals	T1-T11
Scalene	
Anterior	C3-C4
Middle	C5-C6
Posterior	C6-C8
Inspiratory, accessory	
Sternocleidomastoid	C2-C4 and accessory N. (XI)
Trapezius	C1-C4 and accessory N. (XI)
Expiratory	
Rectus abdominus	T6-T12
Transversus abdominus	T6-L1
Internal and external obliques	T6-L1
Pectoralis major	Medial and lateral pectoral N. (C5-T1)

Table 1.2: Muscles of respiration and their innervation. Adapted from [5].

expiration such as cough is impaired.

1.3.2 Effect of Spinal Cord Injury on Respiratory Phases

Inspiratory phase

For neurologically intact individuals, the diaphragm is the main inspiratory muscle. Along with intercostal muscles and scalene muscles, the diaphragm allows the chest wall to move with a single degree of freedom along the relaxation characteristic [31].

People with spinal cord injury at C2 and above will have the diaphragm paralysed completely. They usually need a ventilator. People injured at C3-C5 can take small breaths, while C6 are able to take deep breaths [32].

In the case of low cervical cord injury (below C5-C8), the function of the diaphragm is retained, while the intercostal muscles are paralysed completely. Without the pulling force supplied by the intercostal muscles, when the diaphragm contracts during inspiration, the expansion of the ribcage is limited. The scalenes are innervated around C6 (shown in Table 1.2), therefore some residual functions of these muscles can remain. Estenne and Troyer have found that the electromyography (EMG, see page 20 in Chapter 2) activity of scalene in individuals with tetraplegia can indicate upper rib cage motion [31, 33]: when the EMG activity of scalene is weak, a paradoxical decrease in anteroposterior diameter of the upper rib cage during inspiration is more likely to happen. This confirms the finding of Danon et al. [34], who also found this paradoxical upper rib cage movement in a C1 tetraplegia patient.

Expiratory Phase and Cough

As Table 1.2 shows, expiratory muscles are innervated in the thoracic level of the spinal cord. Thus subjects with tetraplegia have severely compromised expiratory muscle function [35]. Consequently, expiratory activities in tetraplegia individuals depend only on the elastic recoil of the diaphragm. Cough in these subjects can be severely impaired because that the cough action requires rapid contraction of the thorax which can not be achieved solely by the elastic recoil of the diaphragm. Cough is important to facilitate the clearance of the sputum retention and to minimise pulmonary infection. Limitation of cough can also increase the risk of asphyxia. Therefore, for tetraplegic individuals, cough assistance [36,37] is often required.

However, there were some findings indicating that, although the main expiratory muscles are paralysed, most C5-C8 tetraplegic subject can still generate a small expiratory reserve volume [38, 39]. This indicates that although all the well-known muscles of expiration are paralysed, most tetraplegic subjects are still able to activate some muscles that can overcome the elastic resistance to deflation of the chest wall and cause emptying of the lungs [35]. Troyer, Esterne et al. found that the *clavicular portion* of the pectoralis major plays a crucial part in the mechanism of active expiration in tetraplegic subjects [40]. Because of the inwards movement of the upper rib cage caused by the *clavicular portion* of the pectoralis major, the intrathoracic pressure increases. This pressure increase will be transferred to the abdomen via the downwards movement of the diaphragm. As a result, in contrast to neurologically intact subjects who contract the abdominal muscles forcefully and have inward motion of the abdomen, the anteroposterior diameter of the abdomen of tetraplegia people increases [35]. Estenne and Gorini have concluded that this paradoxical expansion of the abdomen during expiration of tetraplegia subjects was observed because of the contraction of the pectoralis major, not of the diaphragm [41].

Estenne and Troyer later carried out some experiments to investigate the expiratory muscles during the cough process [42]. They concluded that in tetraplegic subjects the *clavicular portion* of the pectoralis major also plays a major role during coughing.

1.4 Respiratory Therapies

Tetraplegia can lead to paralysis of respiratory muscles, thus compromising the respiratory function. The damage level of tetraplegia to the respiratory function depends on the level of the spinal cord injury. To patients with spinal cord injury at different level, the respiratory therapies required can be different. The level of the spinal cord injury and respiratory therapies required are summarised as follows:

- **C1 – C3:** The diaphragm is paralysed completely. There is no voluntary respiration in this case and mechanical ventilation is mandatory.

- **C3 – C5:** Some diaphragm function is reduced. As a result, the respiratory function is compromised. Ventilation may be mandatory in this case.
- **C5 – T1:** Diaphragm is intact. The accessory inspiratory muscles and expiratory muscles (mainly the abdominal muscles) are affected. In this case, forced respiration such as cough is compromised, thus assistance for such need is required. Patients in this category are the main targets of this study.

The following sections describe some of the common respiratory therapies available for patients with spinal cord injury at different levels.

1.4.1 Mechanical Ventilation (MV)

Mechanical ventilation (MV) is often the first method used to assist respiration in tetraplegia. This method has a relatively long history among all the respiratory therapies in SCI patients. Tobin has written a comprehensive book on the principles and practice of MV [43]. High cervical injury patients (above C4) are often required to use this method, due to the failure of both main inspiratory and expiratory muscles. MV is a method that uses ventilators to generate the pressure difference between the atmosphere and the lung, thus leading to mechanical ventilation. Hence, there are two ways of generating pressure difference between the atmosphere and the lung, which are called negative pressure ventilation and positive pressure ventilation.

Negative pressure ventilation This method, also known as iron lung, can be traced back to 1929 when Philip Drinker and Louis Agassiz Shaw first developed it. They invented a large container that encloses the whole human body except the head. This machine can evacuate air in the container through a pump that was connected to it, generating subatmospheric pressure around the chest and abdomen. Nowadays, this method is still in use. Ventilators for this method have been developed to be smaller devices, such as jacket and cuirass.

Positive pressure ventilation This method has become increasingly popular. Positive pressure ventilators increase the pressure in the patient's airway through an endotracheal or tracheostomy tube, as shown in Figure 1.7. The positive pressure allows air to flow into the airway until the ventilator breath is terminated. Subsequently, the airway pressure drops to zero, and the elastic recoil of the chest wall leads to passive exhalation.

No matter what kind of MV is used, surgical operation can be avoided. However, long-term MV can lead to complications of the airway and the lung [44]. So when patients can support their own ventilation, withdrawal of MV (known as weaning) should be considered without delay.

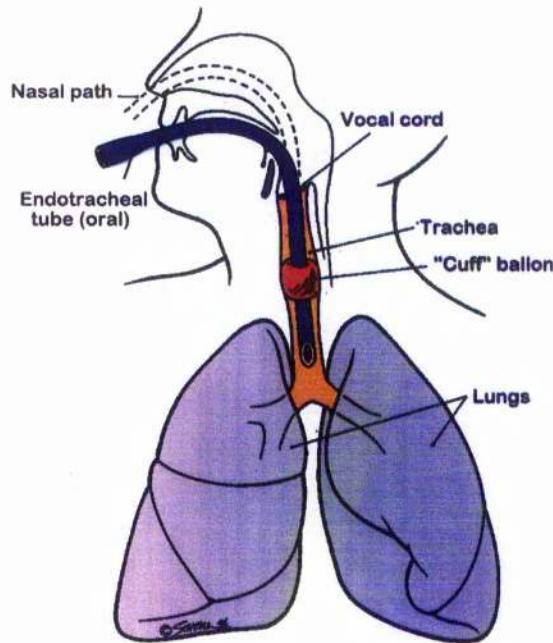


Figure 1.7: An illustration of the endotracheal tube of a positive pressure ventilator. Adapted from <http://library.umsmmed.edu/pe-db/pe-intubation.html>

1.4.2 Diaphragm Pacing (DP)

Also known as phrenic nerve pacing, diaphragm pacing (DP) is an alternative for patients who otherwise have to use MV [24, 25]. This is an FES method which applies electricity to stimulate the contraction of the diaphragm. It was confirmed that tetraplegic patients were able to meet long-term, full-time ventilation requirements using phrenic nerve stimulation of the conditioned diaphragm [26]. Surgical operation (usually thoracotomy) is required in DP to place an electrode around the phrenic nerve, usually in the thoracic area. The electrode is connected to an implanted subcutaneous radiofrequency receiver. An external transmitter sends radio signals to the receiver via an antenna over the receiver. A sample DP device is shown in Figure 1.8. A relatively new surgical improvement called intramuscular-diaphragm pacing has been studied [45]. This technique uses laparoscopic surgery to place intramuscular diaphragm electrodes into each hemidiaphragm near the phrenic nerve motor points. This is less invasive than using phrenic nerve electrodes via thoracotomy.

The diaphragm is given rhythmic electrical impulse via the electrodes to contract. As a result, DP works in the inspiratory phase.

DP has relative low complications with the airway and the lung. Pacers are easy to use, and highly portable. However, this method can only be applied to selected patients with intact phrenic nerve and normal diaphragm function. For patients with C3–C5 tetraplegia, the phrenic nerve can be damaged. Thus the phrenic nerve functionality must be confirmed before the pacing is considered.

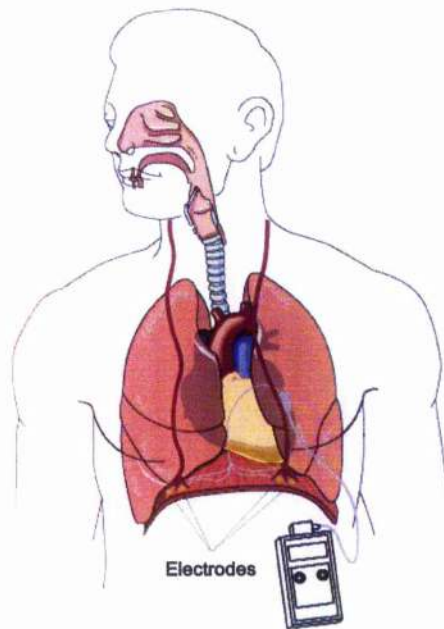


Figure 1.8: The laparoscopic implant procedure used for diaphragmatic pacing requires insertion of four trocars into the abdominal cavity. Electrodes are inserted through these trocars into the phrenic nerve motor points the places where the phrenic nerves enter the right and left hemidiaphragms [46].

1.4.3 Stimulation of the Abdominal Muscles

In contrast to DP, stimulation of the abdominal muscles assists expiratory phases. This method is more likely to be applied when the diaphragm function is intact or slightly compromised, while the expiratory muscle and the accessory inspiratory muscles are paralysed, i.e. with C5 – T1 tetraplegia. According to the source of stimulation, this method is divided into the following two categories.

A. Functional Magnetic Stimulation (FMS)

Functional Magnetic Stimulation (FMS) of abdominal muscles has been developed by scientists mainly to restore cough [47–51]. This technique is performed by using a magnetic stimulator and placing the magnetic coil along the lower thoracic spine [48]. According to *Faraday's law*², when the amplitude and duration of the current through the magnetic coil is proper, sufficient current can be generated in the nerves and it can drive the dysfunctional muscles.

FMS of abdominal muscles has advantages as follows: i) it is a noninvasive method; ii) the stimulation is painless. This is an advantage over FES of the abdominal muscles, which applies electricity to the body physically (see next section); iii) as FMS uses a magnetic field to generate electricity, there is no physical contact between the stimulator and human body. However, the design of the magnetic

²Faraday's law of induction states that the induced emf (electromotive force) in a closed loop equals the negative of the time rate of change of magnetic flux through the loop.

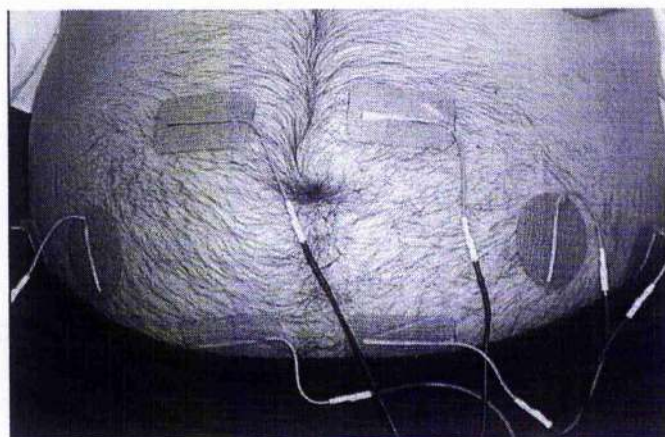


Figure 1.9: The electrodes and the four stimulation channels in FESAM [53].

coil is not as easy as the design of the FES stimulator. The size and winding structure of the magnetic coil can effect the clinical result directly [52]. The magnetic coil is large and requires large electrical current to generate proper magnetic field. Hence, long-term use can overheat the coil. Request for large current also makes the stimulator expensive and less portable.

B. Functional Electrical Stimulation of Abdominal Muscles (FESAM)

The basic concept of Functional Electrical Stimulation of Abdominal Muscles (FESAM) is to apply electrical stimulation to the abdominal muscles during expiratory phases to enhance the contraction of the abdomen, thus assisting quiet breathing and coughing. In the previous study [53], four stimulation channels were used: two channels stimulated the mm. rectus abdominis, while the other two channels stimulated the lateral abdominal muscle group on both sides, as shown in Figure 1.9.

During the early nineties, two groups of scientists have reported pilot studies on the possibility of using FES method to the abdominal muscles to assist cough [27, 54]. Their results were positive. One of these group continued their research on using FES to assist ventilation on nine neurologically intact subjects, and their results provided a basis for future studies with patients in borderline ventilatory failure [28].

This technique has been developed on subjects with spinal cord injury [29, 30, 55–57]. In addition to assistance to quiet breathing, FESAM systems have also been developed to enhance cough [27, 53]. All of these reports have shown increased tidal volume or cough peak flow by FESAM.

Unlike MV or DP, FESAM doesn't require surgery – surface electrode were used. Like other FES applications, the power needed for FESAM is low. The stimulator device is small and portable.

Gollee et al. [53] have developed an automatic control system to control the stimulation according to the respiratory activity. This automatic system is designed to eliminate the requirement of manual manipulation, thus making the FESAM method more convenient for daily life. The control structure of this system is shown in Figure 1.10. Respiratory activity was monitored by a spirometer connected

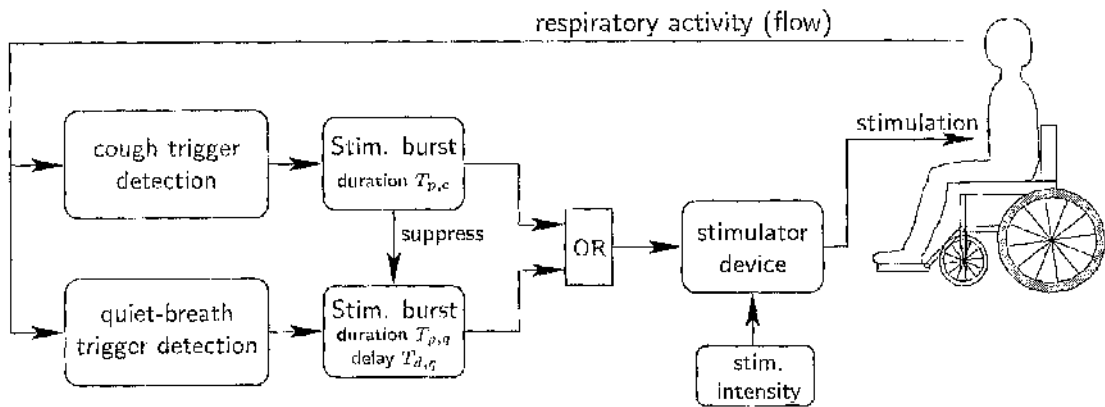


Figure 1.10: The automatic control structure of FESAM [53].

to a face mask worn by subjects. The respiratory flow data was acquired by a computer. The program run on the computer detected the current respiratory activity. The activity was identified as quiet breathing, cough or others. The detection of cough or quiet breathing activates the stimulator device to generate electrical pulses to the electrodes. The amplitude and pulsewidth of the stimulation was set accordingly to support cough and quiet breathing activities, respectively.

1.4.4 Summary of the Respiratory Therapies

This section has introduced some of the main techniques to assist respiratory functions in patients with SCI. Physical techniques such as postural drainage and suction were not mentioned. One of the purposes of this study was to develop an automatic control system that can benefit people most in the daily activity and require least manual control. Hence, long-term usage, portability, ability to self-control are what this study was looking for. These characteristics of the techniques mentioned previously are summarised in Table 1.3.

Tech	Long-term use	Portability	Control	Note
MV	Long-term usage of MV is mandatory to high cervical injury patients. Smaller negative pressure devices such as cuirass are not suitable for long-term use as they may cause chafing and skin damage.	Modern MV usually uses positive pressure tracheostomy tubes. They can be portable.	Respiration cycles can be controlled by preset amount of volume, pressure or time for a cycle. This kind of control is open-loop.	MV devices have been developed for many years. Most hospitals are equipped with MV devices. It is widely used. The negative aspect of MV is that the positive MV can lead to pulmonary complications because it ejects air into the lung directly.
DP	Can be used long-term.	The stimulator is portable.	Control of DP is open-loop.	An alternative to MV. But requires intact phrenic nerve.
FMS	No long-term use report has been published. Large current through the magnetic coil could cause overheating.	The requirement for large current leads to less portable device.	FMS is controlled manually.	This method is less painful than FESAM. But no long-term reported is available and it is mainly researched for assisting cough.
FESAM	Long-term use has been carried out and the results were positive.	Low power requirement makes the device portable. Surface electrode does not require any surgery.	Automatic control system has been developed. Not only quiet breathing, but cough can also be assisted with this technique.	This study applies this method.

Table 1.3: This table lists some main characteristics of the techniques for respiratory therapy mentioned in this thesis.

1.5 Open Issues in the Automatic Control System for FESAM

The automatic control system for FESAM uses a sensor system to record breathing signals. A control system then analyses the breathing signal to detect the breathing activity. The sensor and control system are two essential parts of the entire automatic control system. This section discusses the open

issues of these two systems. These open issues lead to the later contents of this thesis.

Sensor system In automatic control system for FESAM, a sensor system is used to measure the online respiratory activity. In the previous study [53], the system acquires the respiratory data and analyses them online, detecting quiet breathing, cough, and other activities such as speaking. A spirometer connected with a face mask was used. The face mask is uncomfortable and disrupts other activities such as speaking. Other sensors are therefore needed. Chapter 2 discusses the evaluation of using an inertial measurement unit device at the abdomen to detect breathing signals.

Control System In the previous system [53], respiratory activity was detected by analysing the flow rate through the spirometer, its derivative and the similarity of the online flow curve with a standard quiet breathing curve recorded previously. This study introduces six characteristics of the respiratory signal to analyse the respiratory status to minimise the detection error. This issue is discussed in Chapter 3.

Other issues such as system failures are not discussed in this thesis.

2 Experiments with an IMU Sensor System

Summary

Inertial measurement unit (IMU) devices have been used to measure orientation of human body segments in many reports, whilst movement of the abdomen can be used to represent respiratory activities. Experiments with both spirometer and IMU are therefore carried out to explore the possibility of using an IMU device to measure the abdominal movement as breathing signals for the FESAM system. The analysis evaluates the ability of the IMU sensor to detect the onset of respiration and different breathing patterns. Both time and frequency domain are considered in the analyses. Group evaluation and case study are both carried out statistically. The results confirm that the IMU sensor system has the ability to detect the online respiratory status with neurologically intact individuals.

2.1 Introduction and Background

2.1.1 The Role and Requirement of the Sensor in the Automatic FESAM System

The main task of the sensor in this FESAM system is to measure the online respiratory information. A detecting system then analyses the data acquired from the sensor to determine respiratory activity. The role of the sensor is as important as the detecting system.

The sensor used to measure respiratory activities is required to be sensitive to different activities, such as quiet breathing, cough and speaking. A sample of respiratory data acquired from the spirometer is shown in Figure 2.1. In the figure, the three different respiratory activities can be distinguished easily by human eyes. The quiet breathing segment can be differentiated from the cough and deep breathing segments by measuring the amplitude of the data. The cough pattern has distinct sharp curves compared with the other two patterns.

In addition to detect different respiratory patterns, detections of onsets of each inspiration and expiration are also important to the automatic system. This is because that the stimulation is generated in the expiratory phase, as the contraction of abdominal muscles assists expiration. Consequently, as shown in Figure 2.2, the stimulation signal is designed to be generated directly after the detection of the expiratory onset and end when the inspiratory onset is detected.

In the previous study [53], measurements of the airflow at the mouth by a spirometer with a low dead-space full face mask provided the respiratory signal to the detecting system. By analysing this breathing signal online, the system can: i) differentiate breathing patterns between quiet breathing,

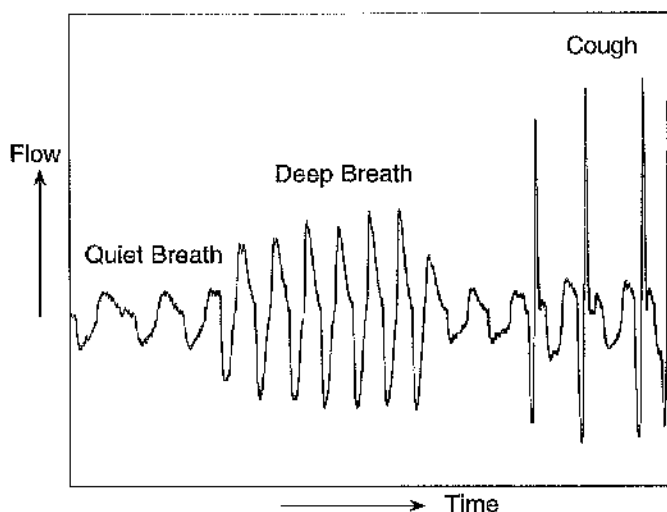


Figure 2.1: Sample respiratory data acquired from the spirometer.

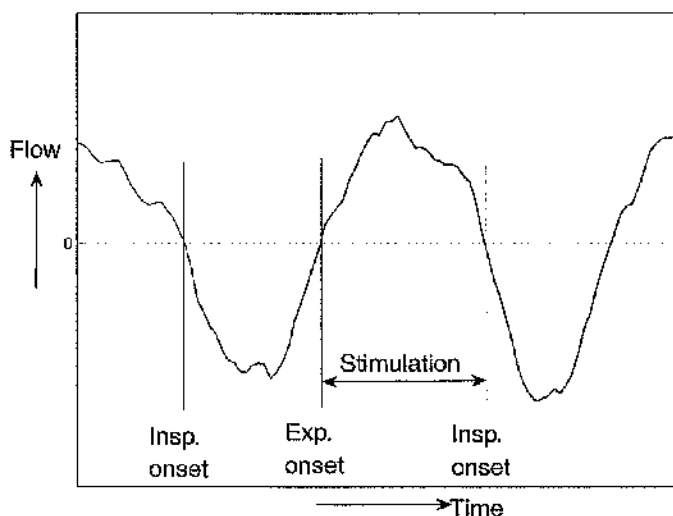


Figure 2.2: Sample respiratory data of quiet breathing acquired from a spirometer. The double arrow line shows when the electrical stimulation is applied. The stimulation is active from the onset of expiration to the onset of inspiration.

cough, and other activities such as speaking; ii) detect the onset of expiration in patterns of quiet breathing and cough, and give corresponding trigger signals for the electrical stimulation.



Figure 2.3: A portable spirometer (Microloop, Micromedical, Chatham, UK [58]). A face mask can be connected to the tube of the spirometer. This spirometer is connected to a computer via the RS232 interface. Breathing data will be collected in the relevant software on the computer at real time. Adapted from http://www.micromedical.co.uk/products/proddetail2.asp?spiro_id=7.

However, the detection device of spirometer with a face mask is not the most suitable device to detect the breathing signal for long-term use due to its inconvenience. A device that could detect the respiratory process indirectly (i.e. not from the mouth and nose directly) is desired to be an alternative to acquire breathing signals. The signal acquired from this device is required to be able to: (i) be analysed in real-time; (ii) detect different respiratory patterns (quiet breathing, cough, speaking) qualitatively; (iii) detect the onset of expiration in patterns of quiet breathing and cough.

In the next sections candidates for the sensor for this system are introduced.

2.1.2 Spirometer

A spirometer is an apparatus which measures the volume of air inspired and expired by the lungs. It is the device to perform spirometry test, the most common of the Pulmonary Function Tests (PFTs). In addition to the spirometry test, spirometers can also be used to record respiratory activities. As shown in Figure 2.3, a spirometer device can be connected to the serial port of a computer and record the respiratory signal online.

The measurement of air flow during respiration is a direct and straightforward way to represent respiration. This device is therefore used in previous studies of FESAM systems [28, 29, 53]. In the previous studies, subjects wore a face mask which connected to the spirometer. The disadvantage of using spirometer is that it cannot be used over a long-term period. The face mask is inconvenient and uncomfortable with respect to daily activity.

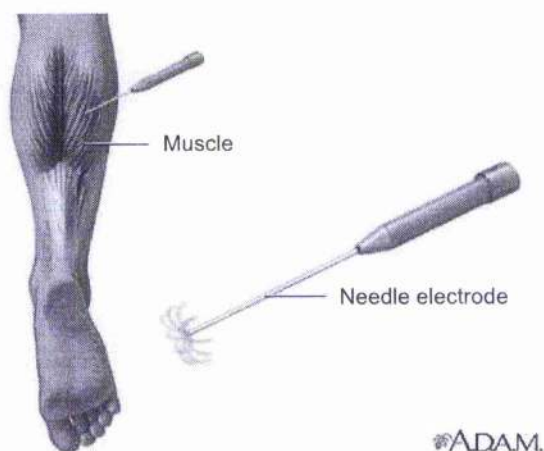


Figure 2.4: Electromyography (EMG) test with a needle electrode. Adapted from <http://www.nlm.nih.gov/medlineplus/ency/imagepages/9741/htm>.

2.1.3 Biopotentials

Biopotentials have been applied to extract command and feedback signals for FES systems [59]. The biopotential for FES systems can be the electrical potential across the nerves, or the electrical activity inside the brain.

Electrical Potential across Nerves

Human muscles can be activated by the action electrical potential transmitted across the nerve systems. The information of such electrical potential, such as its electricity, can be used to represent the status of body functions. For example, the electrical potential across the neurons and the nerves to activate the abdominal muscles can be used to represent the state of these muscles.

Two techniques are available to measure the electrical potential across nerves. They are electromyography (EMG) and electroneurography (ENG).

As shown in Figure 2.4, the EMG technique typically uses a needle electrode to acquire information about the state of the muscle and its innervating nerve. The EMG can also be performed by a surface electrode [60], which is painless and non-invasive to the patient. Experiments have been done using the EMG recordings from sternocleidomastoid (SCM) muscles to control a FES system for hand control of tetraplegic individuals [61].

The ENG technique typically uses cuff electrodes to measure the conduction velocity and response latency of peripheral nerves. The applications of ENG have been reported in FES foot drop correction system [62] and hand grasp neuroprosthesis [63] (shown in Figure 2.5).

To use EMG signal as stimulation trigger for FES systems, it is essential to place the electrodes (electromyography) over the muscles that can be voluntarily controlled [64]. A common problem with

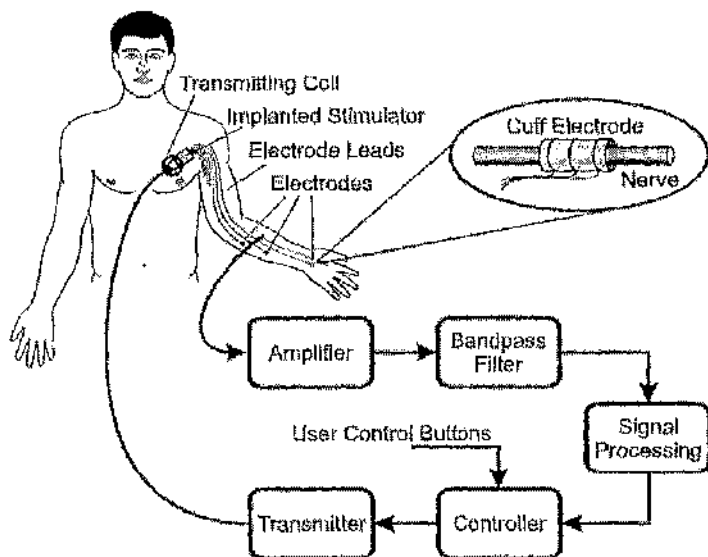


Figure 2.5: Electroneurography (ENG) in a closed-loop hand grasp neuroprosthesis system. Adapted from [63].

using the EMG signal to command the stimulation is the stimulation artefact. A blanking device is usually needed to eliminate the stimulation artefacts that are much bigger than the EMG signals. When the EMG signals from the muscle that is stimulated are used [65, 66], the elimination of the stimulation artefact is more essential.

Two disadvantages of the ENG method in terms of this study are: i) ENG has limitation of selectivity in terms of nerves; ii) it requires invasive nerve cuff electrodes.

Therefore, the open issues for using electrical potential across nerves to control the stimulation to assist breathing can be summarised as follows: a voluntarily controlled muscle or suitable nerve is needed. The electrical potential measured should be able to represent the state of respiration. The abdominal muscles are not suitable as they are paralysed with tetraplegic individuals.

Electrical Potential inside the Brain

Electroencephalography (EEG) measures the electrical activity (impulses) of the brain. The electrical impulses between the brain cells are usually recorded by electrodes placed on the scalp. The EEG signal can be used for a Brain-computer interface (BCI) [67] to provide FES command. This technique is painless and noninvasive. Experiments have been reported on two able-bodied subjects and one neuroprosthesis user to test a EEG-based control of a hand grasp neuroprosthesis [68].

Despite the advantage of no requirement for surgery, it is difficult to pick up individual EEG signals from large groups of neurons in the brain. Another issue for applying EEG is that the electrodes on the scalp are difficult to apply, leading to a complex system. In addition, available EEG experiments

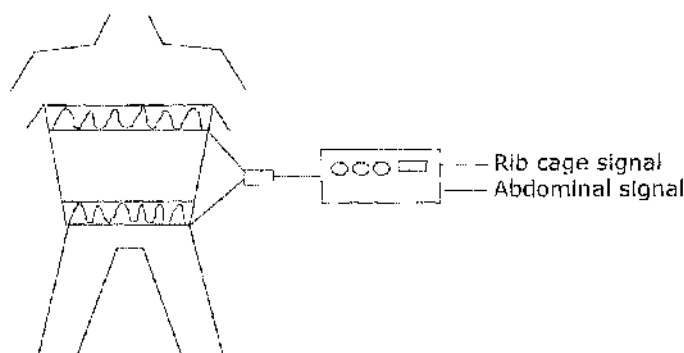


Figure 2.6: A Respiratory Inductive Plethysmograph (RIP) system. Adapted from <http://www.imt.liu.se/bit/staff/tomst/rip.html>.

on FES control were all carried out by doing some deliberate activities, such as hand grasp. These experiments requires training. While no experiment has shown features of EEG signal during voluntary respiration phases, this technique is potentially interesting but not practical at present.

2.1.4 Respiratory Inductive Plethysmography (RIP)

Due to the limitation of biopotential application in tetraplegics, the change of the circumference of the chest wall and abdomen is considered to be an alternative. These detections have been investigated in many applications. Respiratory inductive plethysmography (RIP) is one of these applications.

RIP was originally used in sleep studies [69] and has been used for the study of ventilation during exercise [70, 71]. The RIP device typically consists of sinusoidal arrays of electrical conducting wires with a continuous low voltage electrical current passing through. Detection of the change of the current will represent the rate and depth of excursions of the chest wall and abdomen. The RIP device is worn by subjects encircled the ribcage and the abdomen, as shown in Figure 2.6. The change of circumference of the upper body is therefore recorded and used as breathing signal to analyse ventilation.

RIP devices can be made into portable snugs, and they are commercially available (Lifeshirt [72], Vivometrics, Ventura, CA). This method is a noninvasive measurement.

2.1.5 Electroglottography (EGG)

Electroglottography (EGG) is a technique which measures the change in electrical impedance across the throat during speaking. This method can give information on the closure of vocal folds, and has been used widely in the study of voice analysis [73]. It is possible to use this technique to measure the movement of the abdomen to detect the status of respiration.

EGG is performed by wearing a belt with two electrodes attached around the neck. The waveform of EGG can be similar to the spirometer data, with distinctive difference between different speaking

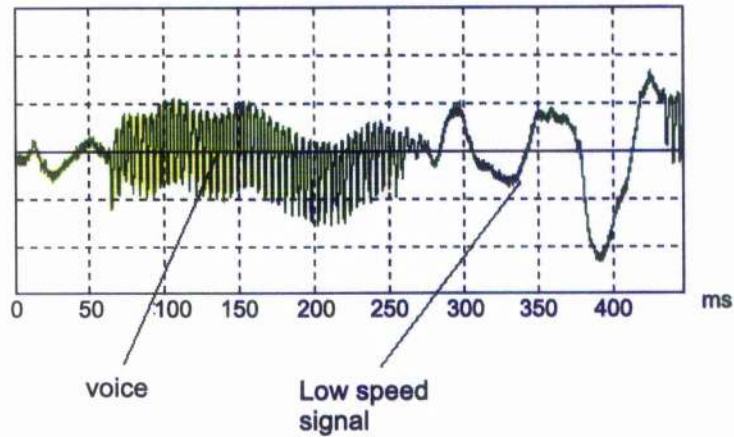


Figure 2.7: A raw waveform of Electroglottography recorded during speaking. Adapted from <http://aune.lpl.univ-aix.fr/~ghio/pedago-EggUK.htm>.

activities (Figure 2.7). However, again, no systems controlled by EGG signal in real-time has been reported.

2.1.6 Inertial Measurement Unit (IMU)

An inertial measurement unit (IMU) typically contains accelerometers and gyroscopes to detect motion. The IMU device works by using the accelerometer signal to continuously correct the orientation estimation obtained by mathematical integration of the 3D angular velocity measured by the gyroscopes [74, 75]. The involvement of accelerometer reduces the integration drift that originates from errors in the gyroscope signal. Magnetometers can also be applied to compensate for the orientation estimation error [76]. IMU devices can be made conveniently portable (Figure 2.8), and they are commercially available (Xsens Technologies B. V., the Netherlands [77]).

Various applications of IMU in the biomechanical field have been reported. Mayagoitia [78] has used four uni-axial seismic accelerometers and one rate gyroscope mounted on the skin to obtain the kinematics of gait in the sagittal plane. Moreno [79] has applied an IMU which contained bi-axial accelerometers and a rate gyroscope to the measurement of foot and shank orthotic segments kinematics.

When the IMU test is performed, the IMU device is usually attached to a belt worn around the body segment. This is a convenient non-invasive method to detect body motion. Consequently, IMU devices have potential to detect the abdominal movement during respiratory phases, thus representing respiration.

One disadvantage of using one IMU device to detect movement is that the overall movements of



Figure 2.8: A commercial IMU device developed to detect human motion [77]. Adapted from http://www.xsens.com/index.php?mainmenu=products&submenu=human_motion.

the body are also detected. When the IMU device is attached at the abdomen, it will detect movement as long as its position is changed. Therefore the experiments with a IMU device in this study require that the subjects sit still on the chair. As a result, the IMU device will detect only the movement of the abdomen, i.e. the relative movement of abdomen to the body. It is thought that this disadvantage can be solved by using another IMU device attached to the chest wall so that the body movement can be eliminated by comparing the two signals from these two devices.

2.1.7 Summary of the Device and Experiment

Signals acquired from the sensor device in this study are required to be able to: (i) be used as command in real-time; (ii) represent different respiratory patterns (quiet breathing, cough, speaking) qualitatively; (iii) detect the onset of expiration in patterns of quiet breathing and cough. At the same time the sensor itself is preferred to be: (iv) noninvasive; (v) portable and convenient. Note that the first requirement of the sensor focuses on the application of the sensor signals on control systems. If there is no reported control systems using the sensor signal in real-time as command, the corresponding evaluation of using this sensor in this study will be “potential”. Any sensor device that cannot fulfill all of these requirements will not be considered. A summary of these characteristics of the sensors mentioned previously is shown in Table 2.1.

The summary table shows that the methods of (surface) EMG, RIP and IMU are potential sensors for the tasks required by this study. In this thesis, the evaluation of using an IMU device is discussed.

The ability of the IMU device to detect different breathing patterns and the onset of inspiration/expiration are the main aspects we wanted to evaluate. The IMU device was used to detect the relative movement of the abdomen. The airflow at the mouth and nose was employed as reference to evaluate the signal from the IMU device. The airflow was acquired by a spirometer. Experiments were conducted with 5 neurologically intact people to record different respiratory patterns: (a) quiet breathing, (b) cough (including continuous cough and single cough), (c) deep breathing and (d) speaking (including loud reading and talking). Signals from the spirometer and IMU were recorded

Sensor	i Real-time	ii Different patterns	iii Detect onset	iv Non-invasive	v Portable
Spirometer	Yes	Yes	Yes	Yes	No
EMG	Yes	Potential	Potential	Yes*	Yes*
ENG	Yes	Potential	Potential	No	No
EEG	Potential	Potential	Potential	Yes	Not Known
RIP	Yes	Yes	Yes	Yes	Yes
EGG	Potential	Potential	Potential	Yes	Not Known
IMU	Potential	Potential	Potential	Yes	Yes

Table 2.1: This table lists the main characteristics of all the sensors mentioned in this study. Refer to the characteristics discussed in Section 2.1.7. *Only refers to the surface EMG.

synchronously. Breathing signals from different breathing patterns were then extracted and analysed separately. Inspiratory / expiratory onset time points of breathing signals were compared. This shows the ability to represent respiration in real-time. The ability to detect different breathing patterns are evaluated by comparing: i) amplitudes of quiet breathing, deep breathing and coughing signals in the time domain; ii) FFT areas of different breathing pattern samples including speaking in the frequency domain.

2.2 Methods

2.2.1 Devices

IMU device

The IMU device used was the Xsens MT9-B Motion Tracker (Xsens Technologies B. V., The Netherlands [77]). The Xsens MT9-B IMU contains 3D gyroscopes, 3D accelerometers and 3D magnetometers. Its algorithm is shown in Figure 2.9. The 3D driftless orientation was obtained by a sensor fusion algorithm [74, 75] where the measurement of gravity (accelerometers) and magnetic north (magnetometers) compensate for otherwise unlimited increasing errors from the integration of rate of turn data (gyroscope). For details refer to the MTx-B technical documentation [77].

During experiments, the IMU device was attached to an elastic belt worn around the abdomen.

Spirometer

The spirometer (Microloop, Micromedical, Chatham, UK [58]) was used with a low dead-space full face mask (Hans Rudolph Inc., Missouri, USA [80]) to record the airflow at the mouth as a reference for the breathing signal acquired by the IMU device. The spirometer has a turbine wheel, whose revolution is proportional to the volume of the airflow (V) through it. The revolutions are counted by electronic sensors, and differentiated into flow rate (v). The flow rate v is used as the breathing signal

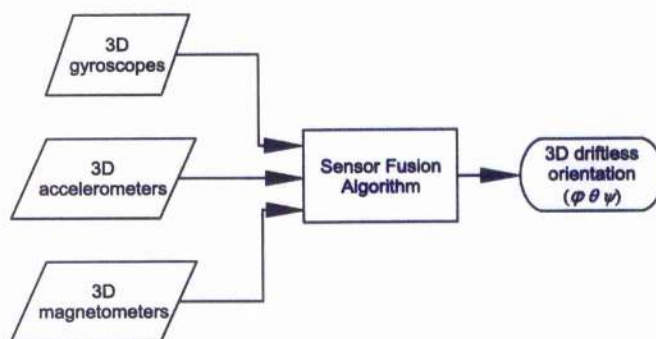


Figure 2.9: The MT9-B IMU algorithm.

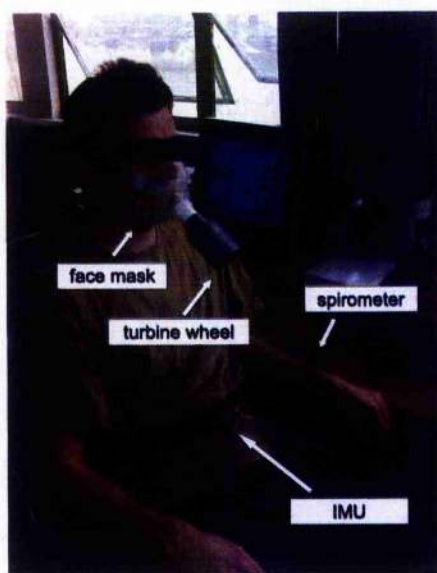


Figure 2.10: A subject during experiment, wearing both face mask (through the turbine wheel connected to the spirometer) and the IMU (attached to an elastic belt around the abdomen).

(B).

Others

Both the spirometer and the IMU were connected to a computer via an RS232 interface. The outputs from both spirometer and IMU were acquired and processed in the Simulink modelling environment (The Mathworks, Massachusetts, USA [81]). The data sampling frequency of the spirometer and IMU was 50Hz and 10Hz respectively. A picture of one of our subjects during experiment is shown in Figure 2.10.

Subject	Gender	Age (years)
01	Female	26
02	Male	25
03	Male	32
04	Female	27
05	Male	26

Table 2.2: Subject information.

2.2.2 Subjects

Subjects recruited for this study were 5 neurologically intact people (Table 2.2). The experimental protocol was explained to all the subjects and then an information sheet and consent form were given to them. They were fully aware that they were free to withdraw from the study at any time and without having to give a reason. The experiment was approved by the local ethics committee at the University of Glasgow.

2.2.3 Experimental Protocol

Experiments were carried out with subjects in sitting posture. During experiments, subjects were required to sit quietly, and place their hands on the arms of their chair.

At the beginning of each experimental session, quiet breathing pattern (QB) was first recorded. This series of QB signals was used for the normalisation of signals for analysis (see Section 2.2.5). QB pattern recorded first could also help subject calm down, eliminating experimental errors caused by anxiety. Other breathing patterns were then recorded. These patterns include forced respirations (cough, C, and deep breathing, DB) and speaking (SP). In order to test the sensor's ability to detect a single change of pattern, cough pattern includes single cough (SC) and continuous cough (CC). Speaking patterns were first recorded asking subjects to read (R) loud. Talking pattern (T) was last recorded when subjects were having a conversation with the experimenter. To evaluate sensor's ability to detect different breathing patterns continuously, different patterns of DB, CC, SC, R were recorded consecutively into 3 sets. In these sets, the four patterns were ordered randomly, along with a short period of QB pattern between them as an inter-experimental rest.

Figure 2.11 describes the experimental protocol. Each subject took one experiment. In the experiment each subject took, there were three parts:

- Part i: 1 minute stable quiet breathing (QB).
- Part ii: three separate sets of different breathing patterns. Every set follows the order of $QB + X_1 + QB + X_2 + QB + X_3 + QB + X_4$, where $X_{1/2/3/4}$ was selected from pattern DB, CC, SC and R, as shown in the bottom part of Figure 2.11. QB was included as inter-experimental rest.
- Part iii: 2 minute talking (T).

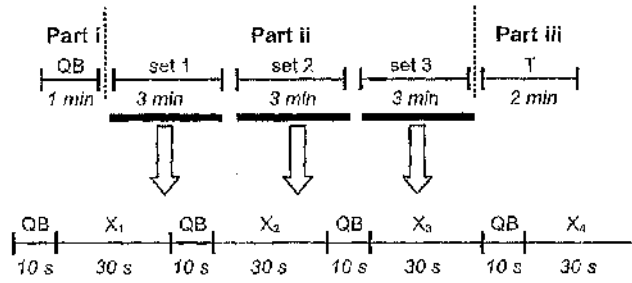


Figure 2.11: Experimental protocol. QB - Quiet Breathing, T = Talking. The space between lines indicates rest. The bottom series of lines explains how each set of part ii is formed. The 10 seconds QB patterns were included as inter-experimental rest. X_1 , X_2 , X_3 and X_4 were patterns of deep breathing (DB), continuous cough (CC), single cough (SC) and loud reading (R), in random order. Note that in part ii, the R pattern lasts actually 60s as people tend to take less breath when reading.

Subjects can take some rest between each part and each set in part ii, as the space between each line in Figure 2.11. It should be noted that in the part ii of experiment, QB patterns were sometimes more than 10s in order to give subjects enough inter-experimental rest.

Before the experiment with each subject, the position of the IMU device on the belt was tested. The IMU device was attached to different positions on the belt. The subject did some QB and DB patterns with each position and the data were recorded. The final position was decided by the highest breathing signal recorded. By such tests with 5 subjects, it was decided to put the IMU device on the umbilicus position.

2.2.4 Data Processing Overview

The data processing of the acquired sensor signals is shown in Figure 2.12. The aim of data processing was to obtain breathing signals which: (i) were synchronised with the voluntary respiration; (ii) had distinct characteristics with different breathing patterns (QB, DB, C, S). In case of the spirometer, the breathing signal was represented by the flow rate (v) at the mouth and nose; while in case of the IMU the breathing signal was represented by the relative displacement of abdomen (d). v and d were obtained within the pre-processing sections in Figure 2.12.

The flow rate v and displacement d were converted into sensor signals B_{raw}^{spiro} and B_{raw}^{IMU} . These signals at this stage were raw signals that needed filter processing. As Figure 2.13 shows, signal B_{raw}^{IMU} had an offset, whilst signal B_{raw}^{spiro} had high-frequency noises. The offset and noises were removed by a highpass and lowpass filtering respectively.

All of the original and filtered signals from both devices with 5 subjects are shown in Appendix A. It can be seen that the high pass filter introduced about 5s settling ripples, and both filters added small amount of phase shift to the signals.

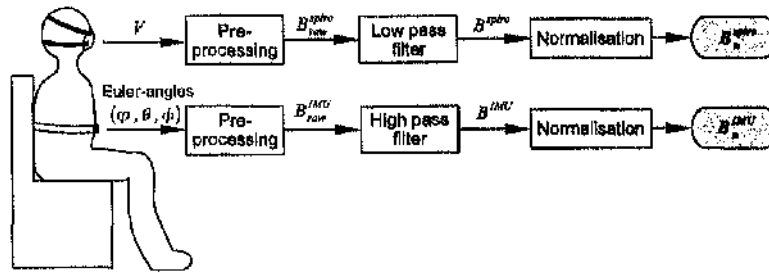


Figure 2.12: Data processing. The processing of IMU data is discussed in Section 2.2.5, and the processing of spirometer data is discussed in Section 2.2.6.

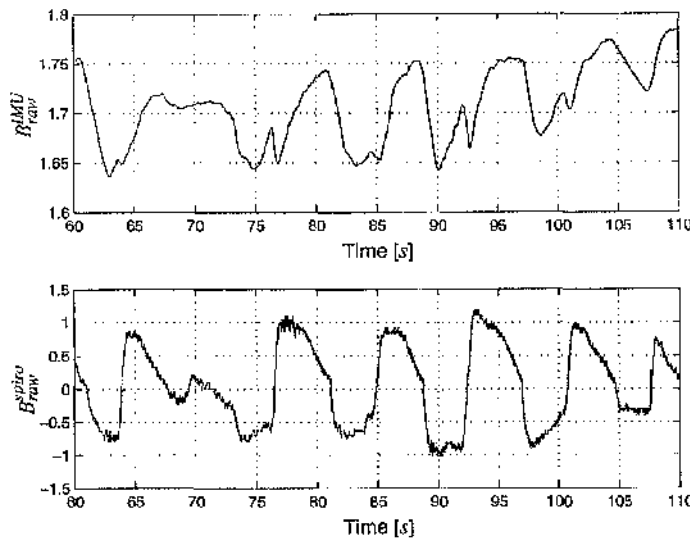


Figure 2.13: A sample set of raw breathing signals from the spirometer and IMU. It can be noticed that the IMU raw signal has an offset, whilst the spirometer signal has high-frequency noises.

2.2.5 Data Processing of the IMU Signal

Pre-processing

The pre-processing of the IMU signal mainly converts the Euler-angles measured by the IMU device into the displacement (d) of the abdomen. Due to the definition of Euler-angle, there will be a mathematical singularity when pitch θ approaches $\pm 90^\circ$. In this study, the position of the IMU device attached at the abdomen was specifically selected to avoid such singularity. The background of this position relates to the two co-ordinate systems in the IMU system.

As shown in Figure 2.14, two co-ordinate systems were defined in the IMU system: (1) global earth-fixed, \mathbf{G} and (2) body-fixed, \mathbf{S} . The co-ordinate systems were both right-handed.

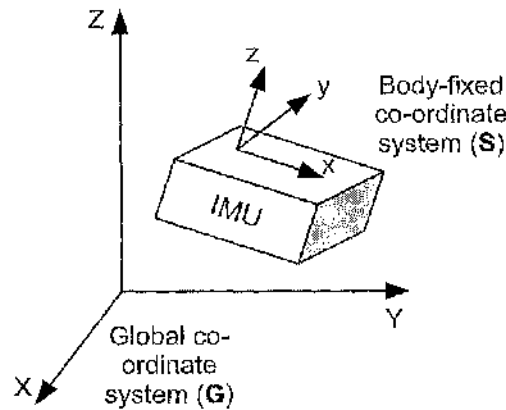


Figure 2.14: Co-ordinate systems of the MT9-B IMU system. The global co-ordinate system G was defined as: X positive when pointing to the local magnetic North; Y according to right handed co-ordinates (West); Z positive when pointing up.

The orientation data was of the body-fixed co-ordinate system S with respect to the global co-ordinate system G . The orientation data can be presented in different conventions [77]. They are:

- Unit Quaternions (also known as Euler parameters)
- Euler angles, roll, pitch, yaw
- Rotation Matrix

Among these conventions, Euler angles is simpler and more convenient to transfer to the relative displacement of the abdomen. Besides, the mathematical singularity when pitch approaches $\pm 90^\circ$ can be easily avoided when the IMU device is positioned head to the horizontal line. This can be seen in Figure 2.10 which shows a subject wearing the IMU device during experiment.

Euler-angles (φ , θ and ψ) are of XYZ earth-fixed type, defined as rotations around X, Y and Z axis -- roll, pitch and yaw/heading in terms of aeronautics, as shown in Figure 2.15. The Euler angles in the IMU system are defined as follows:

- φ =roll=rotation around X, defined from $[-180^\circ \ 180^\circ]$
- θ =pitch=rotation around Y, defined from $[-90^\circ \ 90^\circ]$
- ψ =yaw=rotation around Z, defined from $[-180^\circ \ 180^\circ]$

A sample output with the Euler-angles convention is listed in Table 2.3. The recording file contains the Euler angles of φ , θ and ψ along with the sample time.

The displacement (d) of a 3D movement of the IMU can be obtained by a trigonometric operation with each Euler angle. This displacement with respect to the global co-ordinate system G can be

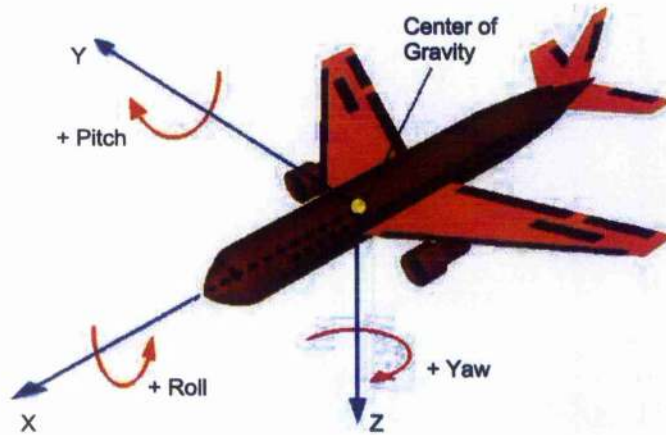


Figure 2.15: Euler-angle systems in aeronautics. The picture is adapted from http://www.mrfizzix.com/spaceflight/Pages/In_Space.htm. In the Euler-angle system of the IMU device, Roll= φ , Pitch= θ and Yaw= ψ .

Sample Time	φ (roll) [deg]	θ (pitch) [deg]	ψ (yaw) [deg]
0.000	134.465912	-18.929155	0.811353
0.010	134.093460	-18.992971	0.673081
0.020	133.698212	-19.109470	0.490710
0.030	133.264557	-19.352758	0.227078
...

Table 2.3: A sample data acquired by the IMU with the Euler angles convention. The Euler angles of φ , θ and ψ are recorded along with the sample time.

projected on the global plane of XY , XZ and YZ as components d_{XY} , d_{XZ} and d_{YZ} . A 3D unit movement (displacement \hat{d}) was defined as it can be projected on the three planes as a rotation with a unit radius. Figure 2.16 shows the displacement component of a unit movement on the YZ plane, \hat{d}_{YZ} . The arrow shows the rotation around the X axis. The rotation radius is a unit length. The component \hat{d}_{YZ} can be calculated from the trigonometric operation of the rotation angle φ . Therefore, all the displacement components of a unit movement can be calculated as:

$$\begin{cases} \hat{d}_{YZ} = 2 \sin(\varphi/2) \\ \hat{d}_{XZ} = 2 \sin(\theta/2) \\ \hat{d}_{XY} = 2 \sin(\psi/2) \end{cases} \quad (2.1)$$

The resultant displacement can therefore be calculated as

$$\hat{d} = \sqrt{\hat{d}_{YZ}^2 + \hat{d}_{XZ}^2 + \hat{d}_{XY}^2} \quad (2.2)$$

The actual rotation radius is not know. Besides, the useful data about the rotation is the relative values between a series of rotations, i.e. rotation radius will be eliminated. The unit displacement

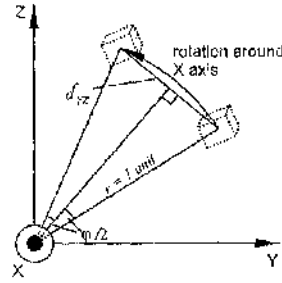


Figure 2.16: A unit 3D movement projected on the YZ plane. It can be understood as a rotation around the X axis (roll) at a unit radius. \hat{d}_{YZ} is the displacement component of \hat{d} on the YZ plane. \hat{d}_{YZ} can be obtained from the trigonometric operation of the roll angle ϕ .

was therefore used to represent the breathing signal B . As the IMU is attached to and moved with the abdomen, the zero point of the B signal can not be fixed. Hence, the \hat{d} signal have an offset. Therefore, the breathing signal at this stage is a raw data with offset, as

$$B_{raw}^{IMU} = \hat{d} \quad (2.3)$$

This offset needs to be removed to obtain the relative movement of the abdomen during breathing.

Filter Processing – Removing the Offset

There are frequency component at around 0Hz in the frequency spectra of the raw IMU signals. Figure 2.17(a) show a series of signal B_{raw}^{IMU} in both time and frequency domain during the QB pattern with subject 02. It can be found that: (i) the main frequency component of the QB pattern was around 0.3Hz-0.5Hz, which corresponds to a normal breathing rate of 20-30 min^{-1} ; (ii) there was a high frequency component around zero because of the offset.

A high pass filter was applied to signal B_{raw}^{IMU} to remove this offset. Figure 2.17(b) shows the time and frequency domain of the filtered signal. The figure shows that the high zero frequency component of the offset in the frequency domain was removed by the highpass filter, whilst other parts of the signal information were unaffected.

The main guide for choosing an appropriate highpass filter is to keep most information of the desired signal in the passband, while cut off the zero frequency component by the stopband. An infinite impulse response (IIR) Butterworth filter was selected as the Butterworth filter has both flat stopband and passband and no ripples.

Generally speaking, the pass frequency of the high pass filter is set below the lower limit of the QB band, say 0.2Hz, while the stop frequency is set as low as 0.01Hz to retain most desired signal informations.

The filter was realised by the *Digital Filter Design* block in the Simulink Library. The filter configuration parameters are listed in Table 2.4. The passband frequency (F_{pass}) and stopband frequency

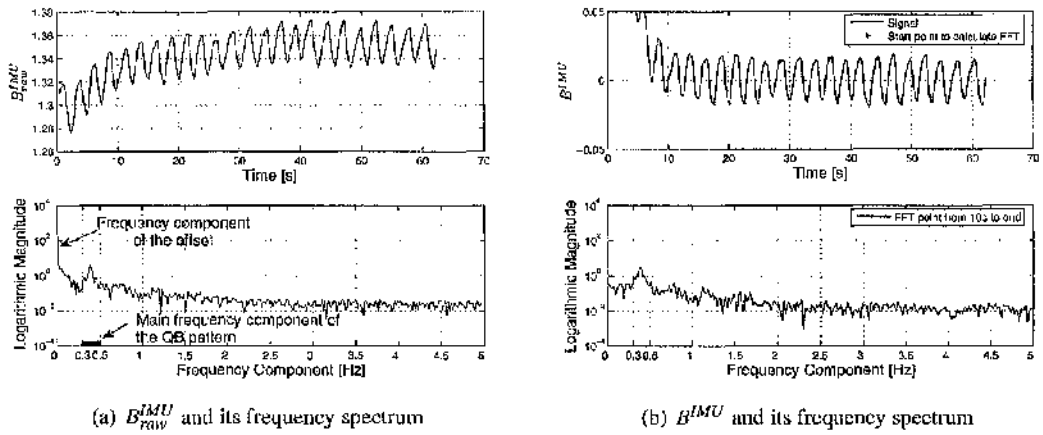


Figure 2.17: Figures showing how the high pass filter works to remove the zero-frequency offset of the raw IMU signal B_{raw}^{IMU} . Figure 2.17(a) shows the raw signal and its frequency spectrum. The filtered signal B^{IMU} and its frequency spectrum is shown in 2.17(b). The large value of B^{IMU} before 10s is due to the settling characteristic of the high pass filter. The FFT frequency spectrum is therefore calculated from 10s onwards.

Design	F_{stop} (Hz)	F_{pass} (Hz)	F_s (Hz)	A_{stop} (dB)	A_{pass} (dB)
IIR Butterworth	0.01	0.2	10	20	1

Table 2.4: The configuration for the highpass filter to remove the offset of the IMU raw signal. The stop and pass frequency were set as 0.01Hz and 0.2Hz respectively. Sample frequency (F_s) was set as 10Hz.

(F_{stop}) were set as 0.2Hz and 0.01Hz respectively. The passband ripple (A_{pass}) and stopband attenuation (A_{stop}) were specified as 1dB and 20dB.

Its magnitude and phase response figure is shown in Figure 2.18. It can be seen that this filter will introduce a phase-shift of around 10° – 30° to the original signal. This phase-shift will lead to a delay within 0.36s in the IMU raw signal.

After this filtering processing, the offset of the raw IMU signal B_{raw}^{IMU} is removed, and the signal B^{IMU} was obtained.

Normalisation Process

As the amplitude of B^{IMU} has little actual physical meaning, it is normalised before the evaluation with the spirometer signal. The normalised signals from the spirometer and IMU device could be then compared qualitatively. The normalisation process for both signals was the same. Therefore this process for IMU signal is discussed the Section 2.2.6 together with the spirometer signal processing.

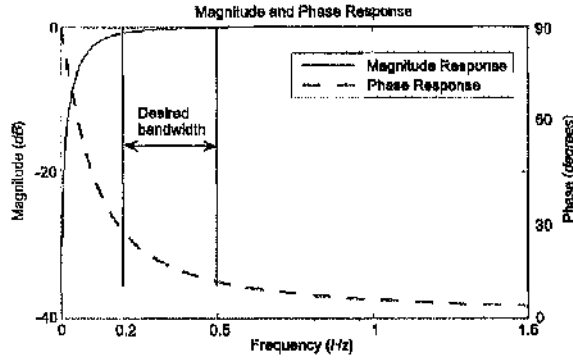


Figure 2.18: The magnitude and phase response of the highpass filter used to remove the offset of the IMU signal. The desired bandwidth is in the interval of $[0.2\ 0.5]$ s as marked. It can be seen that in the desired bandwidth, the phase-shift of the filter is around 10° – 30° .

Design	F_{stop} (Hz)	F_{pass} (Hz)	F_s (Hz)	A_{stop} (dB)	A_{pass} (dB)
IIR Butterworth	3	1	50	20	1

Table 2.5: The configuration for the lowpass filter to remove the high frequency noises of the spirometer raw signal. The stop and pass frequency were set as 3Hz and 1Hz respectively.

2.2.6 Data Processing of the Spirometer Signal

Pre-processing

As mentioned before, the pre-processing of the spirometer signal was to differentiate the air volume (V) at the mouth into the flow rate (v):

$$B_{raw}^{spiro} = v = \frac{dV}{dt} \quad (2.4)$$

It should be noted that the signal V was filtered during the acquisition process by a median filter. This filter worked by taking the average of the original signal over the last 10 samples to remove unwanted noise.

Filter Processing – Removing noise

The signal v differentiated from V was found to be still noisy. A low pass filter was therefore applied to the raw v signal. Figure 2.19 shows how this low pass filter worked.

As the figure shows, the main guide for this lowpass filter is to remove the unwanted high frequency component of the signal ($[3\text{Hz}\ 50\text{Hz}]$ in this sample case). The filtered signal is denoted as B^{spiro} . The filter was realised by the *Digital Filter Design* block in the Simulink Library. The lowpass filter configuration parameters are listed in Table 2.5. The passband frequency (F_{pass}) and stopband frequency (F_{stop}) were set as 1Hz and 3Hz respectively. The passband ripple (A_{pass}) and stopband attenuation (A_{stop}) were specified as 1dB and 20dB .

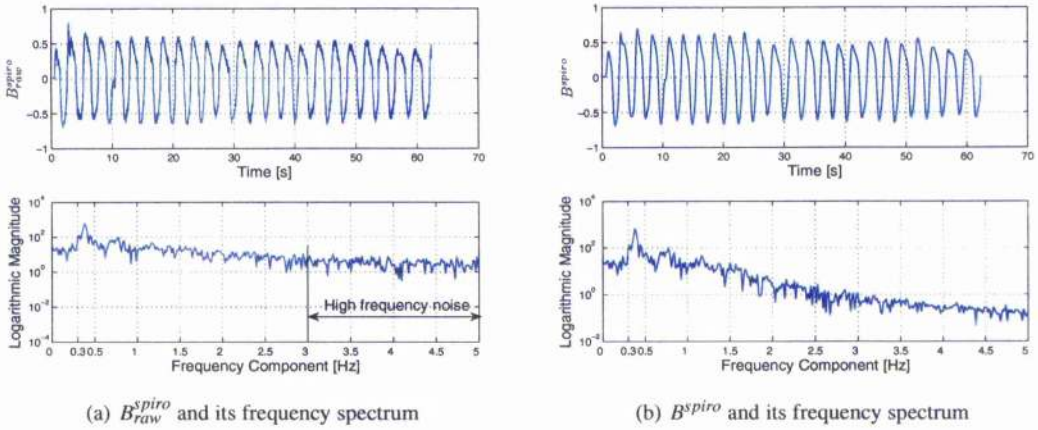


Figure 2.19: Figures to show how the low pass filter works to remove the high frequency noise of the raw spirometer signal B_{raw}^{spiro} . Figure 2.19(a) shows the raw signal and its frequency spectrum. The filtered signal B^{IMU} and its frequency spectrum are shown in Figure 2.19(b). Note that this series of signal is the same as shown in Figure 2.17.

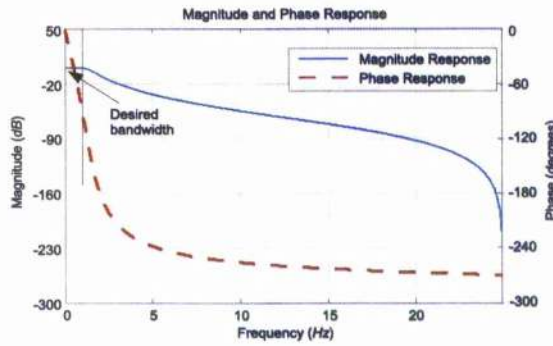


Figure 2.20: The magnitude and phase response of the lowpass filter used to remove noise of the spirometer signal. The desired bandwidth is marked. It can be seen that in the desired bandwidth, the phase-shift of the filter was around $[-80^\circ - 50^\circ]$.

The magnitude and phase response figure is shown in Figure 2.20. It can be seen that the lowpass filter will also introduce a phase-shift to the spirometer signal within the interval of $[-80^\circ - 50^\circ]$. For the signal in the time domain, this usually leads to a delay small than 1s.

After this filtering processing, the high frequency noise of the raw spirometer signal B_{raw}^{spiro} is removed, and the signal B^{spiro} was obtained.

Normalisation Process

After the filter processing, the spirometer signal B^{spiro} and the IMU signal B^{IMU} are normalised. The principles of the normalisation process of both signals are the same. Therefore, the signals from both devices are denoted as B^k .

The purpose of the normalisation process is to remove the physical unit of the signals by setting up

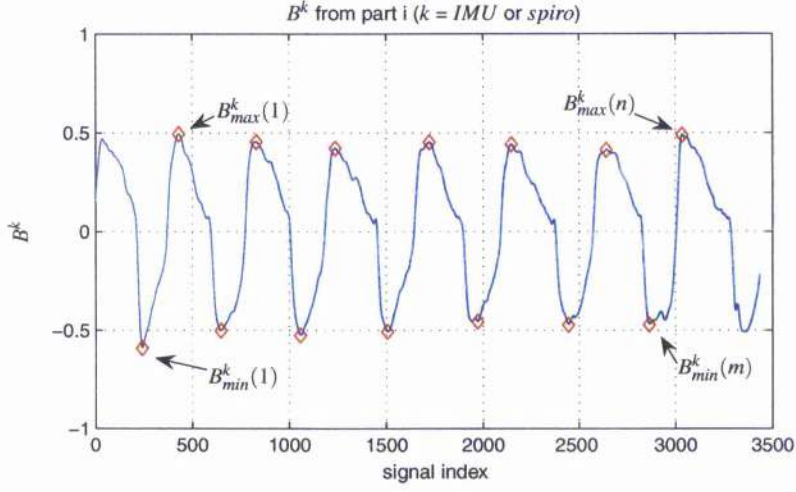


Figure 2.21: This figure shows the maximum and minimum peaks used to normalise signals. The signal used was from the part i of experiment.

a new relative unit system. This new relative unit system defines the amplitude of the inspiration and expiration phase of quiet breathing to be 1. The signal value is then recalculated using the ratio of 1 to the original QB amplitude.

In order to find the ratio to recalculate the signal quantities, the mean amplitude of QB signals (\bar{a}) was first calculated from the data acquired from a signal containing only QB cycles. This signal was typically the recording from the part i of the experiment. Figure 2.21 shows the peak points selected for the normalisation process. B_{max} and B_{min} were arrays of the maximum and minimum values, and n and m are their indices. Then

$$\bar{a}^k = \frac{1}{2} \left(\frac{\sum_{i=1}^n B_{max}^k(i)}{n} - \frac{\sum_{i=1}^m B_{min}^k(i)}{m} \right), \quad (2.5)$$

The breathing signals (B^k) are normalised as B_n^k by:

$$B_n^k = \frac{B^k}{\bar{a}^k}, \quad (2.6)$$

where

$$k = \begin{cases} IMU & \text{the IMU device} \\ spiro & \text{the spirometer device} \end{cases} \quad (2.7)$$

A sample signal before and after the normalisation is shown in Figure 2.22. It can be seen that after the normalisation, the signal B_n^{IMU} is recalculated so that the amplitude of the QB phases are around ± 1 .

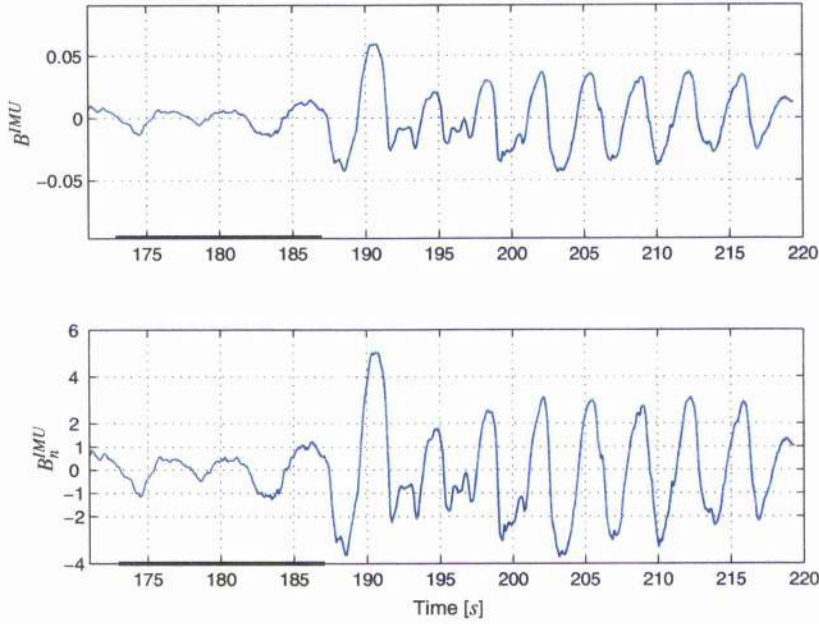


Figure 2.22: A sample IMU signal shows the normalisation process. B_n^{IMU} denotes the normalised IMU signal. The bold lines in the figure indicate the quiet breathing phases, and the breathing pattern after the bold line is deep breathing. It can be found that after normalisation, the amplitude of the quiet breathing phases are around ± 1 , and the deep breathing amplitudes are recalculated.

2.2.7 Methodology of Analysis

Detection of Onset of Expiration and Inspiration

To evaluate the ability of the IMU to represent breathing signals in real-time, the time of each onset of expiration and inspiration of the IMU signal (B^{IMU}) was compared with the signal from the spirometer (B^{spiro}). The normalisation processing does not affect the positions of the onset of expiration and inspiration.

Figure 2.23 shows the onset of expiration and inspiration denoted as (T_{exp}) and (T_{insp}). They are picked by a MATLAB *m* program. This program can automatically pick the zero-crossing data points and output both their values and indices.

The phase-shift of the onset timing (ΔT) is calculated by subtracting timings of the onset points of signal B_n^{spiro} from the corresponding signal B_n^{IMU} , as

$$\begin{cases} \Delta T_{insp} = T_{insp}^{IMU} - T_{insp}^{spiro} \\ \Delta T_{exp} = T_{exp}^{IMU} - T_{exp}^{spiro} \end{cases} \quad (2.8)$$

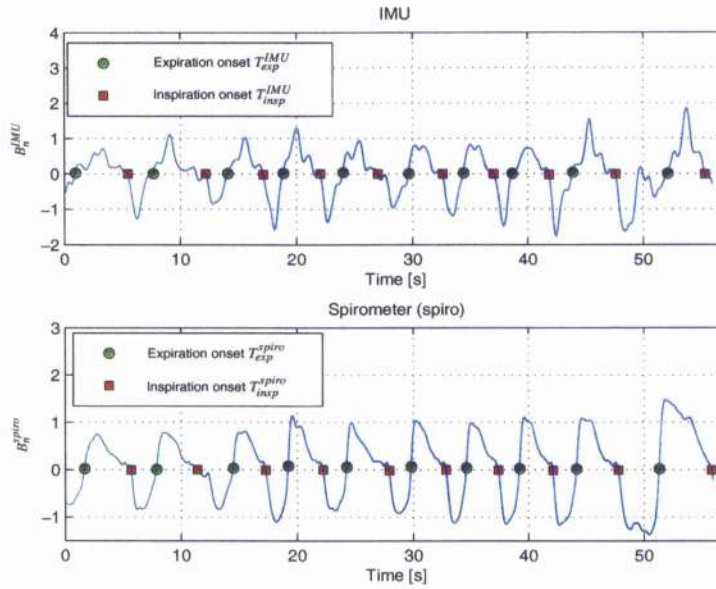


Figure 2.23: A sample series of QB data showing the detection of inspiratory and expiratory onsets.

The phase-shifts of each breathing pattern during both inspiratory and expiratory phases were analysed separately. The QB pattern was analysed with the signal from part i of the experiment. Each set of part ii of the experiment has around 30 *seconds* cough pattern. They were extracted and combined together for analysis. Deep breathing patterns were analysed the same way. Due to the experimental failures described in Section 2.3.2, only the acceptable recordings were analysed. An overview of the recordings with 5 subjects is presented in Section 2.3.1.

The statistical method used to analyse the distribution of the phase-shift was the Box Plot, as shown in Figure 2.24. A box plot can provide visual summary of the *five-number summary* of a data set. They are: 1) the minimum (smallest observation which is not an outlier); 2) the lower quartile (which cuts off the lowest 25% of the data); 3) the median (middle value); 4) the upper quartile (which cuts off the highest 25% of the data); 5) the maximum (largest observation which is not an outlier). The interquartile range (*IQR*) is calculated by subtracting the lower quartile from the upper quartile. When a data value lies $1.5IQR$ lower than the lower quartile or $1.5IQR$ higher than the upper quartile, this data is considered an outlier. The outliers are marked by red + signs in the figures in this thesis. The box plot can be notched. In a notched box plot the notches represent a robust estimate of the uncertainty about the medians for box-to-box comparison. Boxes whose notches do not overlap indicate that the medians of the two groups differ at the 5% significance level. Note that this assumes that the distribution of both groups are normally distributed. As this assumption can not be verified for the data sets of the recordings, notches of the box plot in this study are not evaluated.

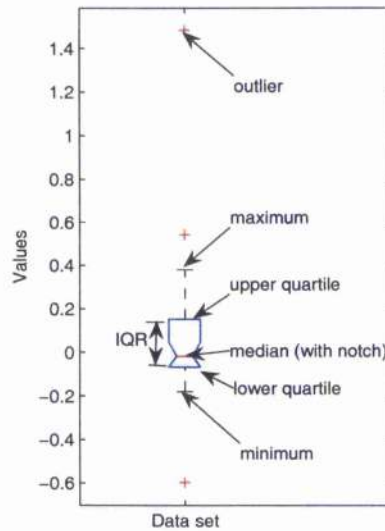


Figure 2.24: An illustration showing the indicators in a notched box plot.

To ensure the data from the two devices were synchronised, the IMU data was first resampled at the sampling frequency of 50Hz . Speaking patterns were not analysed because they were not the main breathing activities we were interested in, as no stimulation was allowed during speaking.

Differentiation between different breathing patterns

One of the important characteristics of the desired sensor was the ability to represent different respiratory patterns. All the processed recording data from both devices are shown in Appendix A. It can be found that amplitude is the most distinctive characteristic to differentiate different breathing patterns in the time domain. Inspiratory and expiratory peaks of the QB, C and DB signals were therefore studied.

A program was developed to auto-detect all the expiratory and inspiratory peaks, as shown in Figure 2.25. This program uses the inspiratory and expiratory positions detected for the analysis of phase-shift to accurately locate the peak values.

The data sets analysed for peak values were normalised, so that the mean peak values of the QB signal was around ± 1 (inspiratory and expiratory). Box plots were also used in this analysis to summarise the distribution of the inspiratory and expiratory peak values with the QB, C and DB patterns.

In addition to the analysis of the amplitude of different breathing patterns in the time domain, the Fast Fourier Transform (FFT) spectra and areas were also analysed to evaluate the signal characteristics in the frequency domain. One typical series of breathing segments of QB, cough, and DB of

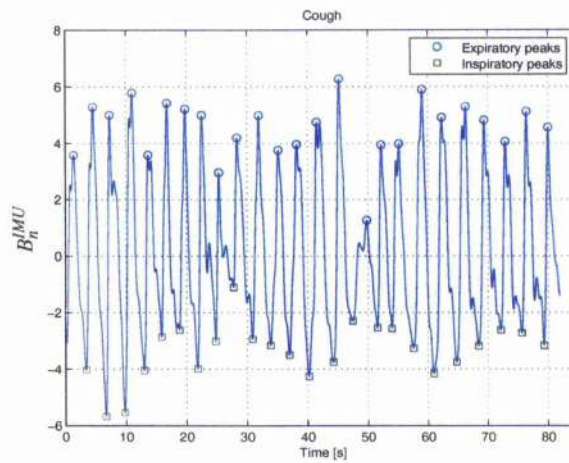


Figure 2.25: The peak points of a cough sample were detected. The peak values are used for the box plot.

each subject were extracted from both IMU and spirometer signal. Their FFT spectra are plotted. The summation of the FFT value (area) was also calculated. This analysis explores the frequency details of both signals which can not be observed from the signal curves in the time domain. This analysis is also useful because the frequency domain analysis is an important aspect of the auto-detection control system described in Chapter 3.

2.3 Results

2.3.1 Overview of the Experiments

Experiments were carried out with 5 subjects. Each experimental session took around 40 minutes. They were started when subjects felt comfortable and relaxed. According to the experimental protocol (section 2.2.3), the recordings of each part of the experiment were indexed as i, ii-1, ii-2, ii-3 and iii. The original and filtered signals of every experiment with 5 subjects are shown in Appendix A.

As reported in Table 2.6, the total time of each part of the experiment, as well as total numbers of the recorded breathing patterns of QB, C, DB and SP were counted. The breathing numbers were counted by counting the number of inspirations from the spirometer signal.

2.3.2 Experimental Problems

By comparing the IMU and spirometer signals presented in the figures shown in Appendix A, it is found that the IMU signals with subject 01, 04 and 05 show some unrecognisable segments during some of the experiments, while the IMU signals with subject 02 and 03 show a generally good result. The unacceptable data sets are considered as experimental problems, and they are summarised as follows in terms of each subject. These experimental problems are thought to be mainly caused by

Sub.	Exp.	Time [s]	number of QB	number of C	number of DB	number of SP
01	i	72	7	/	/	/
	ii-1	225	11	13	7	7
	ii-2	219	13	8	8	6
	ii-3	214	13	13	11	11
	iii	139	/	/	/	12
02	i	62	21	/	/	/
	ii-1	204	20	19	12	17
	ii-2	204	27	19	12	16
	ii-3	218	21	20	13	24
	iii	123	/	/	/	39
03	i	62	9	/	/	/
	ii-1	214	13	16	4	16
	ii-2	226	11	12	4	18
	ii-3	244	11	14	4	16
	iii	123	/	/	/	30
04	i	65	6	/	/	/
	ii-1	302	15	12	5	9
	ii-2	272	11	10	4	9
	ii-3	246	11	10	4	7
	iii	126	/	/	/	14
05	i	93	10	/	/	/
	ii-1	208	11	19	5	10
	ii-2	214	7	13	5	10
	ii-3	212	13	14	9	13
	iii	123	/	/	/	22

Table 2.6: An overview of the experiment result. The last four columns list the total number of breathing patterns recorded in each experiment. The breathing numbers were counted by counting the number of inspirations of the spirometer signal.

the loose attachment of the IMU device at the abdomen. This is discussed in Section 2.4 later in this chapter.

Subject 01 The signals acquired with this subject are shown in Figure A.1–A.5. As the first experimental subject, signals from the first two recordings (data sets i and ii-1) did not clearly represent each breathing cycle. In experiment part ii-2, the IMU signals were clearer, and could be related to the spirometer signals.

- part i: there were some expiratory peaks that could have corresponded to the spirometer counterparts, but the overall signal was unrecognisable concerning the inspiratory and expiratory phases.

- part ii-1: the QB signals at the beginning and in the middle were unrecognisable. The seven cycles of DB were recognisable and corresponded to the spirometer counterpart. Signals during C could also be clearly recognised, while the signals during speaking did not show some of the inspiratory peaks.
- part ii-2: the IMU signal during 120-140s showed similar amplitudes to those of the C pattern while the spirometer signal showed similar amplitudes to those of the QB pattern. Other IMU signals were clear and corresponded to the spirometer counterpart.

Subject 02 The signals acquired with this subject are shown in Figure A.6–A.10. Most of the IMU signals with this subject could accurately represent each breathing cycle of different breathing activities. A noticeable issue with the IMU signals was that there were some offset remaining. Meanwhile, it is found that the median lines of the original IMU signal (B_{row}^{IMU}) generally showed a curve shape. It was different from the median lines of the IMU signal with subject 01, which were generally straight. The IMU device fell off at the end of the experiment part ii-1. This led to the big trough of the IMU signal, while the spirometer signal looked normal.

- part ii-1: the QB signal during 120-140s and the SC signal during 170-200s (when the IMU fell off) do not represent their patterns. Other patterns can be related to their spirometer counterparts.
- part ii-2: the QB signal during 90-100s and SP signal during 140-150s have remaining offsets. Their onsets of both breathing phases were recognisable and corresponded to the spirometer signal.
- part ii-3: the QB signal during 20-30s and 90-110s have remaining offsets.
- part iii: Inspiratory peaks of the IMU signal can be related to those of the spirometer signal, while there are remaining offsets through the whole segment.

Subject 03 The signals acquired with this subject are shown in Figure A.11–A.15. The IMU signals with this subject represented the onsets of both breathing phases accurately compared to the spirometer signals. The amplitudes of the IMU signal during DB and C activities were not as distinctively higher than those of the QB signals as those of the spirometer signals. Moreover, there was one ripple in every IMU inspiratory phase during DB, while the spirometer signals were smooth. The experiment ii-2 and iii-3 were split because the spirometer device was turned off automatically during experiment. The signals of the split parts were combined afterwards. The time index of the splitting position was around 102s in ii-2 and 155s in ii-3.

Subject 04 The signals acquired with this subject are shown in Figure A.16–A.20. Due to an experimental mis-manipulation, the sample frequency of the IMU recording was set as 50Hz when

it should be 10Hz. The data was resampled to 10Hz for the processing. It was found that the IMU signals were mostly unrecognisable, except for the DB and C signals.

Subject 05 The signals acquired with this subject are shown in Figure A.21–A.25. Most onsets of both breathing phases of the IMU signal were recognisable compared with those of the spirometer signal. The amplitudes of the IMU signal during DB activities were lower and more irregular than those of the spirometer signals. Due to the spirometer failure, the data recorded in part ii-1 was split at around 142s and combined afterwards.

- part i: Although the inspiratory and expiratory peaks could be related to the spirometer signal, the IMU signal did not have distinctive transitions in terms of inspiration and expiration.
- part ii-1: Apart from the signal noise, the onsets of both respiratory phases were recognisable and corresponded to the spirometer counterpart except for the speaking pattern. The IMU signal during DB activities during 50-100s had decreased amplitudes, while the spirometer signals showed stable amplitudes.
- part ii-2: The amplitudes of the IMU signals during DB activity were not distinctively higher than those of the signals during QB activity. On the contrary, the spirometer signal showed distinctively higher DB amplitudes than the QB ones.
- part ii-3: The IMU signal during the DB activity at the end showed irregular and low amplitudes, while the spirometer signal showed stable ones.
- part iii: The IMU signal was not distinguishable in terms of amplitude.

A summary of the experimental problems of the recorded data is shown in Table 2.7. Due to the experimental problems found from the recordings, only the acceptable data sets (shown in the table) were used for the analysis of phase-shift and amplitude of the signals from both sensors. Some of the unacceptable data sets were used for the analysis of the frequency characteristics of the signal. They are indicated in Table 2.7.

Sub.	Exp.	Detection of breathing onsets	Amplitude of DB and C	Used for analysis
01	i	bad	/	NO
	ii-1	medium	medium	frequency only
	ii-2	good	good	YES
	ii-3	good	good	YES
	iii	good	/	frequency only
02	i	good	/	YES
	ii-1	medium	good	YES
	ii-2	good (offset)	good	YES
	ii-3	good (offset)	good	YES
	iii	medium (offset)	/	frequency only
03	i	good	good	YES
	ii-1	good	medium	YES
	ii-2	good	good	YES
	ii-3	good	medium	YES
	iii	good	/	frequency only
04	i	medium	/	frequency only
	ii-1	bad	C medium (DB good)	frequency only
	ii-2	bad	C medium (DB good)	NO
	ii-3	bad	C medium (DB good)	NO
	iii	bad	/	frequency only
05	i	bad	/	frequency only
	ii-1	medium	medium	NO
	ii-2	good	medium	YES
	ii-3	good	medium	YES
	iii	medium	/	frequency only

Table 2.7: A summary of the experimental problems of the recorded data. Refer to the details of the experimental problems with the IMU recordings with 5 subject Section 2.3.2. The accuracy of the IMU signal to represent onsets of both breathing phases and forced breathing activities (C and DB) are evaluated as “good”, “medium”, and “bad”. All the data sets recorded from the experiments are shown in Appendix A (from Figure A.1 to A.25). “Good” indicates that most of the IMU data corresponded to the spirometer data. The experimental data is marked as “medium” when there were some segments of unacceptable signals. “Bad” signals were totally unacceptable IMU signals. The data set was considered acceptable for the analysis of phase-shift and amplitude when it was at least evaluated as good once. The data sets which were evaluated as “frequency only” were only used for the frequency domain analysis discussed in Section 2.3.4.

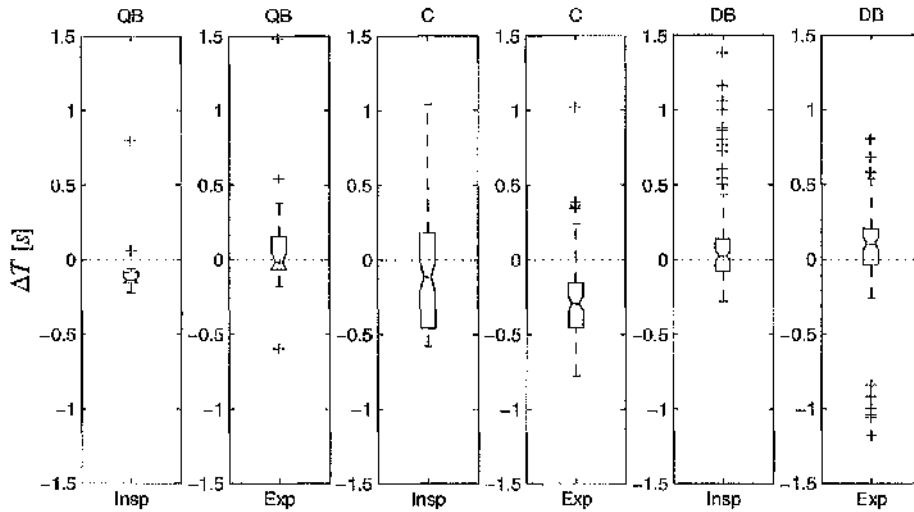


Figure 2.26: Box plots of the phase-shifts during different breathing activities and respiratory phases with all the subjects. Note that there are some recordings which are not included in this analysis due to the experimental problems.

2.3.3 Detection of Onset of Expiration and Inspiration

The phase-shifts between the signals from the two sensors were analysed during different breathing activities and different respiratory phases. The data sets with all subjects were analysed together for a group study. In addition, the recordings with each subject were analysed separately for case studies.

A. Group Results

The box plots of the group result are shown in Figure 2.26. It should be noted that the QB data consists of the recordings part i with subject 02 and 03, and the C and DB data consist of the recordings part ii-2,3 with subject 01, 05 and part ii-1,2,3 with subject 02 and 03. The negative phase-shift indicates that the IMU signal preceeded the spirometer signal, and vice versa. The group result showed that all the IQR (acquired by subtracting the lower quartile from the upper quartile, as shown in Figure 2.24) of all the box plots were within the interval $[-0.5 \ 0.5]$ s. Box plots of the QB signals had the smallest phase-shift ranges while the box plots of the C signal had the largest. Most of the boxes of the phase-shift crossed the zero line, except for the inspiratory sets during QB pattern and the expiratory sets during C pattern. They lay in the negative ranges.

Quiet Breathing The boxes of the QB activity during inspiration and expiration presented in the figure show small values and ranges. Medians of the phase-shifts were both negative, while the spread of the expiratory phase-shifts was approximately symmetrical at zero and the box of the inspiratory

phase-shifts was within the range of $[-0.5, 0]$ s. The largest outlier in the inspiratory data sets was around 0.8 s, while there was a 1.5 s outlier in the expiratory data sets. There were a total of 5 outliers spread within the interval $[-1, 1.5]$ s in the QB data sets.

Cough The boxes of the phase-shifts during the cough activities are the largest among the three breathing patterns. The medians of both data sets during the inspiratory and expiratory phases were negative. While the range of the phase-shift during the inspiratory phase was within $[-1, 1]$ s, most of the phase-shifts during the expiratory phase lay within the interval of $[-0.5, 0]$ s. There was no outlier in the inspiratory data sets, while the largest outlier in the expiratory was at around 1 s. Most of the outliers in expiratory phases were due to the data sets with subject 05. This can be seen from the case studies described later.

Deep Breathing The range of the phase-shifts during both respiratory phases were approximately symmetrical at zero. Both boxes lie within the interval $[-0.5, 0.5]$ s. There were a large number of outliers in the inspiratory data sets within the interval $[0.5, 1.5]$ s, which was due to the data sets with subject 05. In addition, outliers in the expiratory data sets around -1 s were due to the data sets with subject 03. They can be seen from the case studies described later.

B. Case Studies

Due to some abnormal outliers in the box plots of the results of the group study, case studies were carried out among individual subjects. The case studies among the data sets from subject 01, 02, and 03 confirmed that the phase-shift between the two signals during expiratory phases of cough activities tended to be negative. This indicated that during the expiratory phase of cough activities, the IMU signal preceded the spirometer signal. The phase-shifts with all the data sets with subject 05 generally tended to be positive.

Subject 01

The data sets ii-2 and ii-3 with subject 01 were analysed. Thus no phase-shift analysis during QB activity is presented. The box plot results are shown in Figure 2.27.

The figures show that the phase-shifts during inspirations of the C and DB patterns with subject 01 were approximately symmetrical at the zero line and within the interval $[-0.3, 0.3]$ s. There was only one outlier at around 0.4 s in the inspiratory box plots. While the spread of the phase-shifts during the expiration of the C pattern lay within $[-0.25, 0]$ s, the spread of the phase-shifts during the expiration of the DB pattern lay within $[0, 0.5]$ s. The largest outlier of the four box plots with subject 01 was at around 1 s (from the expiratory phase-shift during the C pattern).

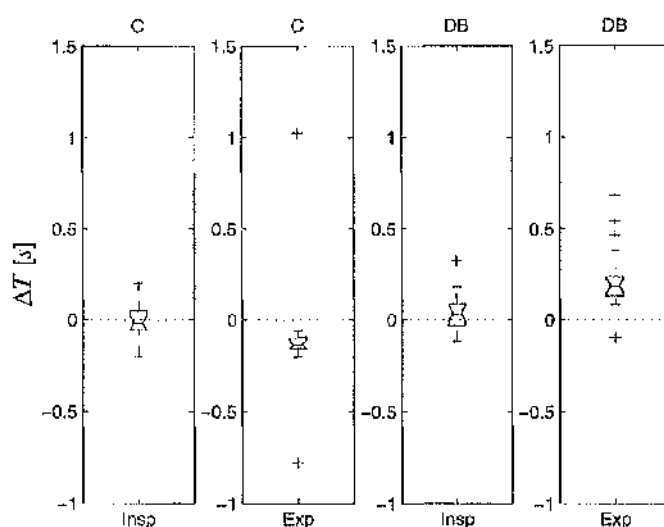


Figure 2.27: Box plots of the phase-shifts during the inspiratory and expiratory phases of C and DB activities with subject 01. The acceptable data sets with subject 01 were ii-2 and ii-3, therefore no phase-shift during QB activity was analysed.

Subject 02

The data sets which were analysed for subject 02 were i, ii-1, ii-2 and ii-3. The box plot result are shown in Figure 2.28.

The phase-shifts with subject 02 had the smallest range among all the data sets with the 4 subjects that were analysed. Including the outliers, the phase-shifts during all the analysed data sets with subject 02 were within the interval $[-1 \ 1]$ s. The box of the expiratory data set during DB pattern was symmetrical at the zero line and within $[-0.2 \ 0.2]$ s, while all the other boxes lied in negative intervals. The intervals of the QB pattern (both respiratory phases) and the DB pattern during inspiratory phase were around $[-0.2 \ 0]$ s, while the intervals of the C pattern (both respiratory phases) were around $[-0.6 \ -0.4]$ s.

Subject 03

The data sets which were analysed for subject 03 are i, ii-1, ii-2 and ii-3. The box plot results are shown in Figure 2.29.

The phase-shifts during expirations of the DB pattern had a large range from -1 s to 0.5 s. Other ranges of the phase-shifts with subject 03 were within the interval $[-0.5 \ 0.5]$ s. The phase-shifts during expirations of the C activity were all negative while the phase-shifts during expirations of the QB activity were all positive. Other boxes all crossed the zero-line.

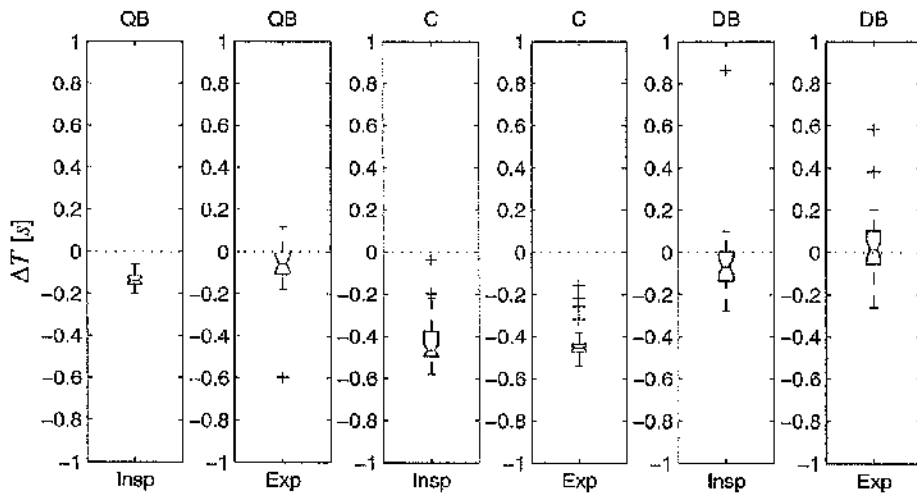


Figure 2.28: Box plots of the phase-shifts during different breathing activities and respiratory phases with subject 02. The data sets which were analysed are i, ii-1, ii-2 and ii-3.

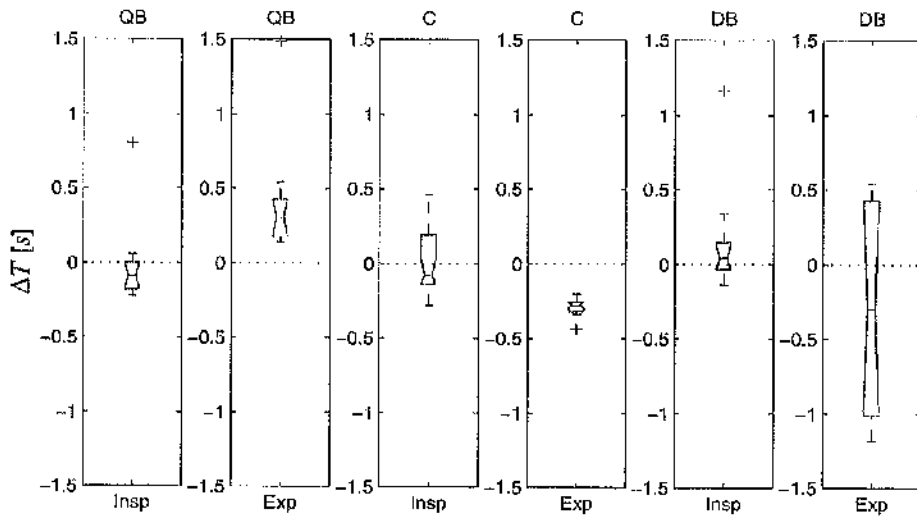


Figure 2.29: Box plots of the phase-shifts during different breathing activities and respiratory phases with subject 03. The data sets which were analysed are i, ii-1, ii-2 and ii-3.

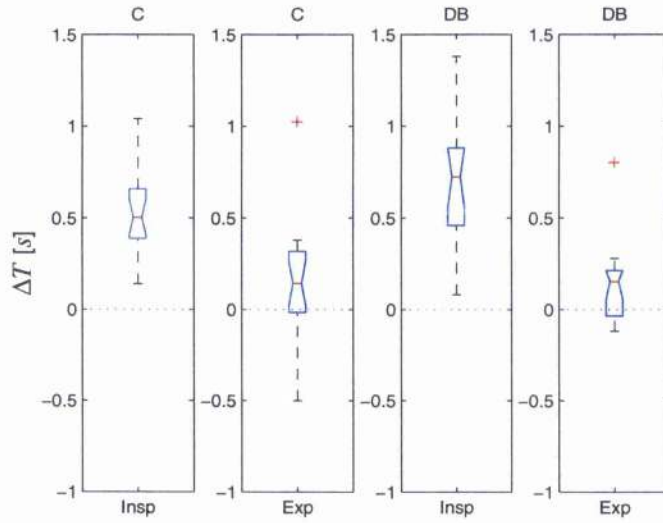


Figure 2.30: Box plots of the phase-shifts during different breathing activities and respiratory phases with subject 05. The acceptable data sets with subject 05 are ii-2 and ii-3, therefore no phase-shift during QB activity is analysed.

Subject 05

The data sets which were analysed for subject 05 were ii-2 and ii-3. Therefore no phase-shift data during the QB activity is presented. The box plot results are shown in Figure 2.30.

The figures show that most of the phase-shifts with subject 05 were positive and within the interval $[0 \ 1.5]s$. The median of the phase-shift data set during inspirations of the DB activity was as high as $0.7s$, and this box plot had a large range of distribution with the upper limit at around $1.5s$. This abnormal distribution resulted in the large outliers in the group box plot.

2.3.4 Differentiation Between Different Breathing Patterns

The ability of the breathing signals acquired from the IMU device to represent different breathing patterns was evaluated in both time and frequency domain. In the time domain, the peak values during different breathing patterns were compared. In the frequency domain, the FFT spectra were used to analyse different breathing patterns.

There were two recorded breathing patterns which were not analysed by the methods described above. They were the single cough (SC) and speaking (SP) patterns. The SC pattern was included mainly to see the reaction of the device to rapid and random changes of different breathing patterns. The magnitude change of the IMU signal could verify the ability of the IMU to react to rapid and random changes of the breathing patterns. The SP patterns were not particularly analysed, as the amplitude of the sensor signal during this activity changed in a complex way.

A. Time Domain Analysis to the Signals

In the time domain, in order to investigate the ability of the IMU to differentiate between breathing patterns, the expiratory (positive) and inspiratory (negative) peak values of C and DB patterns were evaluated by a box plot. The distribution of the peak values during QB pattern was also analysed to compare the two sets of signals from both devices. The analysis for peak values was carried out with all the acceptable data sets. No case studies were carried out as the peak values were easy to observe from the signal figures shown in the appendix.

The box plots are therefore shown with QB, C and DB signals separately. Acceptable data sets with different subjects were combined in terms of breathing patterns. With each pattern, the boxes representing the IMU and spirometer signals are shown in a group.

The group results show that the spreads of the magnitudes of the spirometer and IMU signals are generally within the same range. It could also be found that the IQRs of the IMU signal were larger than the spirometer ones, indicating that the IMU was more sensitive to movement.

1. Peak Values with the Quiet Breathing Pattern

The box plots of the data sets of the peak values with the QB signals are shown in Figure 2.31

The figures show that the medians of the peak values with the QB signals were around ± 1 during inspiration and expiration. The range of the distributions of these data sets were generally as small as 0.5. The positions of the two boxes of the two sensors are similar. One large outlier (-2) existed in the data sets of the IMU signal during the QB inspirations.

2. Peak Values with the Cough Pattern

The box plots of the data sets of the peak values with the C signals are shown in Figure 2.32

The figures show that the boxes of the peak values with the cough pattern lied around ± 5 during inspiration and expiration. The difference between the ranges of both boxes with the two devices

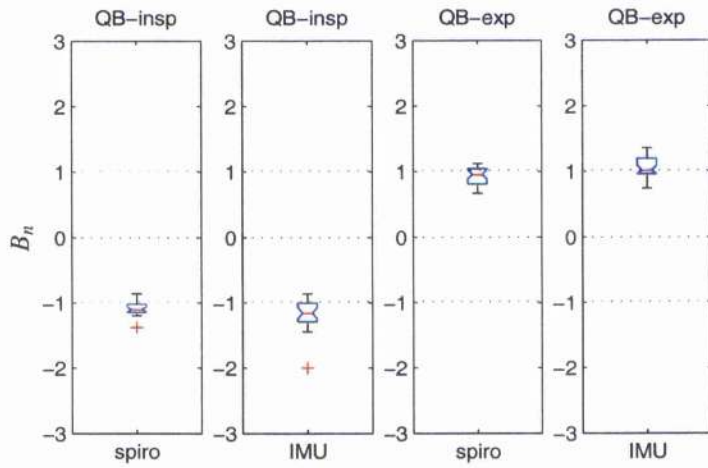


Figure 2.31: Box plots of the data sets of the peak values with the QB signals. The data set used consists of the data set i with subject 02 and 03. The dashed lines indicate normalised value of ± 1 and 0.

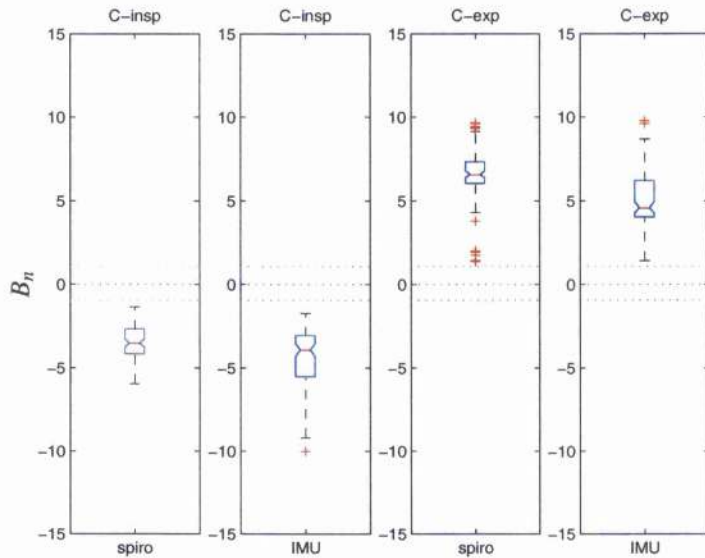


Figure 2.32: Box plots of the data sets of the peak values with the C signals. The data set used consists of the data set ii-1, ii-2, ii-3 with subject 02 and 03, and ii-2, ii-3 with subject 01 and 05. The dashed lines indicate normalised value of ± 1 and 0.

during inspiration was small. In the group of expiratory peaks, the lower outlier of the spirometer signal and the minimum value of the IMU signal were as low as 1, while the upper outliers of the

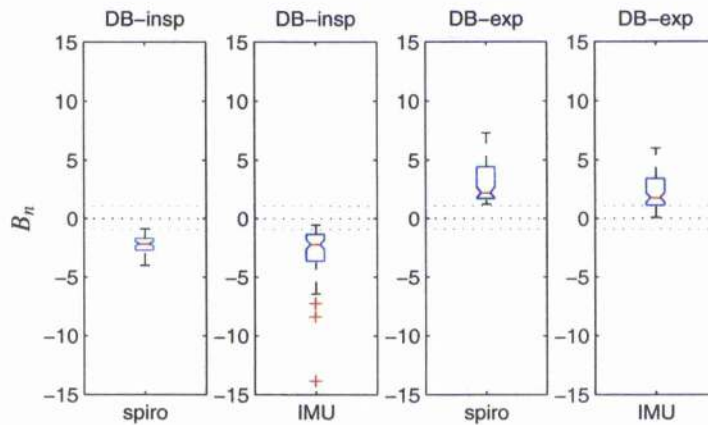


Figure 2.33: Box plots of the data sets of the peak values with the DB signals. The data set used consists of the data set ii-1, ii-2, ii-3 with subject 02 and 03, and ii-2, ii-3 with subject 01 and 05. The dashed lines indicate normalised value of ± 1 and 0.

spirometer and IMU signal are as high as 10. Apart from the outliers, the boxes of the signals from both sensors shared similar ranges. It can be seen that the boxes of the IMU data sets are slightly larger than the boxes of the spirometer data sets.

3. Peak Values with the Deep Breathing Pattern

The box plots of the data sets of the peak values with the DB signals are shown in Figure 2.33

The figures show that the boxes in each group have similar ranges. However the maximum of the IMU signal during inspiration and the minimum of the IMU signal during expiration fall in the interval of $[-1 \ 0]$ and $[0 \ 1]$ (indicating lower peak values than the QB patterns). It can be found that the spirometer maximum during inspiration and minimum during expiration were also as low as -1 and 1 . Apart from this phenomenon, it can be seen that the peak values during the DB activity were not as high as the C peaks.

B. Frequency Domain Analysis of the Signals

To evaluate the frequency characteristics of the signals from both devices, frequency spectra of specified breathing patterns were calculated. The summation (area) of the magnitude of the frequency spectrum was also calculated as this was one of the frequency characteristics in the detection system discussed in Chapter 3. Figure 2.34 shows a sample frequency spectrum analysis of the cough pattern from subject 01. Table 2.8 lists the results from frequency spectrum and area analysis for each subject. It was thought that, although the time domain of the signal was not good, it was possible that the frequency domain of the signal could show some accurate breathing information, such as the FFT area.

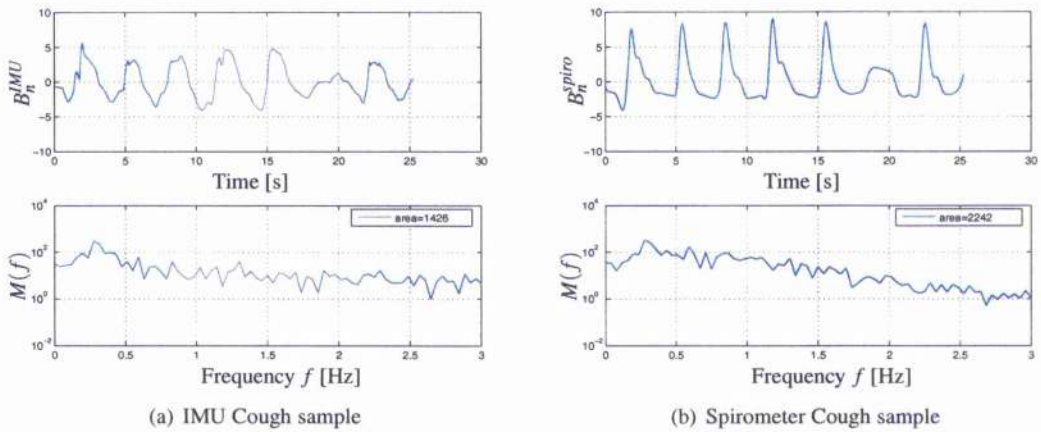


Figure 2.34: Frequency spectra and areas of one series of the cough sample from subject 01. $M(f)$ denotes the magnitude of the FFT spectrum.

		Subject 01		Subject 02		Subject 03		Subject 04		Subject 05	
		IMU	spiro								
QB	$\int M(f)df$	692	923	863	932	1082	1092	900	732	2032	1585
	T [s]	60		60		50		50		80	
C	$\int M(f)df$	1426	2242	4565	3284	2472	2317	2347	2196	2831	2183
	T [s]	25		27		27		40		31	
DB	$\int M(f)df$	1956	2509	906	1206	1691	1215	4259	1332	2944	1557
	T [s]	30		31		40		47		48	
SP	$\int M(f)df$	2603	1935	1988	2782	3564	2355	2152	2461	2182	1389
	T [s]	120		120		110		110		110	

Table 2.8: Summary of the FFT frequency spectrum analysis of different breathing pattern samples. $M(f)$ denotes the magnitude of the FFT spectrum, and T denotes the period of the signal which is analysed. A sample view of the cough pattern from subject 01 is shown in Figure 2.34. Note that pattern SP include both the reading and talking pattern.

In the results for subject 01-04, the FFT areas from both sensors of the QB breathing patterns were distinctively smaller than other patterns. At the same time the relationship between the areas of C, DB and SP patterns varies sharply both for the IMU and spirometer signal. In the spectra areas of the IMU signal for subject 02, the areas during cough were much larger than DB and T patterns. For subject 01 and 03, the T pattern had the largest spectra areas. In case of subject 04 and 05, DB pattern had the largest spectra areas.

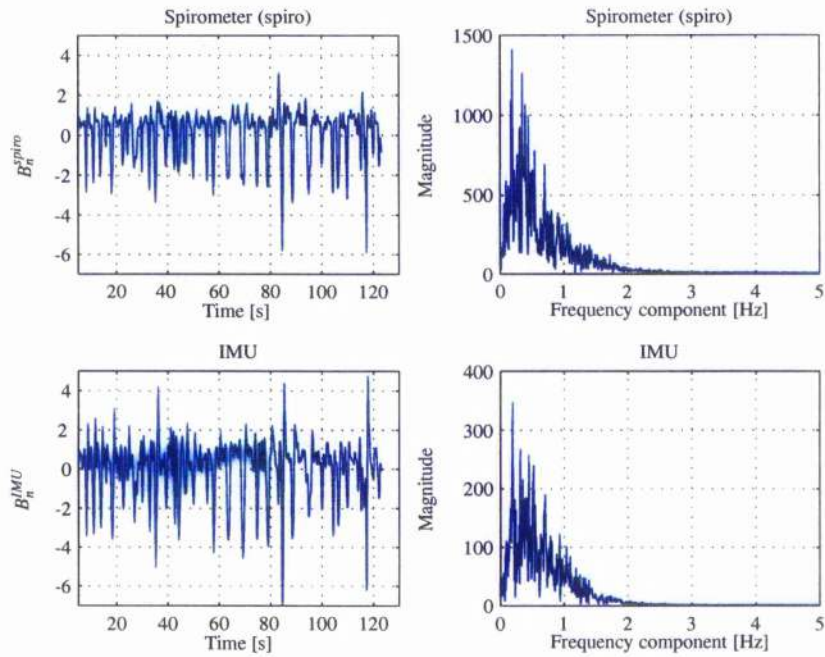


Figure 2.35: Speaking signals from both sensors in both time and frequency domain. Left plots show the signal in time domain. Right plots show their frequency spectra. This is from the experiment part iii of subject 03.

C. Single Cough Pattern

The single cough (SC) pattern was included in the part ii of the experiment mainly for testing the reaction of the sensor to abrupt breathing pattern change.

Most of the original signals from both sensors showed that the SC activities were mostly accurately presented. This confirmed that the IMU device was able to represent rapid pattern changes (from QB to C). Sample data recordings from both devices including the SC patterns can be found in Appendix A.

D. Speaking Pattern

Speaking patterns (include reading and talking) were not statistically analysed. One sample of the speaking patterns were shown in Figure 2.35 along with their frequency spectra. It can be seen that the signal B^{IMU} was similar to B^{spiro} with respect to time and frequency domain.

2.4 Discussion

2.4.1 Phase-shift between the Airflow at the Mouth and the Abdomen Movement

The plots of the group results presented in Figure 2.26 show that most of the phase-shifts (ΔT) of signals from the two devices were within $[-0.5 \ 0.5]$ s. This indicates that when the breathing signal was used to determine the onset of stimulation, the phase-shift of the two devices could be limited to the range $[-0.5 \ 0.5]$ s.

The sign of the phase-shift indicates which signal precedes the other one. There were certain causalities between the movement of the abdomen and the airflow at the mouth. This causality exists in certain breathing activities and certain respiratory phases. There were also breathing situations where no causality between the two signals existed. In this case, the sign of the phase-shift was beyond prediction.

Physiological Analysis of the Causality between the Movement of the Abdomen and the Airflow at the Mouth with Neurological Intact People

Positive phase-shift ΔT indicates that signal B^{spiro} precedes signal B^{IMU} , and vice versa. Which signal precedes the other depends mainly on the causality of the movement of the abdomen (d) and the airflow at the mouth during certain breathing patterns.

Figure 2.36 shows the causalities between the diaphragm, abdomen and the airflow at the mouth during different breathing situations. There is no causality between the airflow at the mouth and the movement of the abdomen during inspiration and quiet expiration, as both of them are the result of the diaphragm movement. When forced expiration (expiration of the C and DB activities) occurs, the contraction of the abdominal muscles will lead to the exhalation of the airflow at the mouth. Thus, during expirations of cough and deep breathing, the movement of the abdomen causes the airflow at the mouth. The physiological explanation of this causality is presented in the following paragraphs.

As discussed in Section 1.1, during inspiration of neurologically intact people, diaphragm is the primary muscle [2]. The diaphragm contracts from a flat sheet to a dome-shape sheet during inspiration. On the one hand, the volume of the thorax is increased by this contraction, and then the intra-thoracic pressure is decreased, thus the air is sucked in. On the other hand, the contraction of the diaphragm increases the intra-abdomen pressure, hence the volume of the abdomen is increased. Therefore, B^{spiro} and B^{IMU} are both the result of diaphragm movements during inspiration – they don't have causalities.

During quiet expiration of neurologically intact people, the primary expiratory muscles, the abdominal muscles, are not usually used, i.e. this expiration process is passive. The recoils of the diaphragm and the thoracic cage pull back the diaphragm, hence reverse the inspiration process. In this case, there is no causalities between the movement of the abdomen and the airflow at the mouth.

The expirations of forced breathing activities such as cough and deep breathing are active processes. Abdominal muscles are primary expiratory muscles. They pull the abdomen inwards directly,

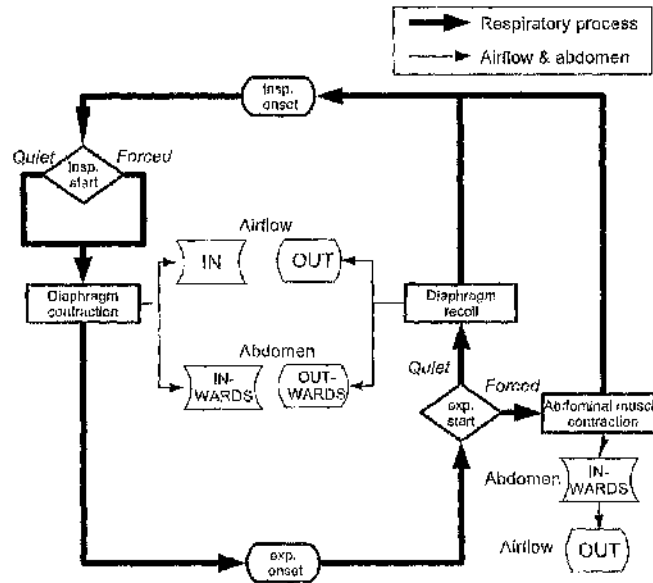


Figure 2.36: A flowchart of the respiratory cycle of neurologically intact people. During inspiration and quiet expiration, airflow at the mouth (signal B^{spiro}) and the movement of abdomen (signal B^{IMU}) are both result of the diaphragm movement. During forced expiration (cough and DB), the airflow is the result of abdomen movement.

thus the diaphragm upwards, reversing the inspiration process. During these breathing activities, the movement of the abdomen causes the airflow at the mouth. The IMU signal therefore should precede the spirometer signal (phase-shift ΔT negative).

Analysis of the Phase-shift Results

The group results and case results (except with subject 05) of the phase-shift analysis showed that the phase-shifts during expiratory phases of the cough activities were mainly negative. This result corresponds with the conclusion that the abdominal movement caused the airflow at the mouth. The result with subject 05 did not correspond with this conclusion. But it was found that most of the phase-shifts with this subject were positive (Figure 2.30). The result of the phase-shift with subject 05 was therefore considered an abnormal result.

The group results of the phase-shift during the expiratory phase of DB activities showed an approximately symmetrical distribution at the zero phase-shift. The case results with each subject confirm that the phase-shift during this activity did not always lie in a negative interval as expected. A possible reason for this result is that the deep breathing activity was not as strong as the cough activity. Thus during the DB activities, the abdominal muscles may not have been used actively. During the experiment, the subjects were asked to take a breath as deep as possible, without specific requirement for a strong exhalation. It was observed during the experiments that in the expiratory phases of deep breathing, subjects tended to exhale in a relaxing way. On the other hand, during the expiratory phases

of coughing, strong abdominal contraction tended to be necessary. One evidence of this explanation is that, signals during deep breathing were generally smaller than the signals during the coughing, as shown in the original signals presented in the figures in the appendix. Another possible cause was that the subjects may have used the intercostal muscles during DB. In this cause, the air flow at the mouth was directly caused by the contraction of the intercostal muscles, instead of the backward movement of the diaphragm caused by the contraction of the abdominal muscles. Therefore, the phase-shift between the air flow at the mouth and the abdominal movement would be decreased.

During the breathing situations where no causality between the abdominal movement and the air-flow at the mouth existed, the results from both group study and case studies show an uncertain distribution in terms of the sign of the phase-shifts. This uncertainty was expected.

Analysis of the Abnormal Results

There are four abnormal results found in the box plots of the phase-shifts. They are: i) one large outlier (at around 1.5s) in the box plot of the expiratory phase during QB activity; ii) large spread of outlier (from 0.5s to 1.5s) in the box plot of the inspiratory phase during DB activity; iii) large outliers (at around -1s) in the box plot of the expiratory phase during DB activity; iv) generally positive phase-shift values in the data sets with subject 05. The first three abnormal result can be found in the group results shown in Figure 2.26. The fourth one can be found in the case result with subject 05 shown in Figure 2.30. By analysing both the group and case results, it was found that all these four abnormal results were only related to certain data sets with subject 03 (problem i and iii) and 05 (problem ii and iv). The result with subject 01 and 02 were generally acceptable and expected.

A. Abnormal Results with Subject 03

One abnormal result with subject 03 was that there was one large phase-shift in the data set i with this subject. The signals from both devices of this data set are shown in Figure 2.37.

The large phase-shift occurred at the last breathing cycle recorded with this experiment, as marked in the figure. The positions of the two expiratory onsets marked by the round markers show that this phase-shift was a big delay of the IMU signal. It can be seen that the signals of this last breathing cycle were distinctively larger and longer than the previous ones. Moreover, there were unusual signal changes during the last inspiration, while the previous ones were all smooth. In Figure A.11 in the appendix, it can be seen that the median line of the last breathing cycle was distinctively lower than the previous ones. Therefore, one possible cause of the delay of the IMU signal is that, during this last breathing cycle, the subject slightly moved the body as he took a stronger breath. The body movement moves the median of the IMU signal and introduces a delay to the IMU signal.

Another abnormal result with subject 03 was that the phase-shifts during expiration of DB activities have a large spread from -1s to 0.5s. The DB signals from both devices are shown in Figure 2.38. Note that this series signal of deep breathing activity consists of the DB segments of data sets ii-1,

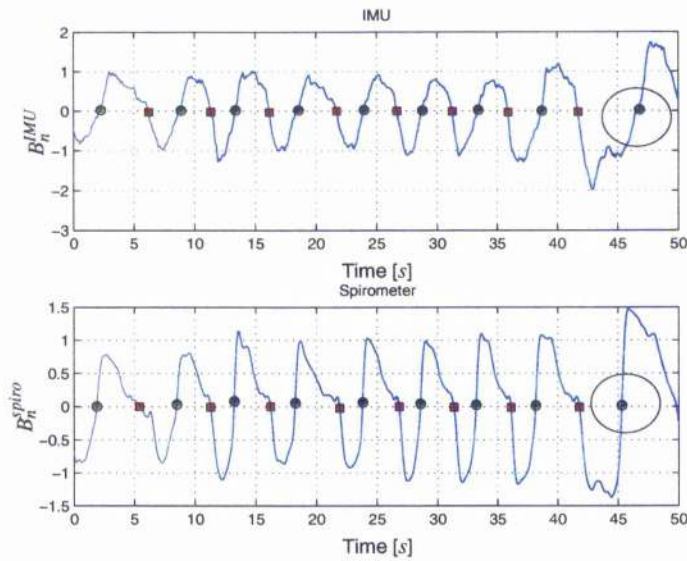


Figure 2.37: The abnormal large phase-shift between the signals from the IMU and spirometer device with the data set i with subject 03. The abnormal expiratory onsets with both signals are marked in the figures.

ii-2 and ii-3 with subject 03.

The figure shows that there was a small oscillation during most of the onsets of expiration (marked by round markers). The onset positions of these expiratory phases were therefore selected manually. These oscillations were the causes of the large spread of the phase-shifts. The signals with subject 03 presented in Figure A.12–A.14 in the appendix show that there were no such oscillations during the cough phases. It is therefore thought that this subject may habitually hold the breath for a short time after he takes a deep breath. The breath holding allows small abdomen movement, which causes the oscillations. When in the coughing activities, the signal shows that the inhalation was stronger and quicker, leading to instant exhalations. This breath holding process was thought to cause this abnormal result.

B. Abnormal Results with Subject 05

The main abnormal problems found in the data sets with subject 05 were that most of the phase-shifts with this subject had large positive values (IMU signal lagged behind the spirometer signal). The large phase-shift values during the expiration of deep breathing activities caused the abnormal issue ii. The signals during the DB activities with this subject are shown in Figure 2.39.

It can be seen from Figure 2.39 and the figures of the original signals with subject 05 in appendix (Figure A.21–A.25) that the IMU signals were “flatter” than the spirometer signals. Also during some continuous breathing activities, the IMU signal was not as stable as the spirometer signals. The weak

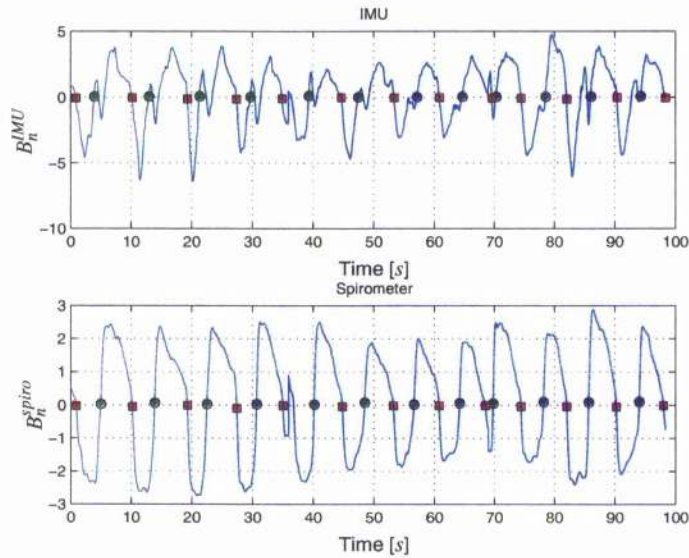


Figure 2.38: The abnormal spread of phase-shift between the signals from the IMU and spirometer device with the DB signals with subject 03. Note that this series signal of deep breathing activity consists of the DB segments of data sets ii-1, ii-2 and ii-3 with subject 03. It can be seen that most of the expiratory onsets of the IMU signal have small oscillations.

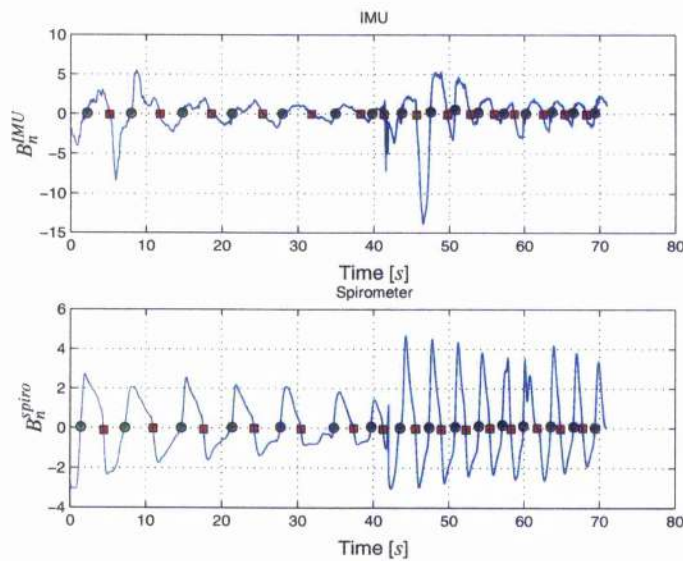


Figure 2.39: Signals from both devices during the DB activities with subject 05. The onsets of both inspiratory and expiratory phases of the IMU signal generally lagged behind those of the spirometer signal.

signals recorded from the IMU could be contributed to the attachment of the IMU at the abdomen. The belt to which the IMU was attached may not have been worn tightly enough by the subject, so that the detection of the movement of the abdomen was not sensitive. This loose attachment of the IMU device to the abdomen could have resulted in the delay of the IMU signal, i.e. positive phase-shifts. Another possible cause of the positive phase-shift was that the subject may have habitually used intercostal muscles during the expirations. When the intercostal muscles dominate the breathing activity, the movement of the abdomen could become less active and strong. Thus, the detection of the movement of the abdomen weakens and have delays.

Phase-shift of the Signals with Tetraplegia

The relationship between the flow at the mouth and the movement of the abdomen could be more complicated in tetraplegic individuals, due to the different damage level to the diaphragm. For instance, for tetraplegia individuals who have partial or complete paralysis in abdominal muscles, when the expiration of forced breathing activity (C and DB) takes place, the abdomen is pulled inwards passively by the diaphragm recoil instead of actively muscle contraction. The level of phase-shift in tetraplegic cases needs to be evaluated.

2.4.2 Detection of Different Breathing Patterns

A. Signal Characteristics in Time Domain

The results of the analyses of the amplitudes of QB, C and DB signals (Figure 2.31–2.33) showed that the IMU sensor had similar ability to differentiate different breathing activities by detecting different signal amplitudes to the spirometer sensor.

The IQRs of the magnitudes of the signals during C and DB activities were higher than the QB ones. This can be explained by the fact that during C and DB activities, the body movements were stronger.

The amplitudes of the DB signals from both devices were lower than those of the C signals. This may be because that subjects breathed less strongly during DB activities than the C activities. This explanation can also be verified by the discussion about the uncertain sign of the phase-shifts during expirations of the DB activities, presented in Section 2.4.1. The possible cause for the uncertain sign of the phase-shift during expirations of the DB activities is that the abdominal muscles were not actively used during the expiration.

During the same breathing activities, the spread of the amplitude of the IMU signals was larger than the spread of the spirometer signals. This indicated that the IMU device was more sensitive to the movement than the spirometer.

The box plots of the amplitudes during DB activities (Figure 2.33) showed some unexpected results. The amplitudes of the inspiratory and expiratory IMU signals both overlapped with the interval $[-1, 1]$, which were the amplitude range of QB. The cause of this unexpected result can be contributed to

the IMU signals with subject 05 (Figure A.22–A.24). As discussed in the previous section about the phase-shift analysis, the IMU signals recorded with subject 05 were “jittery” than the spirometer ones. This was thought to be contributed to the loose attachment of the IMU to the abdomen. The loose attachment also made the IMU recording inaccurate in terms of amplitudes, leading to the unexpected low amplitudes during DB activities.

B. Signal Characteristics in Frequency Domain

In the frequency domain, as shown in Table 2.8, both spirometer and IMU signals had markedly distinctive FFT area with QB signals (except for subject 05). The FFT areas with QB signals were smaller than the other FFT areas with C, DB and SP activities. This is because that the flow-rate during QB activity was lower than during the other activities such as DB and C. The fact that such difference can be represented in the FFT areas of signals from both sensors demonstrates the ability of both sensors to represent breathing signals with correct frequency.

The unexpected high frequency area during QB activity with subject 05 could be attributed to the loose attachment of the IMU device and the sensitivity of the sensor. When the IMU was loosely attached at the abdomen, the movement of the abdomen could have been detected by the IMU sensor less accurately. On the other hand, the loosely attached belt at the abdomen could lead to unwanted vibration of the IMU sensor. This small vibration could be detected by the IMU sensor, leading to the high-frequency noise. Such high-frequency noise could be seen through all the IMU signals shown in the appendix (Figure A.21–A.25).

2.5 Issues and Further Work

2.5.1 Attachment of the IMU to the Abdomen

It was found from analysing the IMU signal in both time domain (Section 2.4.1) and frequency domain (Section 2.4.2) that the attachment of the IMU device is important to acquire correct and accurate breathing signals from the movement of the abdomen.

The IMU signals during the QB activity with subject 01 (Figure A.1–A.5) and 04 (Figure A.16–A.20) were found to be much less recognisable than the signals during DB and C activities. This phenomenon was particularly obvious with IMU signals with subject 04. It can be found that although most of the IMU signals with subject 04 during QB activity were noisy and unrecognisable, the IMU signals during DB activity were as good as the spirometer ones. This phenomenon can be caused by the fact that the attachment of the IMU to the abdomen was not tightly fixed, the movements of the abdomen during QB were not accurately acquired by the IMU as the movements were not intense. When deep breathing occurs, the movements of the abdomen are more intense and stronger, which tends to be easier detected by the IMU.

Pre-experimental tests for the attachment of the IMU are therefore needed for future studies. Such

tests can be a recording with the breathing patterns from the experiment part ii. The attachment of the IMU will be adjusted until the IMU signal are as accurate and correct as the spirometer signals.

2.5.2 Additional Sensor to Detect the Chest Movement

It was discussed previously that one of the possible causes for the inaccurate recordings from the IMU is that the subject may use the intercostal muscles habitually. In this case, the movement of the chest wall could be stronger than the abdomen. It is therefore of interest to detect the movement of the chest as well as the abdomen.

The detection of the chest movement can be achieved by using another set of IMU and belt around the chest. Further experiments should be conducted with both the IMU devices around the abdomen and the chest at the same time. Analysing the strength and the phase-shift of the two signals may find certain breathing activities with certain subjects where breathing signals can be more accurately represented by the movement of the chest than the movement of the abdomen.

2.5.3 Additional Sensor to Eliminate Unwanted Body Movement

An obvious drawback of the detection of the movement of the abdomen by the IMU device is that the sensor detects every movement that it senses. This means that it detects the overall body movement as well as the abdominal movement. As a result, the experiments in this study require subjects to sit still during the recording, allowing only the abdominal movement during breathing activities. The unwanted body movement can lead to inaccuracy of the IMU signal. This can be seen in the IMU signal with subeject 02 shown in Figure A.8. At the end of this recording the IMU device fell off the belt, leading to incorrect recordings.

Using another sensor to detect the movement of the body is thought to be a way to eliminate the detection of unwanted body movements. When a "pure" body movement is recorded by another sensor, the "pure" movement of the abdomen can be obtained by subtracting the body movement signal from the abdomen signal. It is also of interest to demonstrate whether the combination of the detection of the movements of the chest and the abdomen can obtain the pure abdomen movement. The unwanted detection of the body movement are also presented by the shift in zero-line of some of the recordings.

2.5.4 Different Situations with Tetraplegic People

All the subjects with this study are neurologically intact people. The difference of the respiratory system between tetraplegic people and neurologically intact people needs to be considered.

It is important to ensure that the movement of abdomen of tetraplegia people can represent respiration. The situation can be more complicated in tetraplegia people due to different extent of damage to the respiratory system. When the respiratory accessory muscle, intercostal muscles, are paralysed, the rib cage may have paradoxical inward motion during inspiration [5], limiting the movement of

abdomen. Troyer has observed during active expiration [42] and cough process [40] in tetraplegic subjects, that there were negligible changes in abdominal dimension but marked and reproducible decreases in the dimension of the upper rib cage, because of the clavicular portion of the pectoralis major. Additional chest sensor is therefore considered to be important for tetraplegic people. Experiments with tetraplegic people and additional chest sensor are therefore desired to carry out.

2.6 Conclusions

Experiments with 5 neurologically intact people have been carried out to evaluate the ability of an IMU device attached at the abdomen to detect breathing signals. A spirometer is used as well to acquire breathing signals from the airflow at the mouth. This signal from the spirometer is used as reference to evaluate the signal from the IMU sensor.

It is found that the attachment of the IMU sensor at the abdomen can affect the accuracy of the signal acquired by it. Inaccurate recordings can be caused when the IMU device is attached at the abdomen loosely. Pre-experimental tests with the attachment are therefore thought to be needed for the future experiments.

The phase-shifts between the acceptable signals acquired by the IMU sensor and the spirometer are analysed. The results indicate that the good phase-shift between the two signals can be limited to the interval $[-0.5 \ 0.5]$ s. The negative phase-shifts during the expiratory phase of coughing activities correspond with the physiological fact that the abdominal muscle contraction causes the airflow at the mouth.

The amplitudes of breathing patterns of QB, DB and C of the signals from the IMU and spirometer are also analysed (with the acceptable signals). The IMU sensor can differentiate between different breathing activities with different signal amplitudes. The frequency analysis result which shows distinctive small FFT areas with QB activities also indicates the ability of the IMU sensor to detect different respiratory activities. This ability of the IMU sensor is found to be similar to that of the spirometer in both the time and frequency domain, except that the amplitudes detected by the IMU are more variable. This is thought to be caused by the fact that the IMU sensor is more sensitive to movements.

The IMU signals during the SC and SP activities presented in the figures shown in the appendix confirm that the IMU sensor can detect different respiratory activities. The IMU signals during SC activities show the sensor reaction to rapid change of respiratory activities (between QB and C). Compared with the corresponding spirometer signals, the IMU signals are also distinctive during the speaking activities.

The analyses above suggest that the IMU sensor can be considered to be a portable and convenient alternative to the spirometer sensors. Further work should involve experiments with tetraplegic subjects. In addition, additional sensors should be considered to analyse the movement of the chest wall and to eliminate the effects of the body movement.

3 The Algorithm of the FESAM Control System

Summary

This chapter introduces the automatic control system for FESAM. A basic control system is first introduced. Based on the basic control system, a multi-characteristic control system is developed to use multiple characteristics of the breathing signal to detect breathing patterns. The basic control system and the multi-characteristic control system are evaluated by analysing the data from the experiments discussed in Chapter 2.

3.1 Background and Introduction

No matter whether the breathing signal is acquired from the spirometer or IMU device, it is analysed by the control system for FESAM, as shown in Figure 3.1. The main tasks of the control system are to: i) detect the respiratory patterns in real-time; ii) detect the trigger points for different patterns (e.g. onset of the expiration during quiet breathing or when coughing); iii) generate corresponding stimulation signals for the electrical stimulator at the trigger point. The stimulation signal can control the stimulator when and how long the electrical stimulation will be generated. For FESAM, the electrical stimulation is needed to start at the beginning of the expiratory phase for quiet breathing and at the end of the inspiratory phase for coughing, and stop at the end of expiratory phases.

As shown in Figure 3.2, the period of signals for one detection cycle is from the previous expiration to current inspiration. Due to the limitation of analysing signals in real-time, the system analyses past signals.

A basic control system (BCS) is first developed to perform the tasks mentioned above. On base of BCS, a multi-characteristic control system (MCCS) is developed to enhance the detection of breathing

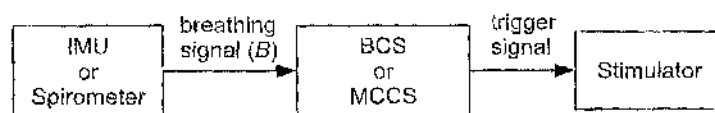


Figure 3.1: The overall structure of the control system for FESAM. The breathing signal acquired from the IMU or spirometer is analysed by the basic control system (BCS) or multi-characteristic control system (MCCS) to generate trigger signals for the stimulator.

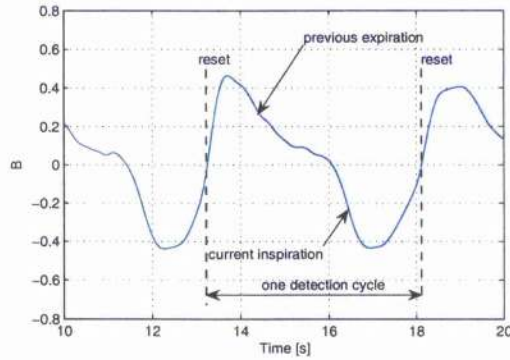


Figure 3.2: Illustration showing one detection cycle for the characteristic detection of the breathing signal. For the detection of the breathing pattern at the end of this detection cycle, the period from previous expiration and current inspiration is analysed.

patterns. Both systems are implemented in the Simulink (Mathworks, United States) environment [81]. The following sections introduce these two systems.

3.1.1 The Basic Control System (BCS)

A basic control system (BCS) was developed in previous studies [53]. This control system detects quiet breathing (QB), coughing (C) and speaking (SP) patterns by comparing some characteristics of the breathing signal with pre-set thresholds. C pattern was detected by analysing the inspiratory breathing signal values. QB pattern was detected by analysing the cross-correlation between the current breathing cycle and a QB cycle reference. The breathing activity will be detected as SP when both C and QB are negated.

The algorithm of the BCS is illustrated in Figure 3.3. The processed breathing signal B is analysed by two main detection blocks which detect QB and C patterns separately. If the C pattern is confirmed, a trigger signal for C pattern will be generated at the trigger point for stimulation. The trigger point for cough is usually before that for QB. As a result, the detection of cough has the priority over the detection of QB. The NOT block in the figure is therefore added to overwrite the QB trigger. When QB pattern is confirmed, the QB trigger is generated only when the C pattern is not confirmed at the trigger point. When neither C nor QB is registered, the control system will not generate any stimulation trigger. In the figure, the speaking pattern represents this case.

The details of the BCS are discussed in [53]. In the later content of this chapter, some of the algorithm of the BCS will be described when necessary.

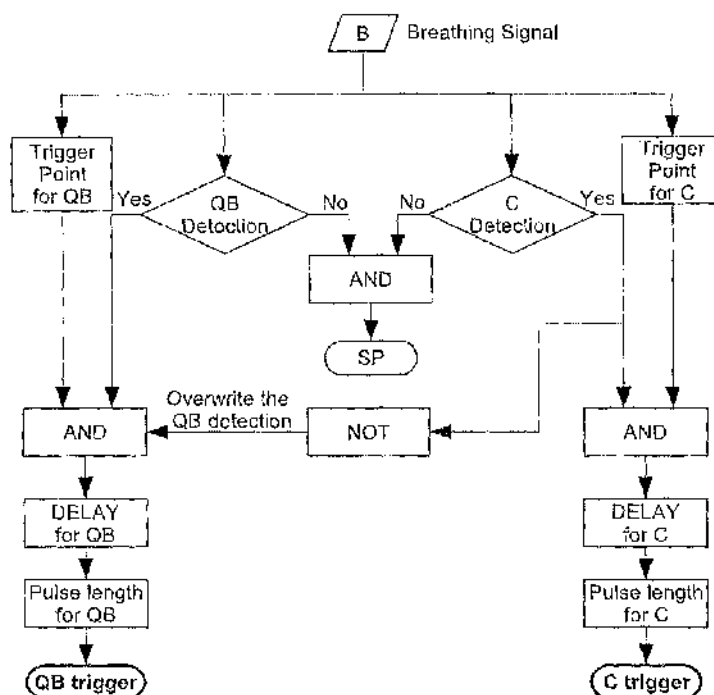


Figure 3.3: A flow chart showing the algorithm of the basic control system (BCS). When the C detection block confirms the cough pattern, the C trigger will be generated after a short delay at the right trigger point. The QB trigger is generated the same way, except when the cough detection is confirmed at the same time the QB trigger is overwritten. QB, C and SP denote quiet breathing, cough and speaking respectively.

3.2 The Multi-characteristic Control System (MCCS)

In the BCS, the main characteristics of the breathing signal which are used for detection are its derivative, sign change, and cross-correlation with the reference signal. Detection errors exist with the algorithm of the BCS. For example, the detection of QB or C can be missed when the key threshold is not crossed. Or, mis-detection (such as detects SP as QB) happens when the key threshold is crossed.

Due to the complicated variations of breathing signals during different activities, it is thought that using more characteristics of the breathing signal can increase the accuracy of the detection. A Multi-characteristic control system (MCCS) is therefore developed.

With the algorithm of the MCCS, QB, C and SP patterns are detected by confirmation of multi-threshold crossings. This algorithm can avoid the errors caused by detections based on sole threshold-crossing. The MCCS is designed to be able to set different priorities to threshold-crossings of different characteristics. This makes the algorithm of the MCCS flexible to different breathing signals from different patients, because it is found that some characteristics can be more distinctive with the breathing signals from some subjects than others. By setting the priorities properly, the algorithm of

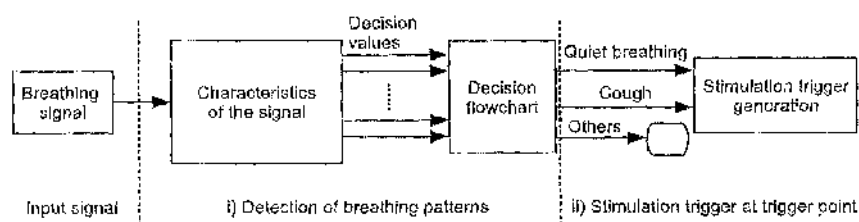


Figure 3.4: A flowchart showing the structure of the multi-characteristic control system (MCCS). There are two parts of this system. The first part (i) detects the breathing pattern and the second part (ii) generates corresponding stimulation trigger. The first part of this system analyses multi-characteristics of the breathing signal and uses a stateflow structure to detect the breathing pattern. Note that when breathing status is detected as “others”, as shown in the figure, the result is linked to a terminator.

the MCCS can also revert to the algorithm of the BCS. The MCCS is therefore an enhancement of the BCS.

With the MCCS, some new aspects of the signal are used, such as the FFT power area of the breathing signal. Combined with the characteristics used in the basic model, a total number of six characteristics of the breathing signal are analysed by a flowchart (stateflow) structure in the control system.

A flowchart illustrating the structure of MCCS is shown in Figure 3.4. The input signal can either be the signals from the IMU or the spirometer. Then different characteristics of the breathing signal are analysed by different sub-systems (represented by one block in the figure). Each characteristic analysis will output a binary value either 0 or 1 to the sub-system of “decision flowchart”. This sub-system analyses the binary values by a stateflow structure, and outputs the decision whether the breathing pattern is QB, C or others. Because it is not suitable to stimulate when people are speaking, the stimulation trigger is only generated when the QB or C pattern is confirmed.

It should be noted that DB pattern was included in the experiment with the IMU device to evaluate its ability to record different breathing patterns. While the MCCS is not specified to detect DB patterns, this pattern is preferred to be detected as QB rather than C.

3.2.1 Typical Breathing Signals of Different Patterns

Before discussing the characteristics of the breathing signal, it is helpful to look at typical signals of the four breathing patterns – QB, DB, C and SP. Figure 3.5 shows a series of samples of these patterns. They are extracted from the second set of the part ii experiment with subject 02 (described in Chapter 2) with the spirometer signal. The time scales of each pattern are the same, and the signals are not compressed or stretched.

The figure shows that QB signals have relative low inspiratory and expiratory magnitude values, while the DB and C signals have large ones. It can also be noticed that the C signals are sharper

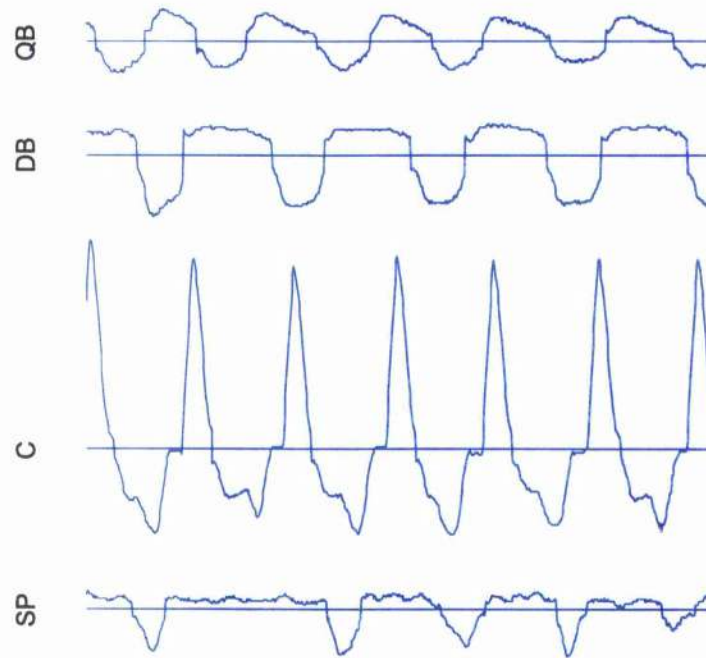


Figure 3.5: Typical breathing signals of QB, DB, C and SP breathing patterns. They are extracted from the spirometer signals of the second set of the part ii experiment with subject 02 (described in Chapter 2). The time scales of each pattern are the same, and the signals are not compressed or stretched.

than the others, due to the fast air exchange. The speaking signals have noisy and irregular expiratory phases.

3.2.2 The Analysis of the Characteristics of Breathing Signal for Detection

Six characteristics are selected in this thesis. They are:

- I. Magnitude of inspiratory signal.
- II. The cross-correlation value of the present breathing cycle and a reference cycle of QB pattern.
- III. The FFT power area over a certain length of the preceding signal.
- IV. The magnitude of expiratory signal during previous breathing cycle.
- V. The number of previous expiratory peaks.
- VI. The derivative of inspiratory signal.

These characteristics are selected for the following reasons:

- I. Similar to the BCS algorithm. The magnitude of breathing signal can be high during the inspiratory phase of coughing patterns.
- II. Similar to the BCS algorithm. The cross-correlation between the ongoing breathing cycle and a QB reference cycle shows the similarity of current breathing signal to the QB pattern.
- III. This analysis calculates the area of the FFT magnitude over a certain period of the preceding breathing signal. It is found that stronger activities such as cough and deep breathing tend to have larger areas of the FFT magnitude. Comparing this characteristic can therefore help to differentiate C and DB from QB pattern.
- IV. In order to differentiate C from DB and QB patterns, this characteristic is used. Because during the expiratory phase of a cough, the magnitude of breathing signal is often distinctively higher than those of QB and DB patterns.
- V. The number of expiratory peaks during speaking are higher than those of DB and C. The analysis of this characteristic can therefore help to differentiate SP from DB and C.
- VI. similar to the BCS, this analysis helps to differentiate C from DB and QB. Because a quicker and intenser inspiration is often needed for coughing.

Note that the analyses of characteristic IV and V are based on signals from preceding breathing cycles. Assumption that the breathing activity is not changed is needed.

The analysis of the characteristics of the breathing signal is to compare them with their pre-set thresholds. Therefore, in this thesis, there are six sub-systems for the analyses and comparisons. Their outputs are binary values of either 0 or 1.

I. Magnitude of Inspiratory Signal Sub-system

This sub-system is designed to differentiate C from QB pattern. During the inspiratory phases of C pattern, the magnitude of breathing signal can reach higher values than those during QB. A threshold is set in such a way that the breathing signal during the inspiration of C can cross while the breathing signal during the inspiration of QB cannot. As the breathing signal during inspiration is negative, the threshold for this sub-system is a negative value. The binary output of this sub-system is expected to be 1 during C and to be 0 during QB. Note that DB pattern also has high magnitude during inspiratory phases, therefore the output 1 can represent DB as well.

The algorithm of sub-system I is similar to the "C Detection" block of the BCS shown in Figure 3.3. The Simulink structure of this sub-system is shown in Figure 3.6.

The threshold for the inspiratory signal is denoted as TH_{insp} . As the inspiratory signals are negative, when breathing signal $B(k)$ exceeds the threshold, their relationship should be $B(k) < TH_{insp}$.

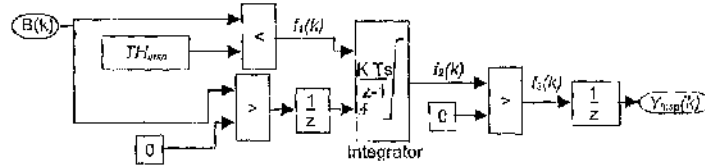


Figure 3.6: The structure of the sub-system I which analyses the magnitude of inspiratory signal. TH_{insp} denotes the threshold for the inspiratory signal. Note that the inspiratory signal is negative. When the breathing signal B exceeds the threshold, this sub-system outputs $Y_{insp} = 1$. The first unit delay block ($\frac{1}{z}$) resets the integrator when expiration starts, and the second unit delay block delays the output one sample point. The second delay avoids missing the trigger point at the beginning of expiration.

In one detection cycle, the threshold-crossing of the magnitude of the breathing signal needs to be held until the end of current cycle. The threshold-crossing status is reset at the beginning of next detection cycle. This holding structure is realised by a *integrator*.

The *integrator* is a *Forward Euler* discrete-time integrator. It has two inputs. As shown in the figure, the top input is the input signal which the *integrator* integrates, and the bottom input is the external reset input whose reset method is set as *rising*. The *initial condition* and *gain value* of the *integrator* are set as 0 and 1, respectively. With these settings, the *integrator* integrates and outputs the input signal from 0. When the reset input signal is rising, say from 0 to 1, the *integrator* resets. Therefore when its input $f_1(k)$ changes from 0 to 1, its output $f_2(k)$ starts to integrate from 0. The integration resets itself when the breathing signal is positive, i.e. the expiration begins. The *integrator* used in this thesis is typically for holding an instant signal for a certain amount of time. A unit delay block is used to avoid missing the trigger point at the beginning of expiration.

At the end, a *unit delay* block delays the outputs signal by one sample period. This can also avoid missing the trigger point at the beginning of the expiration. The whole process can be expressed in the following equations:

$$f_1(k) = \begin{cases} 1 & \text{if } B(k) < TH_{insp} \\ 0 & \text{otherwise} \end{cases}, \quad (3.1)$$

$$f_2(k) = \begin{cases} \int_0^k f_1(k) dk & \text{if } B(k-1) \leq 0 \\ \int_{k_0}^k f_1(k) dk & \text{if } B(k_0-1) > 0 \end{cases}, \quad (3.2)$$

$$f_3(k) = \begin{cases} 1 & \text{if } f_2(k) > 0 \\ 0 & \text{otherwise} \end{cases}, \quad (3.3)$$

$$Y_{insp}(k) = f_3(k-1) \quad (3.4)$$

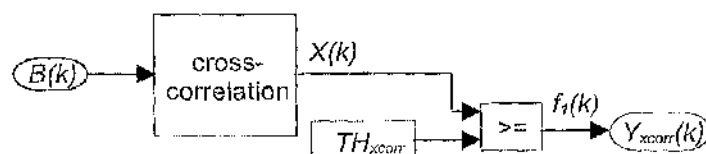


Figure 3.7: The structure of the sub-system which analyses the cross-correlation of the breathing signal with QB reference signal. TH_{xcorr} denotes the threshold for the cross-correlation. The cross-correlation value is calculated with the QB reference signal and the preceding signals of $B(k)$ over a nominal breathing cycle.

Where k and k_0 denote sample instants. k_0 is the sample instant where the inspiratory signal exceeds its threshold.

The breathing signal is normalised before analysis. Therefore, setting the inspiratory threshold $TH_{insp} < -1$ leads to the output signal $Y_{insp} = 1$ when non-QB breathing activities (C, DB or SP) occur. On the other hand, $Y_{insp} = 0$ cannot necessarily indicate the confirmation of QB, because it is not necessary that every speaking or coughing activity needs deep inspiration, especially with tetraplegic individuals.

II. Cross-correlation Sub-system

This sub-system is designed to detect QB pattern. The current breathing cycle is compared with a QB cycle reference. Their similarity is represented by the cross-correlation. The threshold for this sub-system is set as a certain value of the cross-correlation. By comparing the current cross-correlation with this threshold, during QB, the binary output of this sub-system is expected to be 1.

The structure of sub-system II is shown in Figure 3.7. TH_{xcorr} denotes the threshold for the cross-correlation value.

The “cross-correlation” block in the figure calculates the cross-correlation between the current breathing cycle and the reference cycle. A brief introduction to the concept of cross-correlation is needed.

The cross-correlation measures the similarity between two series of signals. Its value is within the interval of $[-1 \ 1]$. When the cross-correlation approaches 1, it indicates that the two signals are similar; when it equals -1 indicates the two signal have a phase difference of 180° ; while the value of 0 indicates that the two signals are not correlated.

The QB reference signal is denoted as $R(k)$. This reference signal has one phase of inspiration and expiration successively. It is obtained by averaging a number of QB signals pre-recorded. The length of this reference signal is denoted as N . The N data points preceding the current breathing signal $B(k)$ are therefore used to compare with $R(k)$. The cross-correlation $X(k)$ is calculated as:

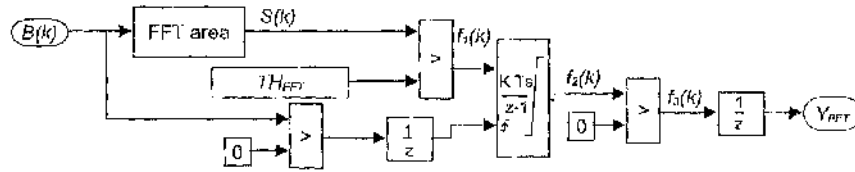


Figure 3.8: The structure of the sub-system which analyses the area of the FFT magnitude of the breathing signal over a certain period.

$$X(k) = \frac{\sum_{k=1}^N R(k)B(k-N+1)}{\sqrt{\sum_{k=1}^N R^2(k) \sum_{k=1}^N B^2(k-N+1)}} \quad (3.5)$$

The cross-correlation value $X(k)$ is within the interval $[-1, 1]$, by its definition. When it approaches 1, the current breathing activity is considered to be identical to the QB reference. The threshold for the cross-correlation TH_{xcorr} is usually set larger than 0.3. Due to the calculating procedure, the cross-correlation maximises at the end of current inspiration, therefore the outcome of the comparison between the $X(k)$ and TH_{xcorr} doesn't need the *integrator* block to hold. The process of this sub-system can be expressed in equations as follows:

$$Y_{xcorr}(k) = f_1(k) = \begin{cases} 1 & \text{if } X(k) \geq TH_{xcorr} \\ 0 & \text{otherwise} \end{cases}, \quad (3.6)$$

This sub-system can distinguish QB pattern from the others. In practice, it is found that the cross-correlation values of the speaking pattern are most distinctive from those with QB pattern.

III. FFT Area Sub-system

This sub-system is designed to differentiate C from QB pattern. It calculates the FFT magnitude of certain points of the breathing signal and sum them up. The summation is understood as the FFT area. This magnitude area value is compared with a pre-set threshold. This threshold is selected in such a way that the FFT area during C can cross it while that during QB cannot. The binary output of sub-system III is therefore expected to be 1 during C.

The structure of the FFT area sub-system is shown in Figure 3.8. The outcome of the comparison is held by an *integrator* until the beginning of expiration.

The FFT area analyses can be found in Section 2.3.4. In Figure 3.8, the block which outputs the power area is a customised sub-system which calculates FFT magnitude and its area. Due to the definition of FFT algorithm, the length of the signal to be calculated should be 2^n ($n = 1, 2, 3, 4 \dots$). The length of the picked signal needs to be longer than the average length of a breath. When the sample frequency is 50Hz, 256 data points ($256 \times 0.02 = 5.12s$) is thought to be an appropriate period (longer than a normal breath) to calculate FFT magnitude.

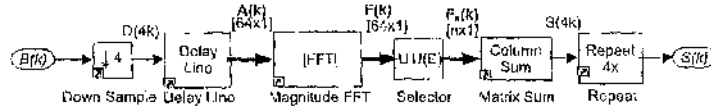


Figure 3.9: The sub-system which calculates FFT magnitude and its area of the breathing signal over a certain period. $D(4k)$ is the down-sampled breathing signal; $A(k)$ is the delayed signal of $D(4k)$ which can then be input to the Magnitude FFT block to calculate the FFT magnitude; $F(k)$ is the FFT magnitude of the down-sampled signal $D(4k)$; $F_n(k)$ is the output of the selector block which extracts the first n data points out of each column of the signal $F(k)$; Signal $S(4k)$ is the FFT magnitude area of the down-sampled signal $D(4k)$.

The FFT magnitude area sub-system is shown in Figure 3.9. During system tests, it is found that the system tends to run slowly when the *Magnitude FFT* block calculates over 256 data points. A *Down Sample* block is therefore used to resample the breathing signal at the rate of 4 times lower. This block resamples 256 data points into 64 ones. The *Delay Line* block delays the signal $D(4k)$ so that a series signal over the period of 64 data points are calculated by the *Magnitude FFT* block. The *Selector* block allows only the first n data points of the 64 points of FFT magnitude to be summed by the *Matrix Sum*. The *Repeat* block is used to resample the down-sampled sum signal $S(4k)$ back to $S(k)$. In practice, it is found that the usage of *Down Sample* can effectively quicken the system calculation while introduce little effect on the comparison.

The process of the FFT area sub-system can be expressed by the following equations:

$$f_1(k) = \begin{cases} 1 & \text{if } S(k) > TH_{FFT} \\ 0 & \text{otherwise} \end{cases}, \quad (3.7)$$

$$f_2(k) = \begin{cases} \int_0^k f_1(k) dk & \text{if } B(k-1) \leq 0 \\ \int_{k_0}^k f_1(k) dk & \text{if } B(k_0-1) > 0 \end{cases}, \quad (3.8)$$

$$f_3(k) = \begin{cases} 1 & \text{if } f_2(k) > 0 \\ 0 & \text{otherwise} \end{cases}, \quad (3.9)$$

$$Y_{FFT}(k) = f_3(k-1) \quad (3.10)$$

Where k, k_0 denote sample instants, and k_0 is where the delayed breathing signal becomes positive (beginning of expiration). TH_{FFT} is the pre-set threshold for the FFT area.

It is found that the FFT magnitude area of C patterns is usually larger than those of other breathing patterns. This is because cough usually has larger breathing signals and quicker changes of them. QB signals have relatively low FFT area values.

It is also found that this FFT area characteristic can help to differentiate SP from QB patterns. However, the threshold set for differentiating C from QB is not suitable, as the FFT area of the SP

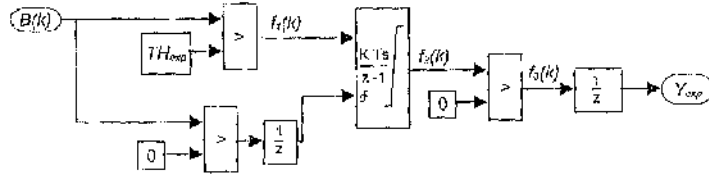


Figure 3.10: The sub-system which analyses the magnitude of the previous expiratory signal. This analysis predicts the current breathing activity assuming that the previous activity is the same.

activities is lower than that of the C pattern. Therefore, a different threshold for differentiating SP and QB is set. This sub-system therefore has two thresholds, denoted as TH_{FFT}^a and TH_{FFT}^b .

IV. The Magnitude of Previous Expiratory Signal Sub-system

It is found that even though the inspiratory breathing signals of the cough pattern may be low, the expiratory signals can be large due to the fast exhalation. This sub-system detects large expiratory signal from the previous expiratory phase. The assumption is that the breathing activity is not changed. Thus, this sub-system predicts the quantity of the current expiratory signal. The predicted expiratory signals are compared with its threshold. The threshold is selected in such a way that C pattern is allowed to cross while QB pattern is not. The structure of the sub-system which analyses the magnitude of previous expiratory signal is shown in Figure 3.10.

The structure of this sub-system is similar to the sub-system I which analyses the magnitude of inspiratory signal. An *integrator* is used to hold the comparison outcome with the expiratory threshold until the beginning of expiration. The process of this sub-system can be expressed by the following equations:

$$f_1(k) = \begin{cases} 1 & \text{if } B(k) > TH_{exp} \\ 0 & \text{otherwise} \end{cases}, \quad (3.11)$$

$$f_2(k) = \begin{cases} \int_0^k f_1(k) dk & \text{if } B(k-1) \leq 0 \\ \int_{k_0}^k f_1(k) dk & \text{if } B(k_0-1) > 0 \end{cases}, \quad (3.12)$$

$$f_3(k) = \begin{cases} 1 & \text{if } f_2(k) > 0 \\ 0 & \text{otherwise} \end{cases}, \quad (3.13)$$

$$Y_{exp}(k) = f_3(k-1) \quad (3.14)$$

Where k , k_0 denote sample instants, and k_0 is where the delayed breathing signal becomes positive (beginning of expiration). TH_{exp} is the pre-set threshold for the expiratory signal.

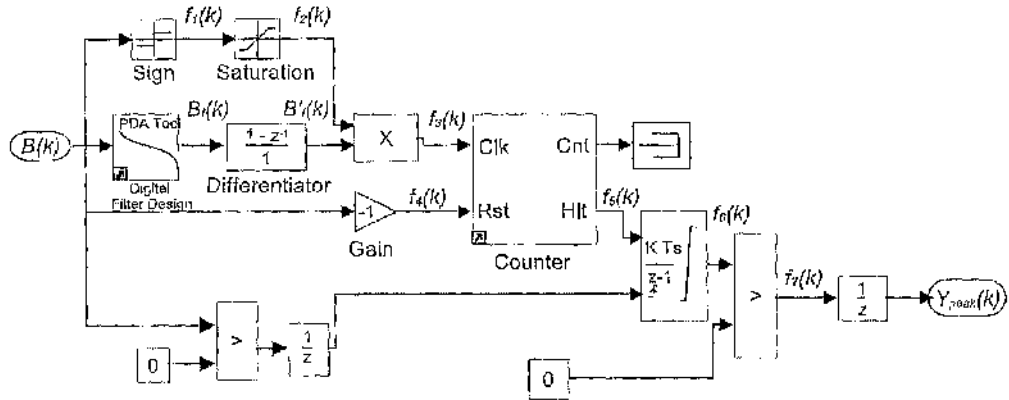


Figure 3.11: The sub-system which counts the peak number of the previous expiratory signal.

The threshold for expiratory signal is set to be large so that only the expiratory signal during the cough activity can exceed it. Therefore, the output of this sub-system can be used as a decision factor to confirm cough.

V. The Sub-system which Counts Previous Expiratory Peaks

The typical breathing signals shown in Figure 3.5 show that during expiratory phases, QB, C and DB usually have not more than two peaks, while SP signals have more regional peaks. This is a distinguishable characteristic of the breathing signals during speaking activities. The task of this sub-system is to count the peak numbers of the breathing signal during expiratory phases. During each detection cycle, the counted peak numbers are compared with a pre-set threshold. The comparison outcome is hold until the end of one detection cycle. The structure of this sub-system is shown in Figure 3.11.

The peak of the magnitude of the breathing signal during expiratory phase corresponds to a zero crossing of its derivative. This zero crossing can be received by the *Counter* block as an trigger event at the *Clk* port. A low pass filter is applied to the breathing signal before counting to avoid counting small peaks due to the signal noise. The digital filter is a IIR Butterworth low pass filter, with parameters of $F_{pass} = 0.2Hz$, $F_{stop} = 1.5Hz$, $A_{pass} = 1dB$ and $A_{stop} = 20dB$. The filtered signal is denoted as $B_f(k)$ in the figure. The *Differentiator* in the figure is a *discrete filter* block which calculates the difference of signal $B_f(k)$. This can be express as:

$$B'_f(k) = B_f(k) - B_f(k - 1) \quad (3.15)$$

Where k is the sample instant. Note that $B'_f(k) = 0$ when $k = 1$.

The counter needs to count only during expiratory phases. Therefore, the sign of the breathing signal needs to be detected. The difference of the breathing signal is only analysed by the counter

when its sign is detected as positive. This function is realised by the the blocks of *Sign*, *Saturation* and *Product*, and be explained by the following equations:

$$f_1(k) = \begin{cases} 1 & \text{if } B(k) > 0 \\ 0 & \text{if } B(k) = 0 \\ -1 & \text{if } B(k) < 0 \end{cases}, \quad (3.16)$$

The *Sign* block outputs 1 for positive $B(k)$, -1 for negative $B(k)$ and 0 for 0 input.

$$f_2(k) = \begin{cases} f_1(k) & \text{if } f_1(k) > 0 \\ \text{eps} & \text{if } f_1(k) \leq 0 \end{cases}, \quad (3.17)$$

The *Saturation* block limits the range of signal $f_1(k)$. The upper and lower limits of $f_1(k)$ are set in inf and eps . The value eps can be understood as a tiny figure close to 0. When signal $f_1(k)$ is below this value, the output $f_2(k)$ is clipped to eps .

$$f_3(k) = f_2(k) \times B'_f(k) \quad (3.18)$$

The *Product* block actually clips signal $B'_f(k)$ to eps when $B(k)$ is negative (inspiratory phase).

$$f_3(k) = \begin{cases} B'_f(k) & \text{if } B(k) > 0 \\ \text{eps} \approx 0 & \text{if } B(k) \leq 0 \end{cases}, \quad (3.19)$$

The main block in this sub-system is the *Counter* block. *Clk* ($f_3(k)$), *Rst* and *Hit* are its input, reset and output port, respectively. The counter block increments (or decrements) an internal counter ($Cnt(k)$) each time it receives a trigger event at the *Clk* port. The value of the internal counter is output at the *Cnt* port, which is not used in this sub-system and connected to a *terminator*. The trigger event in this sub-system is set as "either edge". This means that either the signal at port *Clk* ($f_3(k)$ from the figure) changes from negative to positive or the other way around will be treated as a trigger event. A pre-set threshold for the peak number (TH_{peak}) is set in the block. When the internal counter exceeds this threshold, a binary signal 1 will be generated at the *Hit* port. A trigger event at the *Rst* port will reset the internal counter to its initial state.

The process of the *Counter* block can be expressed as:

$$f_5(k) = \begin{cases} 1 & \text{if } Cnt(k) > TH_{peak} \\ 0 & \text{Otherwise} \end{cases}, \quad (3.20)$$

When the internal counter ($Cnt(k)$) exceeds its threshold, the *Hit* port outputs 1. It should be noted that the internal counter $Cnt(k)$ returns to 0 when the reset value $f_4(k)$ has a zero crossing.

The holding structure which holds the signal $f_5(k)$ value until the end of a detection cycle is the same as those in the sub-systems described previously:

$$f_6(k) = \begin{cases} \int_0^k f_5(k) dk & \text{if } B(k-1) \leq 0 \\ \int_{k_0}^k f_5(k) dk & \text{if } B(k_0-1) > 0 \end{cases}, \quad (3.21)$$

$$f_7(k) = \begin{cases} 1 & \text{if } f_6(k) > 0 \\ 0 & \text{otherwise} \end{cases}, \quad (3.22)$$

$$Y_{peak}(k) = f_7(k-1) \quad (3.23)$$

Where k, k_0 denote sample instants, and k_0 is where the delayed breathing signal becomes positive (beginning of expiration).

Some of the main internal signals during some sample QB and SP activities are shown in Figure 3.12. The top figure shows the original breathing signal $B(k)$, the low pass filtered signal $B_f(k)$, and the undelayed output of this sub-system $f_7(k)$. The bottom figure shows the internal counter $Cnt(k)$ and the saturated derivative of signal $B_f(k)$. It can be seen that during the inspiratory phases, signal $f_3(k)$ is approximately 0, due to Equation 3.18. The internal counter increments when $f_3(k)$ has a zero-crossing. The pre-set threshold for the peak number is 2 in this example. It can be seen that when $Cnt(k)$ exceeds 2, the output signal $f_7(k)$ is generated and held until the start of expiration.

While this sub-system is mainly used to distinguish the SP pattern from others, its analysis is based on the preceding expiratory signals. Therefore, the assumption that the breathing activity is not changed is also needed in this sub-system.

VI. The Sub-system which Analyses Derivative of Inspiratory Flows

This sub-system is designed to detect fast inspirations. The breathing activities which can cause intense inspirations are C, DB and SP.

The derivative of the breathing signal is calculated and compared with a pre-set threshold. The outcome of the comparison is held until the end of one detection cycle. The binary output of this sub-system is expected to be 0 during QB. The structure of this sub-system is shown in Figure 3.13.

The process of this sub-system can be expressed by the following equations:

$$f_1(k) = \begin{cases} 1 & \text{if } B(k) - B(k-5) < TH_{insp} \\ 0 & \text{otherwise} \end{cases}, \quad (3.24)$$

Where k denotes sample instants. Note that the output of the differentiator is 0 when $k < 0$. The differentiator calculates the derivative of the breathing signal by subtracting every 5 data points. Calculating the difference between every 5 points instead of the successive points is to avoid errors introduced by the unexpected data points in the signal, e.g. signal noise.

$$f_2(k) = \begin{cases} \int_0^k f_1(t) dt & \text{if } B(k-1) \leq 0 \\ \int_{k_0}^k f_1(k) dk & \text{if } B(k_0-1) > 0 \end{cases}, \quad (3.25)$$

Where k_0 is the sample instant where the delayed breathing signal exceeds 0, i.e. expiratory phase begins.

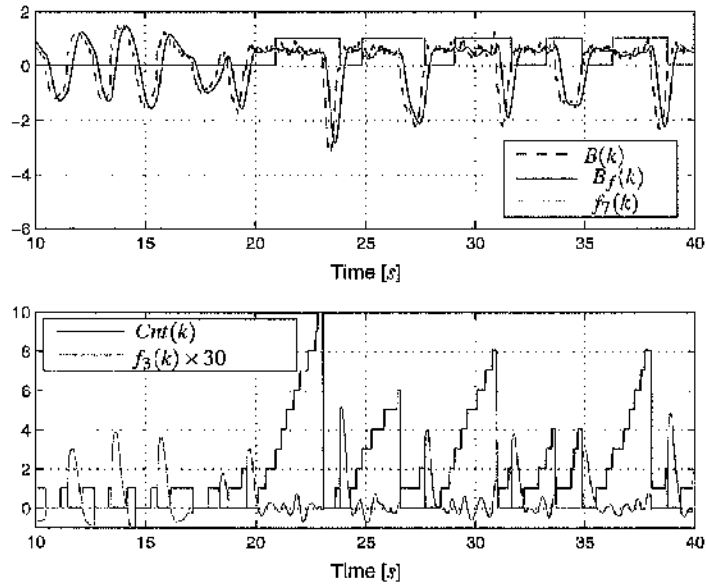


Figure 3.12: Signals showing the process of the sub-system which counts the peak numbers of expiratory signal. In the top figure, signal $f_1(k)$ is the undelayed output signal of this sub-system. $B_f(k)$ is the filtered signal by a low pass filter. It can be seen that this sub-system detected the speaking pattern from the preceding expiratory signals. In the bottom figure, the signal $f_3(k)$ is the saturated derivative of the filtered breathing signal. It shows that during inspiratory phases, its value is approximately 0. When this value has a zero-crossing, the count value $Cnt(k)$ increments. $Cnt(k)$ resets to 0 at the beginning of every expiration. Note that signal $f_3(k)$ is multiplied by 30 to fit the figure.

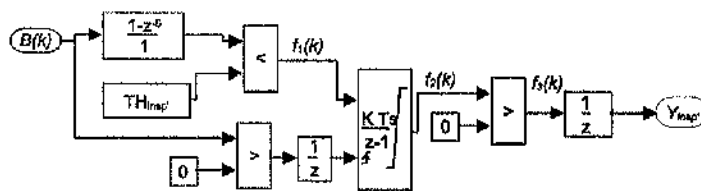


Figure 3.13: The sub-system which analyses the derivative of the breathing signals during inspiratory phase.

$$f_3(k) = \begin{cases} 1 & \text{if } f_2(k) > 0 \\ 0 & \text{otherwise} \end{cases}, \quad (3.26)$$

$$Y_{insp}(k) = f_3(k-1) \quad (3.27)$$

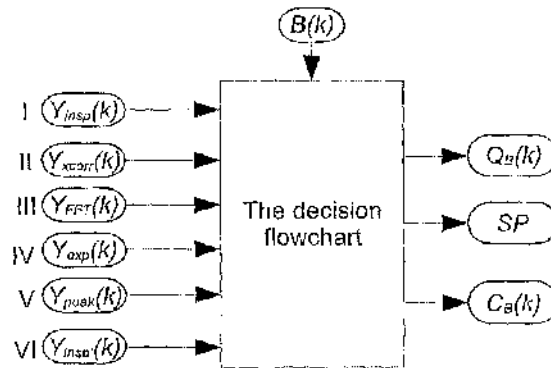


Figure 3.14: Illustrations showing the inputs and outputs of the decision flowchart sub-system of the MCCA. This flowchart analyses the outputs of the sub-systems described in Section 3.2.2 and generates signals which indicate whether the current breathing activity is cough or quiet breathing, or others such as SP. The outputs $C_B(k)$, $Q_B(k)$ and SP indicate the attempt to cough (when $C_B(k) = 1$) or quiet breathing $Q_B(k) = 1$ or other breathing activities such as speaking.

The value of the derivative of breathing signals during inspiratory phases depends on how fast the inhalation process is. In the inspiratory phase of cough activity, the inhalation is usually faster than that during the inspiratory phase of QB activity. This can be seen from the typical breathing signals shown in Figure 3.5. The inspiratory phase of the speaking activities is typically lower than that of cough activities and higher the QB ones. Therefore, this sub-system can distinguish QB from C and SP patterns.

Note that the detection of threshold crossing of this sub-system occurs in the first (descending) half of the inspiratory phase, while the detection of trigger point for cough occurs in the second (ascending) half.

3.2.3 The Decision Flowchart Sub-system which Analyses the Outputs of the Sub-systems which Analyses the Signal Characteristics

One of the differences of the MCCA to the BCS is the decision flowchart sub-system. As shown in Figure 3.14, this decision flowchart analyses the outputs of the sub-systems which analyses the signal characteristics. This flowchart sub-system checks breathing activities using the characteristics of the breathing signal. The output signals of this structure are signals for QB and C attempt ($Q_B(k)$ and $C_B(k)$). QB is confirmed when $Q_B(k) = 1$ and C is confirmed when $C_B(k) = 1$. SP (or other activities) is confirmed when $Q_B(k) = C_B(k) = 0$.

The structure of the flowchart sub-system is shown in Figure 3.15. The start point of the flowchart is when the breathing signal becomes negative (during inspiration). When the flowchart works, the result from the characteristic sub-system I which analyses the inspiratory signal is analysed. When the

inspiratory breathing signal of the current phase exceeds its threshold, the current breathing activity is considered not to be QB. If the inspiratory breathing signal does not exceed its threshold, the current breathing activity is thought to be any possible activities (QB, C and SP). This is because it is found that some of the coughing and speaking signals can be as small as the quiet breathing signals. The second level of the flowchart analyses the result from the sub-system VI which analyses the derivative of the inspiratory signal. If this result shows that the derivative of the inspiratory signal exceeds its threshold, the breathing activity is not QB. After this level, the breathing activity is considered either to be cough or speaking (left side of the flowchart), or quiet breathing or speaking (right side of the flowchart).

To distinguish between the cough and speaking pattern, the results of the sub-system III(a) (FFT power area), IV (previous expiratory signal) and V (number of previous expiratory peaks) are analysed. A high FFT power area result confirms the current breathing signal to be cough, while a low FFT power area result may represent cough or speaking pattern. If the previous expiratory signal is high, the current breathing activity is expected to be cough, assuming the breathing activity is not changed. When the result of the sub-system IV is 0 (no high previous expiratory signal), the cough and speaking patterns will be differentiated by the result of the sub-system V. Large number of peaks of the expiratory signal during previous breathing phase confirms the current breathing activity to be speaking, assuming the breathing activity is not changed, otherwise the current breathing activity is considered to be cough.

To distinguish between the quiet breathing and speaking pattern, the results of the sub-system II (cross-correlation), III(b) (FFT power area) and V (number of previous expiratory peaks) are analysed. If the cross-correlation of the current breathing signal and the reference signal is smaller than the threshold, the signal will be considered to be speaking. If the cross-correlation is higher than the threshold, the exceeding of the FFT power area confirms the current breathing activity to be speaking. Same as the analysis to differentiate cough and speaking, the last level of the flow chart to differentiate quiet breathing and speaking analyses the result of the sub-system V.

The outputs of this flowchart sub-system is the confirmation of the breathing activity – QB, C or SP. When the speaking pattern is confirmed, both outputs of the QB and C ports are 0.

3.2.4 Generation of the Stimulation Trigger

This part of the system generates stimulation trigger signals for cough or quiet breathing accordingly. The stimulation trigger needs to be generated at the right time and have a pulse-length which indicates the length of the stimulation. These features of the stimulation trigger are processed by the “Trigger Point”, “DELAY” and “Pulse length” blocks of the BCS shown in Figure 3.3 on page 66.

In the MCCS, these three blocks are integrated in the “Stimulation trigger generation” block as shown in Figure 3.4 on page 67. The algorithm of this block is remained. Refer to previous papers for details.

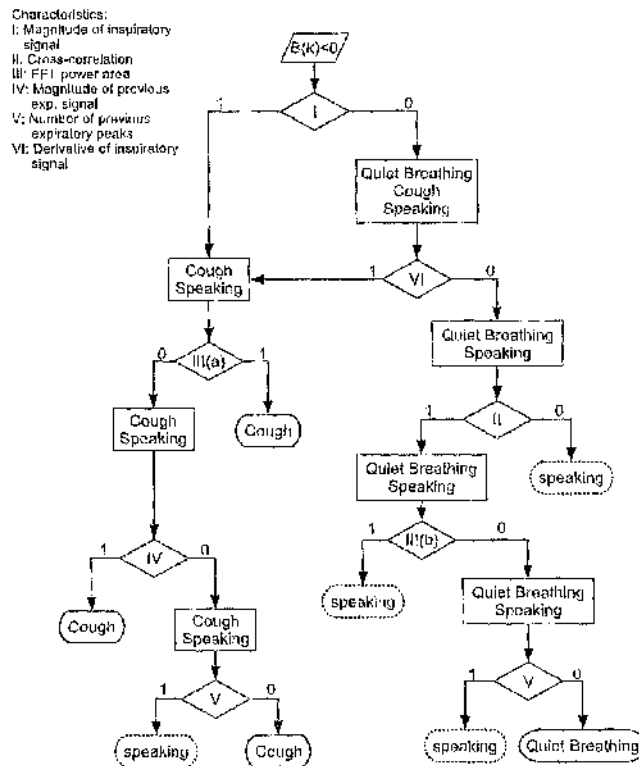


Figure 3.15: The structure of the flowchart sub-system. Note that sub-system III(a) and III(b) have the same structure. They use different thresholds to differentiate C and SP from QB patterns.

3.3 Testing the Multi-characteristic Control System (MCCS)

As an enhancement to the BCS, the performance of the MCCS is tested. Two tests are conducted.

The first one uses both the MCCS and BCS to analyse the same breathing signals. The thresholds for the BCS are first optimised. Then the corresponding thresholds for the MCCS are set to the same values. By changing other thresholds for different signal characteristics, the system performance is evaluated. This test is focused on the detection of SP patterns.

The other test uses only the MCCS. The signals from the experiment with the IMU and spirometer are analysed by the MCCS. By optimising the thresholds for signals from different subjects, the MCCS performance with various types of breathing signals is evaluated.

3.3.1 Improvement of the Detection of Speaking Patterns by the MCCS

At the time, the MCCS analyses six characteristics of breathing signals to detect QB, C and SP, while the BCS analyses two of them. By using the decision flowchart, the MCCS has a more sophisticated detection algorithm. In this section, the improvement by the MCCS to detect SP patterns is presented.

In previous experience, SP patterns can be mis-detected as C or QB in various situations. This is due to the variations of the breathing signal during different speaking situations. For example, the breathing signals during the inspiratory phases of a shout can be similar to those of coughing. When speaking quietly, the inspiratory signals can be similar to QB ones. With the algorithm of the BCS, a shout can be detected as cough and the quietly speaking can be detected as quiet breathing.

When using the detection results from the control system to generate the electrical stimulation for FESAM, mis-detecting SP as QB or C will lead to unwanted stimulation. This is worse than missing stimulation (miss-detecting QB or C), as the electrical stimulation can disturb the process of speaking, or make patient uncomfortable.

The sub-system V of the M CCS is specifically designed to improve the detection of SP patterns. It is found that in most cases of speakings, no matter how the inspiratory phases vary, their expiratory phases share a common feature. That is during the expiratory phases of speak, regional peaks are distinctively high. The sub-system V counts the regional peaks during every expiratory phases and compare them with a threshold. The successive respiratory cycle will be detected as SP if the threshold is crossed. This detection is based on the assumption that the breathing activity is not changed.

One sample test is presented with the spirometer data ii-2 with subject 01 (as described in Chapter 2). The settings of the thresholds for the BCS and M CCS are shown in Table 3.1. The shared thresholds (I and II) are set to the same values. The threshold for sub-system V is set to 4, which means that when the peaks exceed 4 during the previous expiratory phase, the present breathing cycle will be predicted to be speaking. Other parameters are chosen to distinguish between different breathing activities most effectively.

The detection results with both systems are shown in Figure 3.16. The inspiratory phases of the SP pattern with this signal are similar to the C patterns. It is hard to differentiate them by comparing only the magnitude of inspiratory signals. This causes that all the SP patterns are detected as C with the BCS (Figure 3.16(a)).

Most of the SP patterns are detected correctly with the M CCS (Figure 3.16(b)). The first speaking cycle is not detected because the sub-system V can only predict successive breathing cycles. This also causes that the QB pattern after the last SP pattern is mis-detected as SP.

3.3.2 Testing the M CCS with the IMU and Spirometer Signals

The ability of the M CCS to detect breathing activities is evaluated with the IMU and spirometer signals from the experiments discussed in Chapter 2.

The evaluation tests the system accuracy with different data sets acquired from both the spirometer and the IMU. This test can also further evaluate the IMU signal for its suitability to be used for the automatic control system for FESAM.

The tests use the acceptable data sets with the 5 subjects (refer to Table 2.7 on page 44). The system parameters, the six thresholds for the six sub-systems, are adjusted with data sets with different subjects and devices.

Threshold	BCS	MCCS
I	2	2
II	0.3	0.3
III(a)	-	200
III(b)	-	130
IV	-	10
V	-	4
VI	-	-1

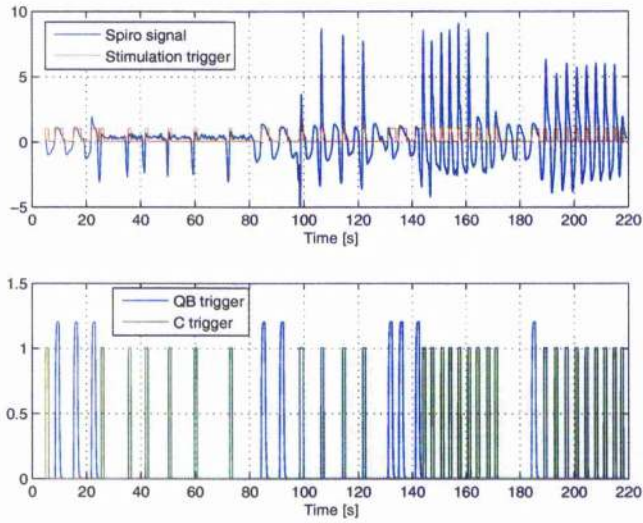
Table 3.1: Thresholds set for the test with both BCS and MCCS to improve the detection of QB, C and SP patterns. Note that the signals are all normalised before the testing. Refer to Section 3.2.2 for details of the sub-system.

The acceptable data sets with each subject are analysed separately with constant system parameters. For the data sets with subject 02 and 03, a cycle of quiet breathing reference is calculated with data sets *i* (a series of quiet breathing), as they are acceptable. For the data sets with subject 01 and 05, as the data sets *i* are not acceptable, the quiet breathing references were calculated with acceptable quiet breathing segments selected from the data sets *ii*.

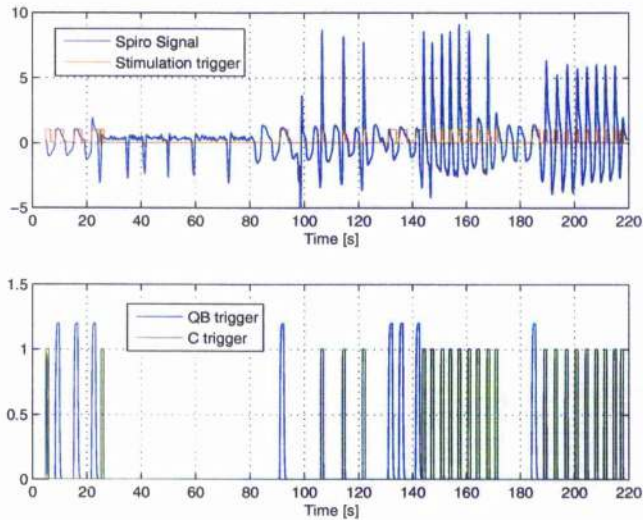
The six thresholds for the six sub-systems are tested with all the data sets with each subject. Each threshold is chosen in such a way that the sub-system can differentiate certain breathing activities most effectively. Due to the different characteristics of the IMU and spirometer signals, the thresholds are adjusted accordingly. The decision of each threshold was made by testing a number of different values, and choosing the one which made the detection most accurate. Each sub-system has a display block which can show the analysed characteristic. A sample view of the display block for the sub-system V is shown in Figure 3.12 in Section 3.2.2. This figure shows the breathing signal along with the numbers of the peaks during previous expiration. In this example, if the threshold for this sub-system is set as 2, the QB patterns can be distinguished from the SP patterns.

After the thresholds are chosen, they are used constantly with all the data sets with the same subject. The total numbers of the QB, C and SP breathing activities are counted. The recorded results include the numbers of: i) QB cycles which have correct stimulation triggers; ii) C cycles which have correct stimulation triggers; iii) SP cycles which have stimulation triggers either for C or QB. The first two results evaluate the ability of the system to detect QB and C activities and generate right stimulation trigger signals. The third result shows the ability of the system to differentiate speaking activities, where no electrical stimulation is allowed.

The SC and DB breathing activities are not evaluated with the MCCS. The reason is that: i) these two activities are included mainly to test the sensitivity of the IMU device to rapid change of breathing activities; ii) the MCCS does not have specific parameters for these two activities, thus the results are



(a) Detection results of the BCS.



(b) Detection results of the MCCS.

Figure 3.16: Detection results of the BCS and MCCS with a sample spirometer signal. Refer to Section 3.3.1 for the configurations of the two systems. In the bottom figures, the magnitudes of the trigger signal for the QB pattern is set 1.2 and that for the C pattern is set 1 to distinguish. The stimulation trigger in the upper figures show either the trigger signal for the QB or C pattern, along with the signal. The MCCS has detected the five speaking patterns, while the BCS mis-detected them as C pattern. Note that the shared thresholds of the two system are set the same

not optimised; iii) they can represent breathing activities other than the QB, C and SP ones in a general sense. Thus, this is a further work which requires the system to deal with various breathing activities

Threshold	Subject 01		Subject 02		Subject 03		Subject 05	
	IMU	spiro	IMU	spiro	IMU	spiro	IMU	spiro
I	2	2	2	2	2	2	2.5	2
II	0.5	0.3	0.7	0.6	0.2	0.5	0.5	0.5
III	200							
IV	2	3.5	3	3	1.8	3.5	3	3.5
V	4	4	3	3	6	4	4	4
VI	-0.5	-1	-1.5	-1.5	-0.5	-0.5	-1.5	-1.5

Table 3.2: Summary of the thresholds of the six sub-systems for the tests of the MCCS with the data sets from the IMU and spirometer. Note that the breathing signals are normalised before the testing. Refer to Section 3.2.2 for details of the sub-system.

that are closer to the daily life.

3.4 Results of the Tests Using MCCS to Analyse the Signals from both the IMU and Spirometer Device

3.4.1 System Parameters with All the Data Sets

The system parameters which are adjusted are the six threshold values, shown in Table 3.2. Refer to Section 3.2.2 for details of the six sub-systems and their thresholds. The thresholds are chosen in such a way that the sub-system can distinguish different breathing activities most effectively. All the data sets were normalised before the testing.

The threshold I is for the characteristic of the magnitude of inspiratory signal. For most subjects, this threshold is set to 2 (IMU test with subject 05 is 2.5), as the average inspiratory peak value is 1 due to the normalisation. Threshold II is for the cross-correlation between the current breathing cycle and a QB reference signal. For most subjects, this threshold is set larger than 0.5. The threshold II of the IMU test with subject 03 is set to 0.2. The third threshold is set to 200 for every data set. This threshold is for the FFT area. It is found that most of the FFT areas during the C activity are larger than 200, while those during the QB activity are distinctively smaller than 200. The threshold IV is for the magnitude of expiratory signal. This threshold aims to detect previous coughs, which have large magnitude during expiratory phases. During the test, it is found that the expiratory peaks during coughing activity varies with different data sets, the thresholds are therefore set accordingly. The fifth threshold is for the peak numbers of the previous expiratory signal. The breathing cycle whose peak number is higher than this threshold is considered as speaking pattern. This threshold is set to more than 3. When the signals are noisy, QB signals can have more than one expiratory peaks, therefore the threshold for the peak numbers is set higher, e.g. 6. The last threshold (VI) is for the derivative

Subject	Quiet Breathing		Cough		Speaking	
	IMU	spiro	IMU	spiro	IMU	spiro
01	7/19	11/19	14/16	16/16	5/15	0/15
02	38/67	59/67	40/42	40/42	7/57	0/57
03	20/31	27/31	24/24	24/24	11/48	2/48
05	9/22	18/22	17/18	11/18	11/23	6/23
Total	74/139	115/139	95/100	97/100	34/144	8/144

Table 3.3: Results of the testing of the MCCS with the signals from the IMU and spirometer. The results are in the form of x/y , where y denotes the total number of the QB, C or SP activities with all the acceptable data sets with each subject. In the columns of QB and C, x denotes the numbers of the QB or C patterns when the system generates the stimulation signal correctly. In the SP columns, x is the number of the breathing cycles where the system incorrectly generates stimulation signals either for QB or C patterns.

of the inspiratory signal. The breathing cycles which have higher derivatives of inspiratory signal are considered to be speaking or coughing pattern. This threshold is set to either -0.5, -1.0 or -1.5.

3.4.2 Testing Results

The results of the testing with the MCCS with both the IMU and spirometer signals are shown in Table 3.3.

The results are in the form of x/y , where y denotes the total number of the QB, C or SP activities with all the acceptable data sets with each subject. In the columns of QB and C, x denotes the numbers of the QB or C patterns when the system generates the stimulation signal correctly. In the SP columns, x is the number of the breathing cycles where the system incorrectly generates stimulation signals either for QB or C patterns.

The system results with the QB and SP patterns with the spirometer signals are better than those with the IMU signals, while the results with the C pattern with subject 05 show the opposite.

Quiet Breathing The detected QB pattern numbers with the spirometer signal are larger than those with the IMU signal. More than half of the total number of the QB patterns are correctly detected with the data sets with the IMU signals with subject 02 and 03. In the spirometer column, the results show that most of the QB patterns are detected.

Cough Most of the C pattern with both signals from the IMU and spirometer are detected correctly. There are 5 out of 100 C patterns missed with the IMU signal and 3 out of 100 with the spirometer signal.

Speaking Only 8 out of 144 S4 patterns with the spirometer signal are mis-detected as either QB or C, while 34 out of 144 with the IMU signal are mis-detected.

3.5 Discussion

3.5.1 Improvement of the Detection of SP patterns

The sample test showed that by adjusting proper thresholds for the MCCA, the accuracy of the detection of SP patterns can be increased. At the same time, the accuracy to detect QB and C patterns is remained. The decision flowchart can be differently functioned by adjusting the thresholds alone. For example, setting the threshold for the cross-correlation sub-system 0 can eliminate the function of this sub-system in the decision flowchart. The decision flowchart can also be adjusted by changing the priorities of the sub-systems in the tree structure.

3.5.2 MCCA Results with QB, C and SP patterns with the IMU and Spirometer Signals

The IMU results with the QB and SP patterns are not as good as the results with the spirometer signal. This can be caused by the inaccurate signals recorded by the IMU device, due to loose attachment. This explanation can be verified by the fact that the results with the IMU signal during the C activities are as good as the result with the spirometer signal. As discussed in the previous section, C signals are more likely to be recorded accurately by the IMU device because this activity allows strong movement of the abdomen, avoiding errors caused by the loose attachment of the IMU at the abdomen.

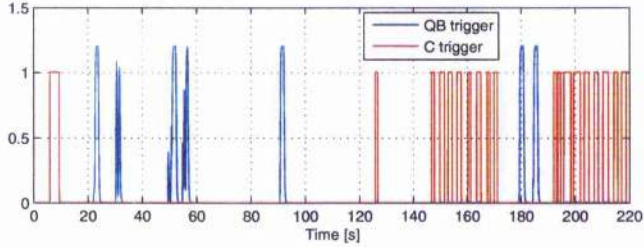
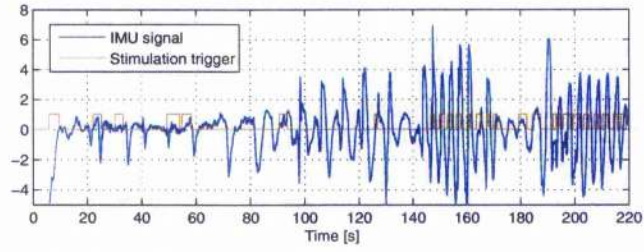
On the other hand, most of the results with the spirometer signals show that the MCCA is able to distinguish QB, C and SP patterns. At the beginning of each detected QB or C activities, the system generates the stimulation trigger accordingly.

The results with data sets ii-2 with subject 01 are shown in Figure 3.17. This is a typical result during the tests. It shows that some of the QB patterns of the IMU signal are not detected as they are recorded inaccurately. On the other hand, the IMU signal during the C activity is recorded accurately. Hence, they are more likely to be detected. The result with the IMU signal also shows four false QB detections during the SP patterns.

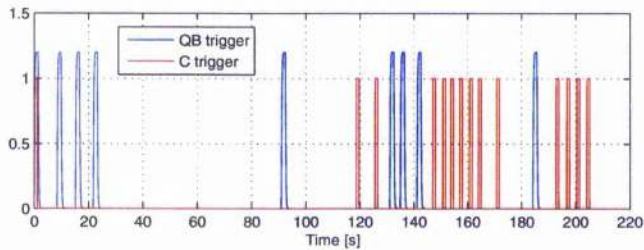
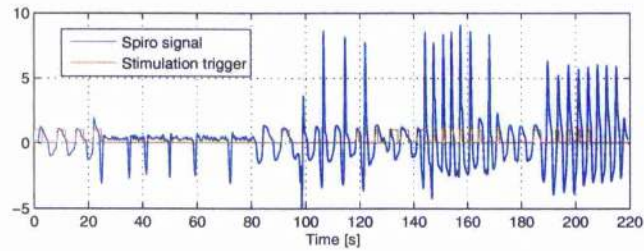
3.5.3 Result with DB and SC patterns with the Signals from the Sensor Experiment

As shown in Figure 3.17, SC and DB patterns are not detected correctly. Most of the DB patterns, with both signals, are detected as cough. Neither the QB nor C pattern during the SC activities are detected correctly.

DB The signals during the DB pattern with this subject is similar to the C pattern. While the DB pattern shares most of the distinctive characteristics of the C pattern, such as high inspiratory magnitude and its derivative, the MCCA tends to detect DB as C pattern.



(a) The results with the IMU signal.



(b) The results with the spirometer signal.

Figure 3.17: The results with data set ii-2 with subject 01. Note that the C activities are from 140s to 170s and the DB activities are from 190s to the end. In the bottom figures, the magnitude of the trigger signal for QB patterns is set to 1.2 and that for C patterns is set to 1 to distinguish them. The stimulation trigger in the upper figures show either the trigger signal for the QB or C pattern, along with the breathing signal.

SC With the threshold of the derivative of the inspiratory flow, it is found that the threshold crossing happens during the expiratory phase of the C pattern, not the inspiratory phase. This causes that the QB pattern after a C pattern be recognised as SP pattern. Meanwhile, the C pattern is not detected as

the threshold of the derivative of the inspiratory signal is not passed.

These two breathing activities can represent the activities during the daily life. Solving these problems are therefore part of further work that is needed to improve the MCCS.

3.6 Conclusion

The MCCS is an enhancement to the BCS. Using more signal characteristics can improve the detection of QB, C and SP patterns. A sample test shows that by adjusting proper thresholds for the sub-systems which analyse different characteristics of the breathing signal, the MCCS increases the accuracy of detecting SP patterns dramatically, while retaining accuracy for detection of QB and C. By using different combinations of the sub-system results (using different thresholds or changing the tree structure), detections can be improved.

Tests are also carried out with acceptable data sets from both the IMU and spirometer device using the MCCS. The results show that the MCCS detects more accurately with the spirometer signals than the IMU signals. With the spirometer signals, the MCCS shows a good detection of the QB, C and SP patterns. The system needs to be improved for SC, DB and other breathing activities that can occur during daily life.

4 Implementation of the Automatic Control System Using a Graphical User Interface

The previous two chapters discussed two parts of the control system for FESAM: the acquisition of the breathing signal (Chapter 2) and the analysis of it (Chapter 3). In Section 4.2 of this chapter, the stimulator which receives the results of the multi-characteristic control system and generates the electrical stimulation accordingly is introduced.

These three parts of the control system are developed in the Simulink environment. The control and configuration of them need relevant knowledge of the software. In addition, the parameters which need to be configured are embedded in the Simulink blocks within the three parts of the system. Therefore, an interface is needed to configure the parameters of the entire system.

A graphical user interface (GUI) is created to integrate the three parts of the control system. Through the panels of this interface, the parameters of the three parts of the system can all be configured graphically. A graphical viewer on the interface panel can also show the acquired breathing signal and the corresponding stimulation in real-time.

The interface of the automatic control system is designed in such a way that every parameter that is related to the stimulation can be accessed on the panel.

When the GUI is initiated, the Simulink models of the whole system are hidden, and only panels of the GUI are visible. People who use this interface don't need to have detailed knowledge of MATLAB or Simulink. For example, medical staff can get access to the control of the system easily through the GUI.

This chapter firstly introduces the structure of the entire automatic control system. The relationships between the three parts of the system and the GUI are also discussed. Then the stimulator part of the system and the GUI are introduced.

4.1 Structure of the Automatic Control System for FESAM

As shown in Figure 4.1, the automatic control system consists of three sub-systems. The first sub-system acquires the breathing signal. As discussed in Chapter 2, the breathing signal can be acquired by either the IMU device or the spirometer in real-time. The system is designed in such a way that the breathing signal can also be loaded from acquired signal files for offline analysis. Adding this feature to the GUI is needed for testing and configuring the system. The analysis of the breathing signal loaded from acquired signal files is therefore not in real-time.

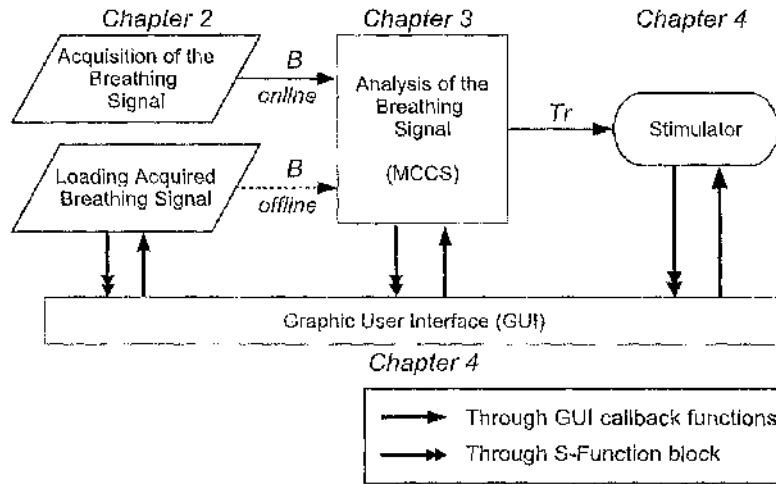


Figure 4.1: Illustration showing the three sub-systems of the automatic control system for FESAM and a graphical user interface (GUI) which configures the system parameters and shows system results. The breathing signal B can be acquired by either the IMU or the spirometer in real-time (online), or be loaded from an acquired signal file (off-line). The interaction between the GUI and the sub-systems are implemented by the GUI callback functions and a S-function block, which are indicated by the arrows in the figure. Refer to the following sections for details.

The breathing signal B is analysed to determine the current breathing activities. The sub-system which analyses breathing signals is discussed in Chapter 3 as the multi-characteristic control system (MCCS). The characteristics of the breathing signal are analysed through a flowchart structure. The output of the analysis is a binary trigger signal (Tr) which indicates when stimulation is allowed. This trigger signal is the logical disjunction of the results of the decision flowchart $Q_B(k)$ and $C_B(k)$, i.e. $Tr = Q_B(k) \vee C_B(k)$. The trigger signal Tr has a certain length as described in Section 3.1.1.

The stimulator delivers electrical stimulation to the abdominal muscles when the trigger signal $Tr = 1$. Pulse width and the start of the stimulation are designed to be manually adjustable for safety reasons. The parameters of the stimulation are configured in the stimulator sub-system.

All the parameters of the automatic control system can be configured through a graphical user interface. This interface also controls the start of the acquisition and analysis. A graphical viewer is embedded in the main panel showing the acquired breathing signal along with electrical stimulation generated by the stimulator. The GUI controls the sub-system through the GUI callback functions from the Simulink, whilst the online results of the sub-systems are transferred to the GUI through a S-function block.

The first two sub-systems of the automatic control system are discussed in Chapter 2 and 3. The following section introduces the stimulator system.

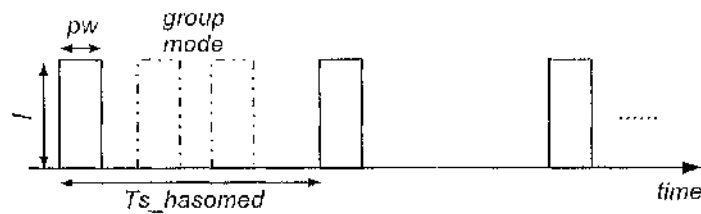


Figure 4.2: The electrical stimulation delivered by the stimulator at one channel. I denotes the current. pw denotes the pulse width. $Ts_hasomed$ denotes the interval between each pulse. The pulses with dash dot lines indicate the grouped pulses when the mode of the stimulator at this channel is set as group mode.

4.2 The Stimulator System

The stimulator delivers electrical stimulation to the abdominal muscles. Multiple channels are used for the FESAM. For each channel, three parameters are needed before the stimulation. They are the current, pulse width and mode for the stimulation.

As shown in Figure 4.2, the current I and pulse width pw relate to the strength of each pulse of the electrical stimulation. Increasing any of them will strengthen the simulation. The mode of the stimulation for each channel can be set as group pulse or single pulse. With the group mode, grouped pulses will be delivered. The interval of the grouped pulses needs to be set in this mode. The interval between each pulse in the single mode or each grouped pulses in the group mode also needs to be set before the stimulation. This interval is denoted as $Ts_hasomed$.

The current and mode for each channel of the stimulation are set constant during stimulation. The pulse width of the stimulation is designed to be adjustable during the stimulation manually. In this way, the stimulation can be stopped or adjusted manually if accident happens. An extra manually controlled switch is also used to start the stimulation delivery for safety reasons. The stimulation is only delivered when this switch is on.

The manual control of the pulse width and the start of the stimulation can be realised either by GUI items on the GUI panel or a DAQ card with a throttle and button. In this thesis the latter is used.

The following hardware section discusses the setup of the stimulator and the DAQ card. The software section later discusses the setup of the configurations of the stimulator system in the Simulink environment.

4.2.1 Hardware

The connection of the PC, stimulator and the DAQ card of the stimulator system is illustrated in Figure 4.3. The stimulator and the DAQ card are connected to the PC via USB.

The stimulator (RehaStim, HASOMED GmbH, Germany, shown in Figure 4.4) for the electrical

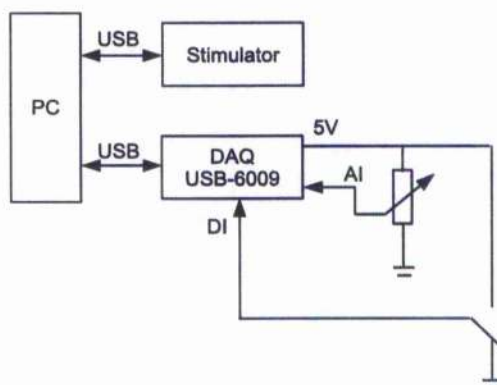


Figure 4.3: The connection of the PC, stimulator and the DAQ card of the stimulator system. The analog input (AI) of the DAQ is realised by a throttle device, whilst the digital input (DI) is realised by a button. The default position of button is shown in the figure (DI=0).



Figure 4.4: The front and rear view of the stimulator (RehaStim, HASOMED GmbH, Germany). Adapted from <http://www.rehastim.de/>.

stimulation has 8 isolated stimulation channels. The electrical current of each channel can be set between 0 and 126mA. Pulse width of the current can be set from 20 to 500 μ s. The frequency range of the stimulator is from 1 to 140Hz.

A DAQ card (DAQ USB-6009, National Instruments, Texas, USA) is used to control the start and the pulse width of the stimulation. The DAQ card has an analog and digital input, and is connected to a PC via USB port, as shown Figure 4.3. The analog input is realised by a throttle, and the digital input is realised by a button. The default position of the button is shown in the figure. In this position, the digital input is 0 (DI=0).

4.2.2 Software

The stimulator and DAQ card are implemented by a stimulator system realised in the Simulink environment, as illustrated in Figure 4.5.

In this stimulator system, the current for four channels (I_1 – I_4) and the pulse mode are held constant

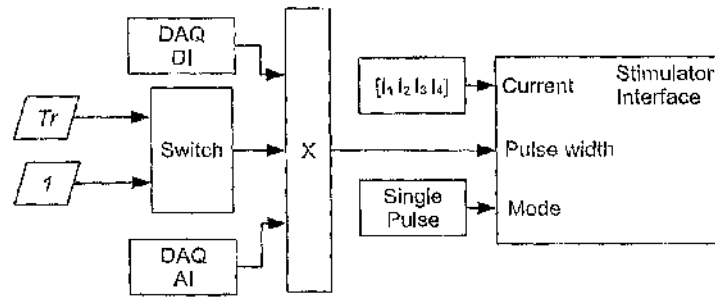


Figure 4.5: Illustration showing the stimulation system which implements the DAQ control and the stimulator interface. The pulse width input for the simulator is the product of three values. The DAQ DI only allows stimulation when the button is pressed. The DAQ AI is controlled by a throttle, and can be changed manually. The switch block chooses the trigger source. When the switch chooses constant 1, the stimulation is completely triggered manually. The current inputs (I_1, I_2, I_3, I_4) are configured by the GUI.

during stimulation. The pulse width of the stimulation is a product of three values shown in the figure. As the default DAQ DI value is 0, the stimulation is only triggered when the button is pressed, i.e. $DI=1$. The switch value is controlled by the GUI either to be the MCCS result Tr or constant 1. When the switch chooses constant 1, the stimulation is completely controlled manually: the electrical stimulation will be generated with the pulse width set by the throttle (DAQ AI) when the DI button is pressed. If the switch chooses signal Tr as the trigger source, the stimulation is generated when $Tr = 1$ with the pulse width of the value of DAQ AI.

The “Stimulator Interface” block is a Simulink mask. Its Simulink interface and parameters are shown in Figure 4.6. The first four parameters (Sample Time, Serial Port, Channels, Main Time) need to be configured before stimulation. Sample time is only for the interface block, not necessarily for the stimulation. The serial port is the port number to which the stimulator is connected to PC. As the stimulation for the control system requires 4 channels, the parameter of channels are set accordingly. The currents of these 4 channels are denoted as I_1, I_2, I_3 and I_4 in Figure 4.5. The main time parameter is the sample time of the stimulation (stimulator), which is the parameter $Ts_hasomed$ shown in Figure 4.2. Note that $Ts_hasomed$ is in *second*, therefore it is multiplied by 1000 to be in *millisecond*. The parameter “Group Time” is needed in the “Group Pulse” mode. The last two parameters can change the frequency of desired channel. They are not used in this control system.

As introduced in the beginning of this chapter, the parameters of the stimulator sub-system can be configured visually by a GUI. With this GUI, the mask parameters of the “Stimulator Interface” block can be configured without opening the mask parameter interface as shown in Figure 4.6. The GUI can also directly set the current for each channel (I_1-I_4) and realise the switch which allows the MCCS result Tr to be the trigger source.

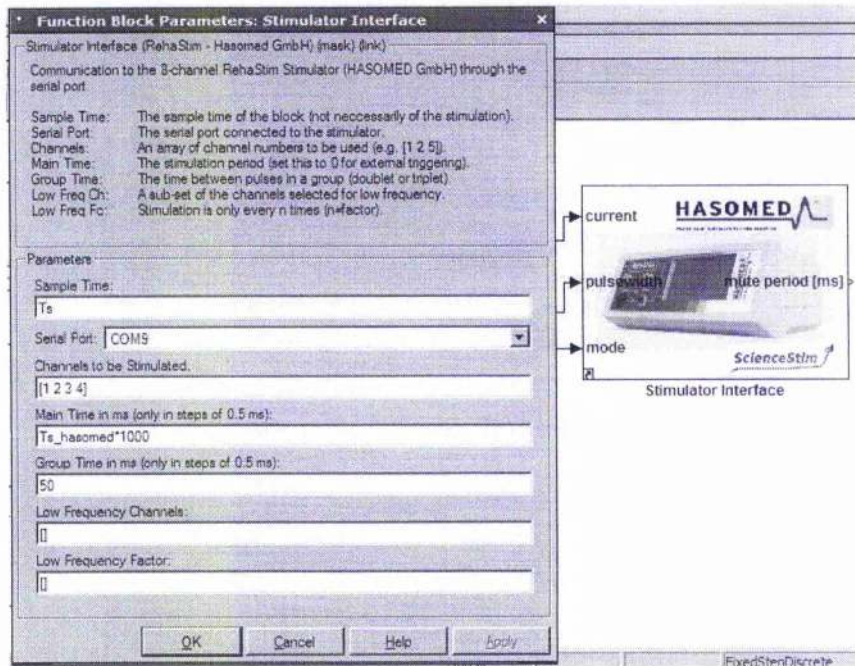


Figure 4.6: The Simulink interface of the stimulator. This interface is a mask structure in Simulink. The mask parameter is shown in the panel on the left. Sample time, Serial Port, Channels and main time are the main parameters that need to be configured. Only 4 channels are used in this system. The sample time and main time parameters T_s and $T_{s_hasomed}$ are both controlled by the GUI of the system.

4.3 The Graphical User Interface (GUI) of the Automatic Control System

The graphical user interface (GUI) of the system controls the stimulation and all the parameters of the system. The main panel of the GUI shows the result of the breathing signal along with the stimulation. Its configuration panel can be activated by a button in the main panel. In the configuration panel, all the system parameters can be configured. The breathing signal can be set to be acquired in real-time (online) or loaded from a local file (offline). At this stage, the spirometer device is implemented to be the source of the breathing signal in real-time.

The GUI has been designed using the Matlab GUI layout editor GUIDE. A GUI consists of two files: one is a *fig* file which has the graphical information of the panel; the other one is a *m* file which controls every callback of the graphical components on the panel.

4.3.1 The Main Panel of the GUI

The main panel of the graphical user interface (GUI) of the system is shown in Figure 4.7.

The popup menu on the top left can change the source of the breathing signal. When the popup menu is set to load the acquired breathing signal from a local file, the “Load” button below it will

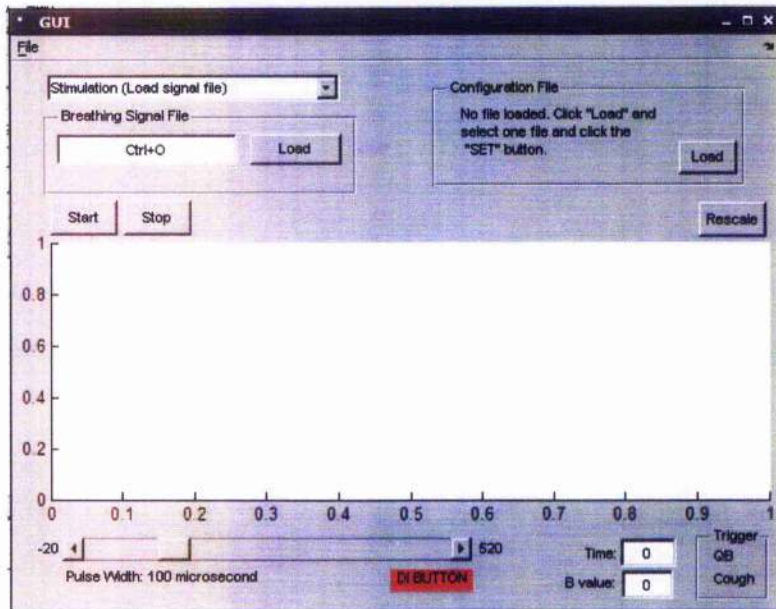


Figure 4.7: The main panel of the GUI of the automatic control system.

be activated. If the data is selected to be acquired in real-time, the GUI will activate the acquisition sub-system of the spirometer or IMU.

All the system parameters can be set by pressing the “Load” button on the top right in the “Configuration File” sub-panel. The configuration panel of the GUI will be activated. This panel is discussed in the next section.

The throttle values (DAQ AI) are shown in the bottom left part of the main panel. The DI button status is indicated by the “DI BUTTON”. When the button is pressed, the background of the button changes from red to green. The slider on top of the DI BUTTON shows the present value of the pulse width which is set by the throttle manually. The maximum value of the pulse width can be adjusted in the configuration panel.

The “Start” and “Stop” button in the middle of the panel starts or stops the automatic control system. When the system is started, the breathing signal will be displayed on the viewer in real-time. The text boxes “Time” and “B value” in the bottom right indicate the values of the stimulation time and the breathing signal value. As shown in Figure 4.8, the breathing signal segments where QB stimulation is delivered are displayed with red lines, while the segments where C stimulation is delivered are displayed with black lines. The font colors of the trigger indicator in the “Trigger” sub-panel in the bottom right also change when stimulation is generated.

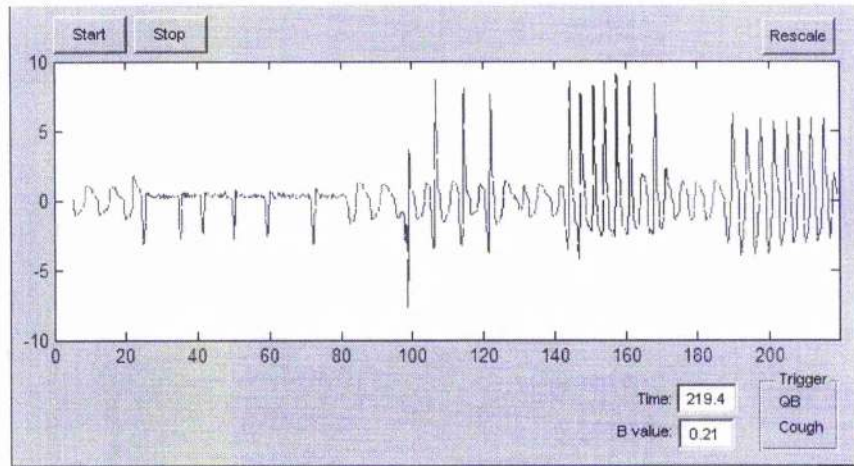


Figure 4.8: The graphical viewer after an offline simulation using a local breathing signal file. The breathing phases which are triggered for QB patterns are drawn in red, and the phases which are triggered for cough pattern are drawn in black. The “Trigger” sub-panel in the bottom right also indicates the stimulation trigger by changing the corresponding font color in real-time.

4.3.2 The Configuration Panel of the GUI

The configuration panel of the GUI is shown in Figure 4.9. During the system testing in Chapter 3, it was found that the system parameters for individual subject can be hold constant, while parameters need to be re-configured for different subjects. The configuration panel is therefore designed to be able to save all the parameters to a local *mat* file. By this feature, different sets of parameters can be specifically saved and loaded for different subjects. The left column of the panel shows the interface dealing with the configuration files. The files can be loaded in the “file list” window. After the loading, pressing the “SET” button changes all the present parameters of the system to the values from the configuration file. The SET button is added to allow adjustment to the parameters loaded from configuration files. For example, after a configuration file is loaded, the parameters can still be adjusted by the sliders. The real parameters in the Simulink model are only changed when the SET button is pressed.

The middle column of the panel controls the six thresholds for the MCCS. The details of the MCCS are discussed in Chapter 3. The parameters can be adjusted either by dragging the slider or typing specific values in the text boxes.

The settings for the stimulator are listed in the right column of the panel. The electrical current of the four channels can be adjusted individually either by dragging the sliders or typing values in the text boxes. The values in the “Pulsewidth Weights” are gains for the pulse widths of the four channels. The “Maximum Pulsewidth” text box configures the maximum pulse width that the throttle can achieve. This value corresponds to the maximum value of the slider in the main panel. The two

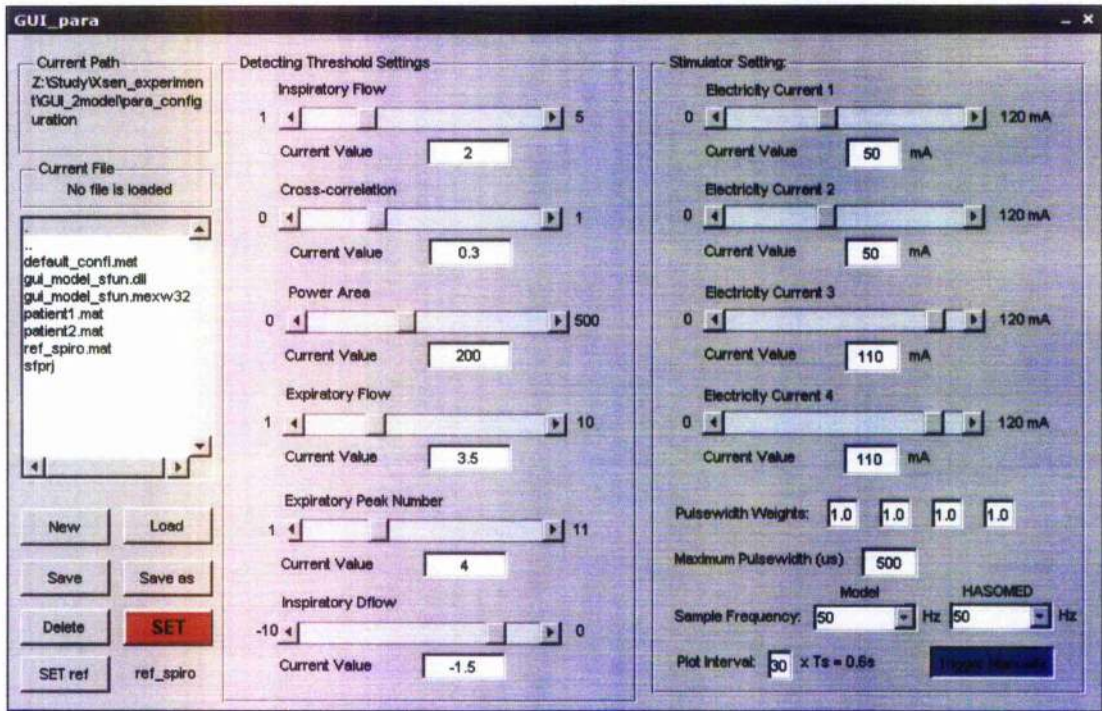


Figure 4.9: The configuration panel of the GUI.

popup menus below set the sample frequencies of the model and the stimulator. The “plot interval” sets the drawing intervals of the graphical viewer in the main panel. This is discussed in detail in Section 4.4. The bottom right button “Trigger Manually” is the switch illustrated in Figure 4.5 which allows the stimulation to be generated according to the system result Tr or manually.

4.4 Integration of the GUI with the MCCS Simulink System

The display window on the main panel of the GUI (shown in Figure 4.8) shows the system results in real-time. The Simulink scope is able to show the result in real-time in the system model, but it is not possible to be embedded it in the panel. The idea of designing the GUI is to hide the whole Simulink model of the system, while using only the GUI panels to control and configure the whole system. Therefore, a real-time viewer (scope) is embedded in the main panel of the GUI. This scope is updated in real-time by a Simulink S-function block. This S-function block also reads parameters from the stimulator system and the breathing signal in real-time, as shown in Figure 4.1.

An S-function is a computer language description of a Simulink block [82]. S-function allows customised functions in a Simulink model. In this study, an S-function is added in the system model which reads the system results and updates the scope in real-time. The flowchart of this S-function is shown in Figure 4.10.

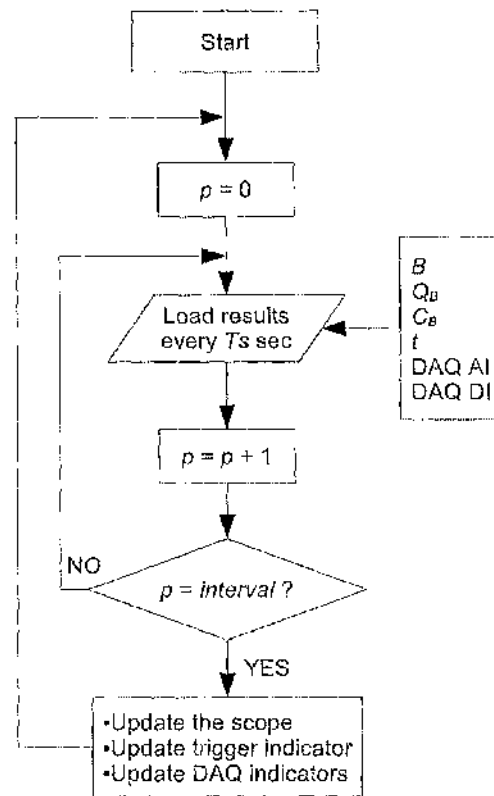


Figure 4.10: Flowchart showing the work flow of S-function block which updates the scope on the main panel of the GUI in real-time. p is a pointer. $interval$ is the parameter which allows the S-function to update the scope in every $interval \times Ts$ seconds. As shown in Figure 4.9, the $interval$ is set 30, so that the scope is updated every 0.6s. The S-function block reads six system results every Ts seconds, which can be adjusted by programming the S-function. The system results are the breathing signal (B), trigger signals for QB and C (Q_B and C_B), present time (t), the throttle value (DAQ AI) which controls the pulse width of the stimulation and the button status (DAQ DI) which allows stimulation. They are all represented in the main panel of the GUI.

The S-function block is inserted in the MCCS system model. When the model starts, the S-function block reads the necessary system results every Ts seconds in real-time. This time interval Ts can be customised in the S-function script. The indicators of the pulse width (DAQ AI), the DI button (DAQ DI), the trigger signals for QB and Cough, and the time and B values on the main panel of the GUI are updated by the S-function. It is found that the system tends to run slowly when the indicators and the scope are updated every Ts seconds, as Ts is set as 0.02s. A plot interval parameter is therefore added, as shown in the bottom right of Figure 4.9. By comparing the pointer p and the interval value, the scope and indicators are only updated every $interval \times Ts$ seconds.

4.5 Conclusion and Further Work

The acquisition of the breathing signal (discussed in Chapter 2) and the control of the MCCA (discussed in Chapter 3) are implemented using a GUI with two panels.

Through the configuration panel of the GUI, the parameters of the acquisition, the MCCA and the stimulator can be set graphically. All the parameters can also be saved and loaded separately. The GUI can switch the modes between triggering the stimulation manually or according to the breathing activities detected by the MCCA.

The system results of the breathing signal, trigger signals for QB and C, pulse width and the status of the DI button are displayed on the main panel of the GUI in real-time.

The GUI is designed in such a way that all the controls and settings of the whole system can be accessed graphically through the two panels. This allows non-technical people (e.g. medical staff) to use the system. However the system needs the presence of MATLAB and Simulink. Further work is needed to transfer the GUI and the Simulink model into one independent system. Potential utilities to realise this include the Real-Time Workshop by the MathWorks, and the LabVIEW Simulation Interface Toolkit (National Instruments, Texas, USA).

5 Discussion

This thesis discussed the experiments (Chapter 2) which use an IMU sensor to detect abdominal movement to represent breathing signals. The experiments are based on the fact that the movement of the abdomen can represent different breathing activities. Previous studies used spirometer to measure the air flow at the mouth to represent breathing signals. Further discussion on the air flow at the mouth and the movement of the abdomen is presented in Section 5.1.

Breathing signals acquired by the sensor (either spirometer or IMU) are analysed by a control system which detects the breathing activities (quiet breathing, cough or speaking and others). This basic control system is enhanced in this thesis (Chapter 3). A multi-characteristic control system (MCCS) is developed to analyse multi-characteristics of the breathing signal. By using additional characteristics of the breathing signal, the accuracy of detecting certain breathing activities can be increased, while the accuracy of detecting other activities remained. There are some potential modifications to the MCCS which can further enhance the detection. They are discussed in Section 5.2.

In Chapter 4, a graphical user interface (GUI) which integrates the sensor, control and stimulator systems is discussed. The possibilities of making this GUI a stand-alone software is discussed in Section 5.3 in this chapter.

5.1 Further Physiological Discussion on the Movement of the Abdomen

A prerequisite for using an IMU device to detect breathing activities is that the abdominal movement synchronises the respiratory phase. The air flow at the mouth is conventionally used to represent the respiratory status. In this study, a spirometer is used to record the air flow at the mouth. The breathing phases whose flow value are negative are considered as inspiration, and the positive flow value represents expiratory phases. The zero-crossing points of the spirometer signal are considered as the onsets of inspiratory and expiratory phases. The IMU device recorded the abdominal movement (AM). Similarly, the outwards AM (negative IMU signal) is considered to represent inspiratory phase, whilst the inwards abdominal movement indicates expiratory phase. In order to evaluate the ability of the AM to represent breathing activities, experiments with both the IMU and spirometer devices are conducted (Chapter 2). The phase-shift between the signals recorded by the IMU and the spirometer is evaluated.

It is found that although the phase-shift between the onsets of inspiration and expiration represented by the IMU and spirometer signal can be limited to within $[-0.5, 0.5]$ s, the timing of the onsets varies

depending on the breathing situation. This result can be explained by the causality of the air flow and the AM, as shown in Figure 2.36 on page 56. For neurologically intact people, the inspiration starts by the contraction of the diaphragm. The air flow and the AM are both results of the contraction. The expiratory phases of non-forced breathing starts by the recoil of the diaphragm. This recoil results in the air flow at the mouth and AM at the same time. The forced expiratory phases (such as cough and deep breathing), on the other hand, is driven by the contraction of the abdominal muscles. This contraction directly results in the AM, while the AIR is the result of the upwards movement of the diaphragm forced by the contraction of the abdominal muscles. In this case, the onsets of respiratory phases represented by the IMU signal precedes those represented by the spirometer signal.

As discussed in Section 2.3.3 on page 45, the analysis of the onsets of respiratory phases represented by both sensors corresponds to the causalities discussed in the previous paragraph. Most of the phase-shifts of the breathing onsets represented by the air flow and AM during the expiratory phase of coughing patterns are negative (Figure 2.26 on page 45). This indicates that the AM precedes the air flow during the expiratory phases of cough.

It is also found that there is no clear causal relationship between the AM and air flow represented by the phase-shift result during the expiratory phases of deep breathing. To investigate this, the habit of the usage of expiratory muscles should be noted. The word habit here refers to the frequency and timing of using different expiratory muscles with different people. It was observed during the recording that some subjects tend to move their chest wall during deep breathing. It is possible that these people tend to heavily use their intercostal muscles to facilitate the forced expiration. In this case, the air flow can be a direct result of the contraction of the intercostal muscles. The phase-shifts of the onsets represented by the two sensors therefore show no clear causal relationship.

The way different people use the abdominal muscles with different people can also be different. J. G. Martin and A. De Troyer have done an experiment to evaluate the role of the abdominal muscles in the adjustment to inspiratory mechanical loadings [83]. They tested 8 neurologically intact subjects, while seated and supine, during different loading breathings. The seated results show that two subjects used their abdominal muscles during the quiet breathing, while all others let the passive recoil of the lung dominate their quiet breathing. During mechanical loading breathing, the seated result shows different abdominal muscle recruitment. The rectus abdominis and external oblique abdominis were recruited separately or together. Also there are some cases where neither muscles was recruited. They found that one subject showed inward movement of the abdominal wall during inspiration. In addition, abdominal muscles can be trained to be used during quiet breathing as well. The relationship between the air flow and AM can therefore be complicated under these circumstances.

No matter how complicated the causality between the AM and air flow is, one advantage of using the AM to represent the expiratory onset of coughing over using the air flow is that the electrical stimulation is best applied before the movement of the abdomen. That is the stimulation trigger represented by the AM works better. Because in order to gain the necessary intra-abdomen pressure for cough, a short breath holding tends to appear at the beginning of the expiratory phase. While the

air flow can not represent this onset point as there is usually still a small amount of air sucked into the airway, the AM can represent this onset accurately. The electrical stimulation triggered by the AM detection can therefore be more effective and efficient.

5.2 Potential Modifications to the Multi-characteristic Control System (MCCS)

The main improvement of the MCCS over the basic control algorithm is the use of more characteristics of the breathing signal. At this stage, the MCCS can analyse six characteristics of the breathing signal. The added characteristics are some distinguishable characteristics of certain breathing patterns, such as the expiratory peaks which are distinctively high during speaking patterns.

As shown in Figure 3.14 on page 79, the MCCS has separate characteristic analysing sub-systems and a decision flowchart sub-system. The advantage of this structure is that the detection algorithm for different breathing patterns can be easily modified by changing the flowchart structure. When one characteristic of the breathing signal with an individual has distinctive ability to detect certain breathing patterns, this sub-system output can be given a higher priority in the flowchart. Similarly, any sub-system result can be ignored by deleting it in the flowchart when this characteristic is not distinctive with the individual.

By revising the structure of the flowchart, the MCCS can be changed back to the basic control algorithm. The MCCS can therefore be seen as an enhancement to the original system. With the structure of separate sub-systems and flowchart, the MCCS has potentials to be upgraded with analyses of more characteristics of the breathing signal. Moreover, the structure of the flowchart has the potential to be more accurate to detect different breathing patterns using more sophisticated algorithms.

5.3 Integration of the Sensor System, MCCS and Stimulator with the Graphic User Interface (GUI)

The structure of the MCCS is also designed to be conveniently connected with the graphical user interface (GUI) which implements the sensor system, MCCS and the stimulator. The aim of designing the GUI is to create a user friendly control panel with which all the parameters regarding the whole automatic control system can be configured. All the potential control of the whole system can be accessed via the panels of the GUI. In addition, the system results (the acquired breathing signal along with the generated stimulation) can be displayed on the GUI panel.

The ideal GUI for the automatic control system is a stand-alone software system which doesn't rely on the presence of MATLAB or Simulink. With the stand-alone software system, the application of the FESAM system can be more accessible by non-technical people. The requirement for the PCs and the expensive software can also be eliminated. Also with fewer unnecessary component of MATLAB and Simulink running, the control system should be running more stable and faster.

Potential tools for creating such a stand-alone software system are the Real-Time Workshop (The MathWorks, US) and the LabVIEW Simulation Interface Toolkit (LSIT), National Instruments, Texas, US.

The Real-Time Workshop generates and executes stand-alone C code for Simulink models. It could be complicated to generate C code of the MCCS as the Simulink model contains customised blocks for the sensor and the stimulator. There is also an S-function written in MATLAB m code in order to update the displays on the GUI main panel. Another issue of using the Real-Time Workshop is the integration of the GUI panel.

On the other hand, the LSIT seems to be more convenient for creating the GUI and transforming the model. The LSIT is designed to link between LabVIEW and the Simulink model directly – no programing code transfer is required. The GUI control for the Simulink model can be designed by the powerful LabVIEW user interface. However, the potential of generating the system without the presence of LSIT is not known.

6 Conclusion and Further Work

This thesis has discussed the three sub-systems of the automatic control system for functional electrical stimulation of abdominal muscles (FESAM): the sensor system, the multi-characteristic control system (MCCS) and the stimulator system.

The experiments for the sensor system mainly investigated the possibility of using an IMU sensor to detect breathing activities for the control system. The sensor for this application is required to be able to accurately represent the breathing activities in real-time. In previous studies, spirometer devices were used. Spirometer devices typically require a face mask. This can be uncomfortable for people who use this system for a long time. The usage of a face mask also restricts the daily life of patients.

During the experiment, the IMU device is attached to the abdomen. Consequently, the abdominal movement recorded by the IMU sensor is used to represent the breathing activity. In order to evaluate the ability of the IMU sensor to represent breathing activities, a spirometer device is also used during the experiment. Signals from both sensors are recorded at the same time in a Simulink model. The recorded signals from both sensor are first processed before evaluation. By normalising the signals, the average amplitudes of the signals during quiet breathing is in the range $[-1 \ 1]$. Using the normalised signals from both sensor, their respiratory onsets and amplitudes are analysed. The results show that although the causal relationship between the signals from the IMU and the spirometer is indistinct, the phase-shift of the onsets represented by the two signals can be limited to the range $[-0.5 \ 0.5]$ s. The ability of the IMU to detect different breathing activities is confirmed by analysing the amplitudes of the IMU signals during different breathing activities.

The breathing signal recorded by the sensor is analysed by a control algorithm which detects the present breathing activity. The basic control algorithm analyses the breathing signal and its derivative during inspiration to detect cough and uses a cross-correlation algorithm to detect quiet breathing. Based on this basic control algorithm, a multi-characteristic control system (MCCS) is developed to analyse multiple characteristics of the breathing signal. The MCCS has separated sub-systems which analyse signal characteristics and a decision flowchart to detect the current breathing activity. The detection algorithm can be adjusted by changing the structure of the flowchart. Different characteristics of the breathing signal can be set with different priority for detecting certain breathing patterns. By ignoring certain characteristic analysis, the MCCS can be reversed to the basic control algorithm. The MCCS is therefore an enhancement of the basic control algorithm.

The output of MCCS for the present breathing activity can be a trigger source for the stimulator

which delivers the electrical stimulation. To make the stimulation safer, the stimulator system is designed in such a way that the pulse length of the electrical stimulation and the start of stimulation are controlled manually by a throttle and button.

The sensor system, MCCS and the stimulator system are integrated by a graphical user interface (GUI). The interface is designed in such a way that all the parameters regarding the automatic control system can be configured visually. The results of the acquisition of the breathing signal and the stimulation delivered by the stimulator can also be displayed by the embedded graphical viewer on the main panel of the GUI. By using this GUI, no further knowledge of MATLAB and Simulink are required. The configuration of each parameter of the system can be easier and clearer. In addition, certain set of parameters can be saved into a local file, and be loaded when needed.

During the analysis of the experiment results with the IMU device, it is found that the attachment of the IMU at the abdomen is essential for the data recording. This is because that the IMU sensor is sensitive. The movement of the body can also be recorded by the IMU sensor. Detecting only the relative movement of the abdomen against the body by the IMU device is therefore a further work. Potential solution to this issue is to use two IMU devices. One device detects the absolute abdominal movement, whilst the other one detects the absolute body movement. The relative abdominal movement can therefore be obtained by subtraction of these two movement.

Future development of the MCCS includes selecting of signal characteristics and creating a more sophisticated decision flowchart. The aim of the future development is to improve the accuracy of the system to detect different breathing activities. By analysing more distinctive characteristics of the breathing signal, different breathing patterns are expected to be more distinguishable. On the other hand, the flowchart which uses the results of the analyses of the characteristics can be more sophisticated. At this stage, the flowchart uses a tree structure. A probability reference algorithm can be added to the flowchart algorithm. A probability table of all the sub-system results of the characteristics during certain breathing activities can be obtained by analysing the breathing signals during the same breathing activities. For example, the probability that the sub-system result of the FFT area is 1 during coughing activities is expected to be high. Before the flowchart reaches a final decision, the current sub-system results need to be compared with the reference table. The decision is confirmed only if a certain similarity of the current sub-system results with the reference is reached.

The GUI of the whole system is expected to be more intelligent in the future. At this stage, the GUI can not revise the structure of the decision flowchart in the MCCS. It can only change the thresholds for the characteristic sub-systems. More features on revising the flowchart structure with easy control are expected. For example, a check box can be added to each of the threshold. When the check box is checked, the sub-system result will not be analysed by the flowchart.

The experiments with the IMU sensor show that the IMU device is sensitive to the body movement. Therefore, using only one IMU sensor for the PESAM on daily base is impossible. The attachment of the IMU at the abdomen needs to be tight. The results from the tests using the automatic control system with both IMU and spirometer signals also show that the IMU signal less easy for the system

to detect breathing activities. However, the experiments show the potential of using an IMU sensor for the FESAM. By using additional IMU sensors, it is possible to remove the problem with the body movement. By further enhancing the MCCS and the GUI, the automatic control system for FESAM can be more accessible and applicable with the IMU sensor for daily life and outside a laboratory environment.

Appendix

A Original Data from the Experiments with IMU

All of the original and filtered signals from both the spirometer and IMU with 5 subjects are shown in this appendix. The signals from IMU and spirometer are filtered by a high pass and low pass filter respectively. Refer to Chapter 2 for the filter information. Note that there are some spirometer signals missing in the figures. That is because the spirometer turned itself off during the experiment. Note that the original IMU signals in the figures have offsets which are indicated in the legend. The offsets is added manually to make the original signals close to the filtered ones.

By observing the figures shown below, individual variation exists in the experiments with 5 subjects. This variation mainly occurs with the IMU signal, while the spirometer signal can correctly represent breathing activities with all the subjects.

The IMU signals with subject 01, 04 and 05 show some large distortions during different breathing activities, while the signals with 02 and 03 coincides with the spirometer signals.

The distorted signal recordings from subject 01, 04 and 05 are thought to be contributed to the attachment of the IMU device to the abdomen. Further details are discussed in Chapter 2.

A.1 Subject 01

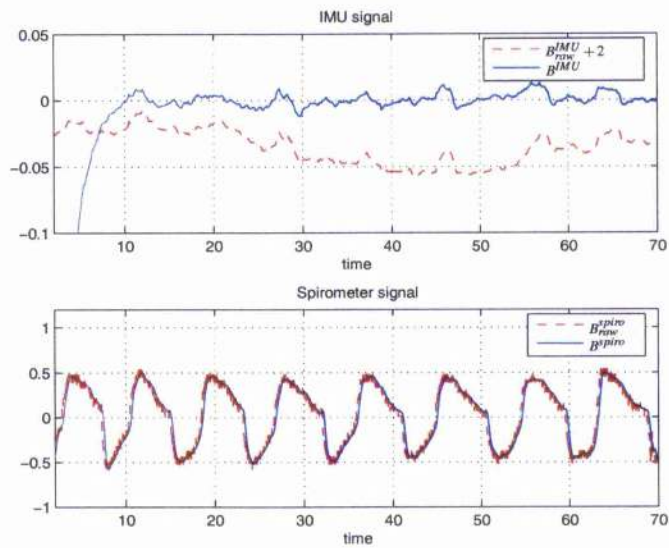


Figure A.1: Original and filtered signal of part i of the experiment with subject 01.

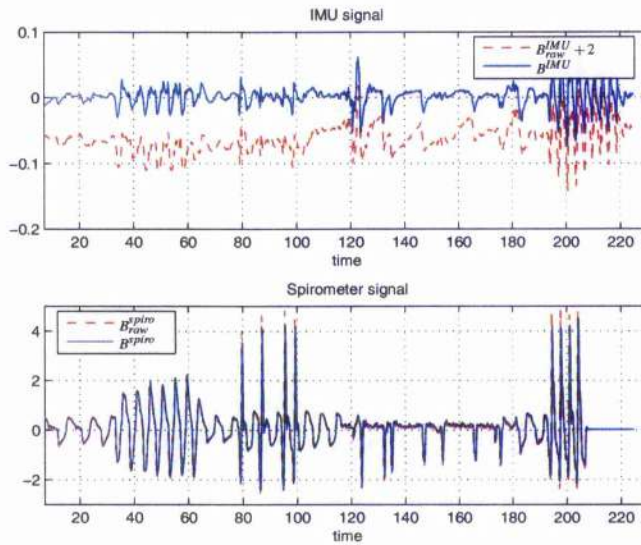


Figure A.2: Original and filtered signal of part ii-1 of the experiment with subject 01.

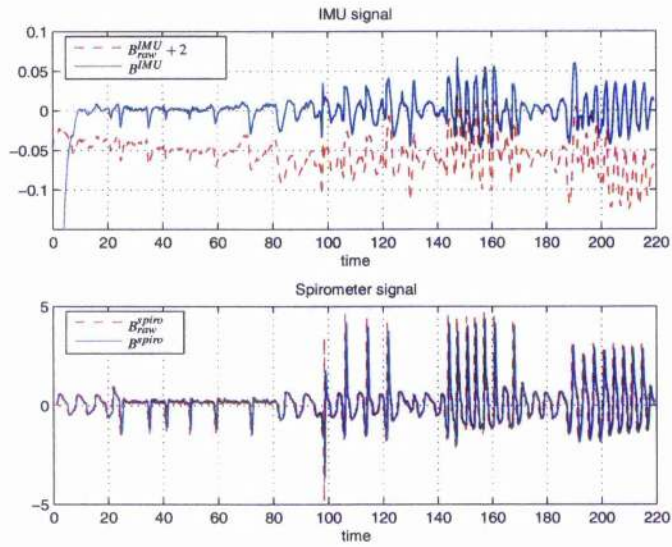


Figure A.3: Original and filtered signal of part ii-2 of the experiment with subject 01.

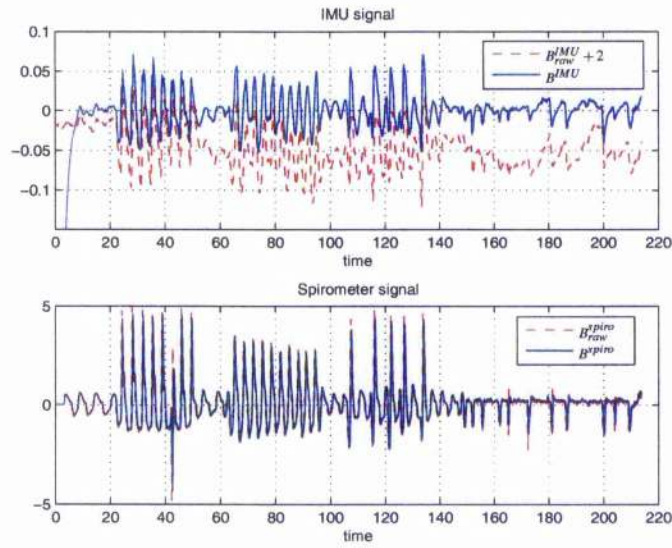


Figure A.4: Original and filtered signal of part ii-3 of the experiment with subject 01.

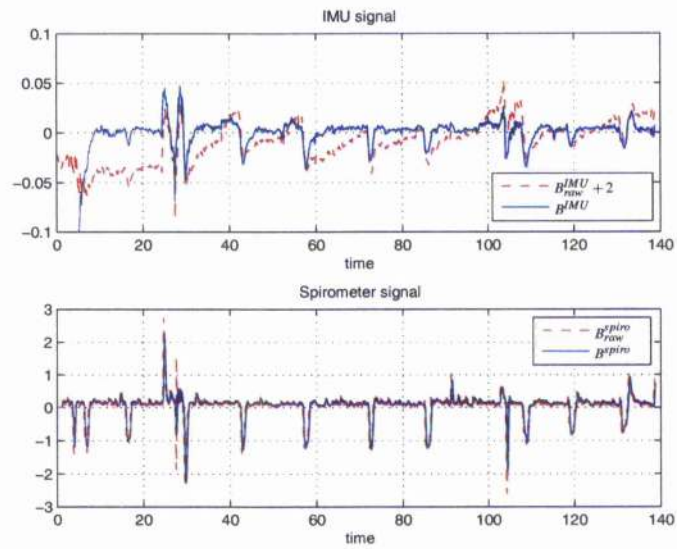


Figure A.5: Original and filtered signal of part iii of the experiment with subject 01.

A.2 Subject 02

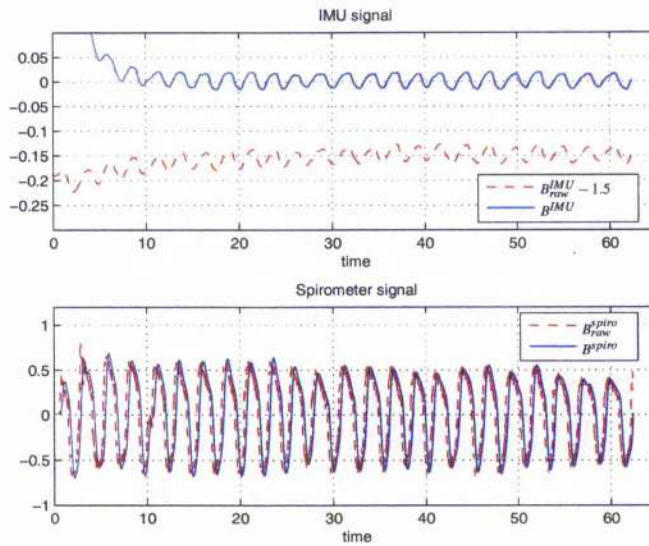


Figure A.6: Original and filtered signal of part i of the experiment with subject 02.

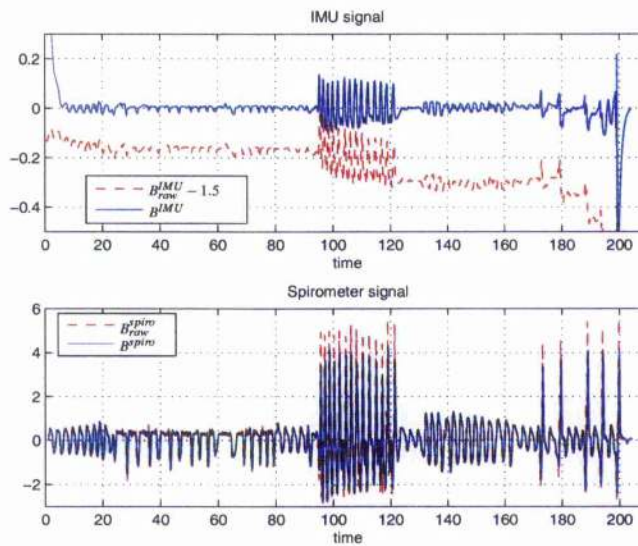


Figure A.7: Original and filtered signal of part ii-1 of the experiment with subject 02.

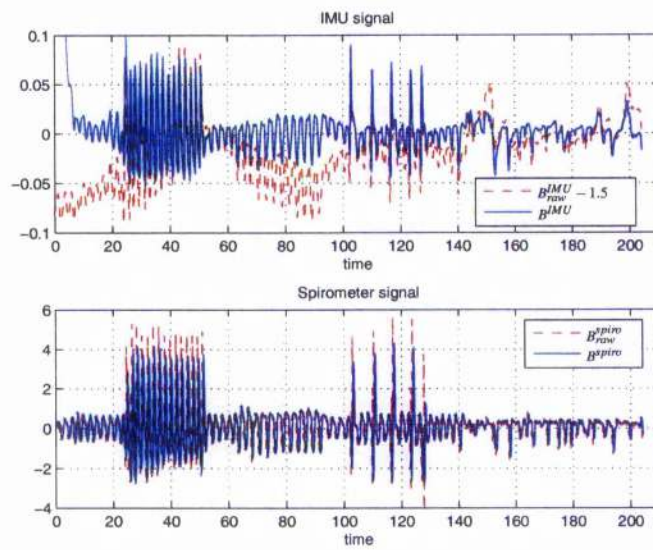


Figure A.8: Original and filtered signal of part ii-2 of the experiment with subject 02.

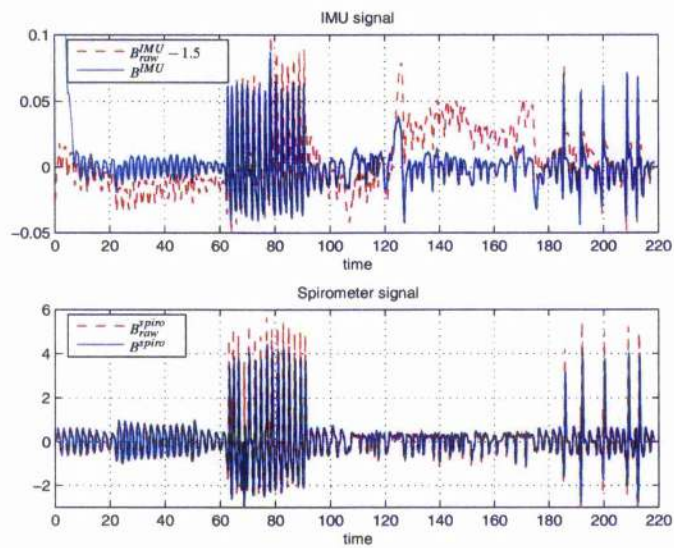


Figure A.9: Original and filtered signal of part ii-3 of the experiment with subject 02.

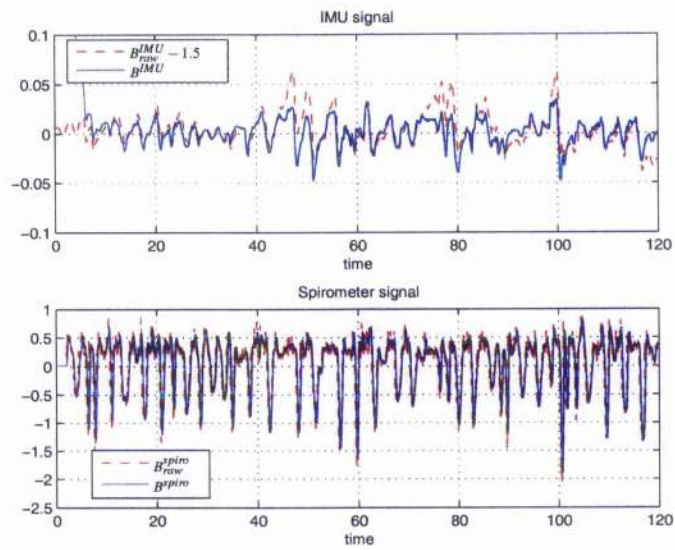


Figure A.10: Original and filtered signal of part iii of the experiment with subject 02.

A.3 Subject 03

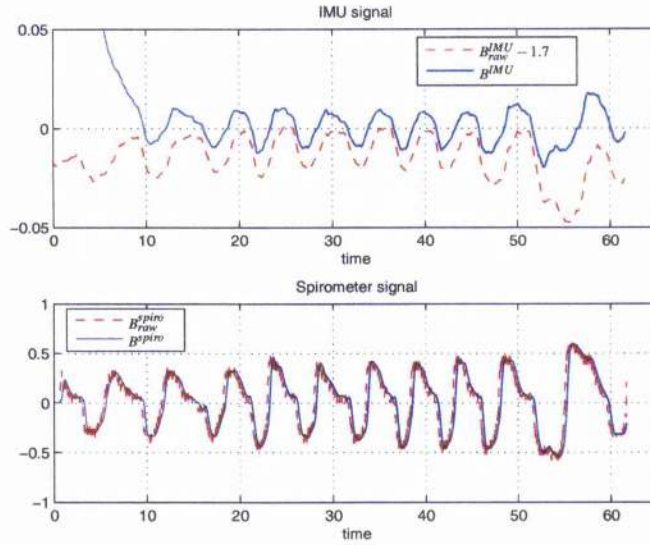


Figure A.11: Original and filtered signal of part i of the experiment with subject 03.

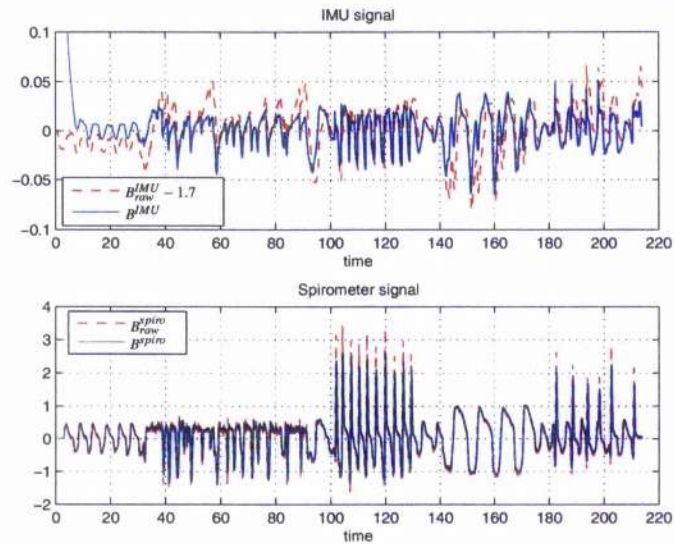


Figure A.12: Original and filtered signal of part ii-1 of the experiment with subject 03.

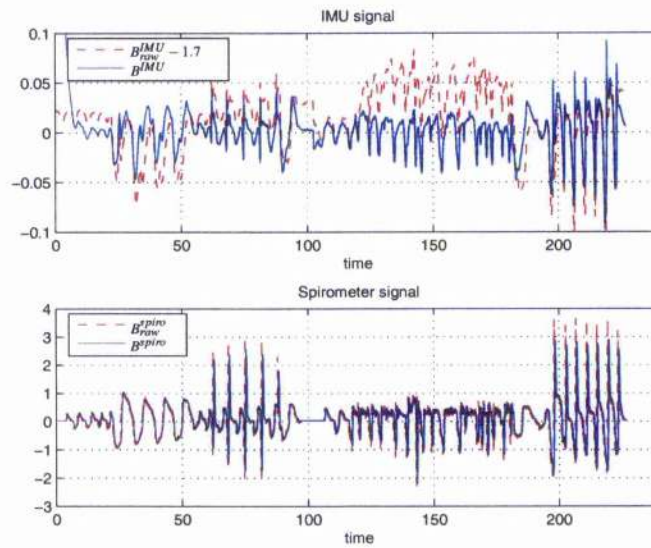


Figure A.13: Original and filtered signal of part ii-2 of the experiment with subject 03.

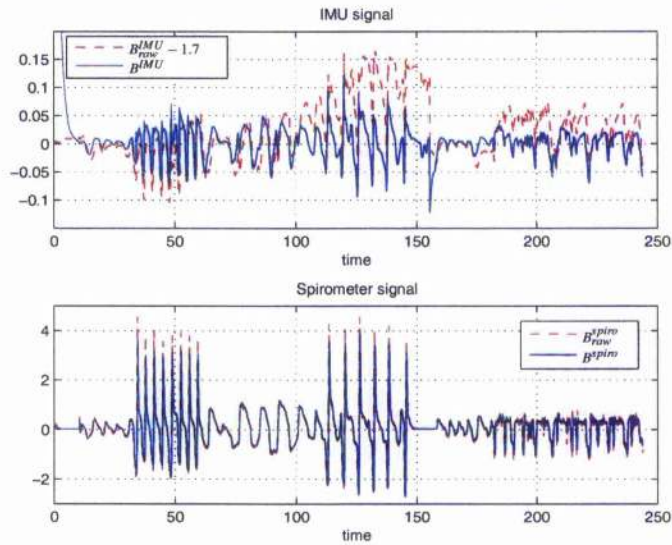


Figure A.14: Original and filtered signal of part ii-3 of the experiment with subject 03.

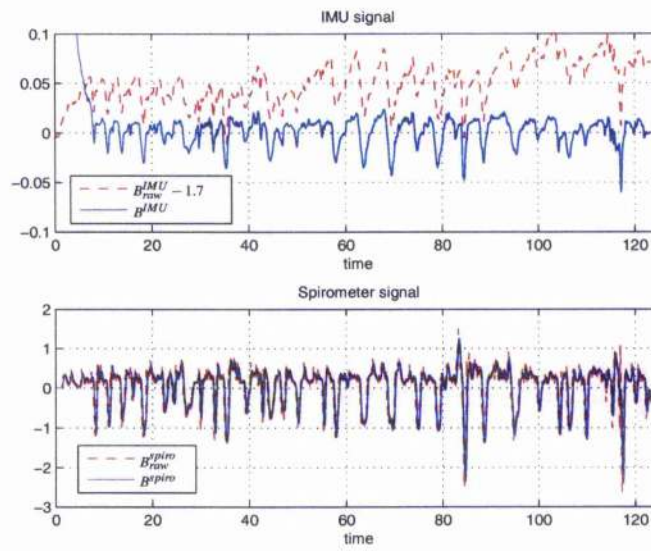


Figure A.15: Original and filtered signal of part iii of the experiment with subject 03.

A.4 Subject 04

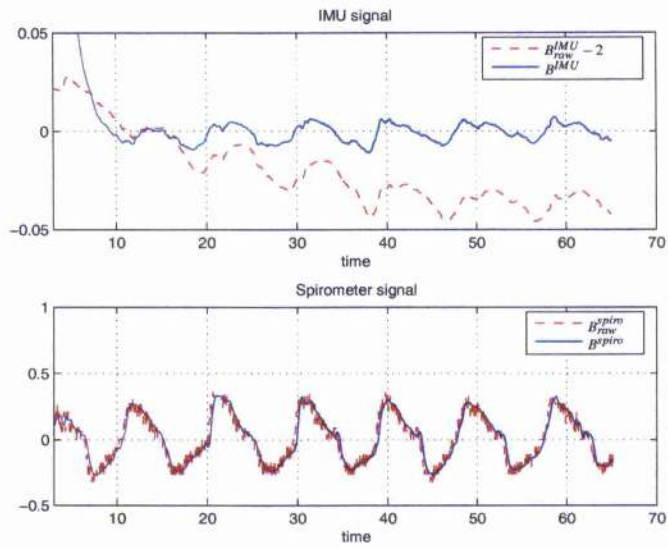


Figure A.16: Original and filtered signal of part i of the experiment with subject 04.

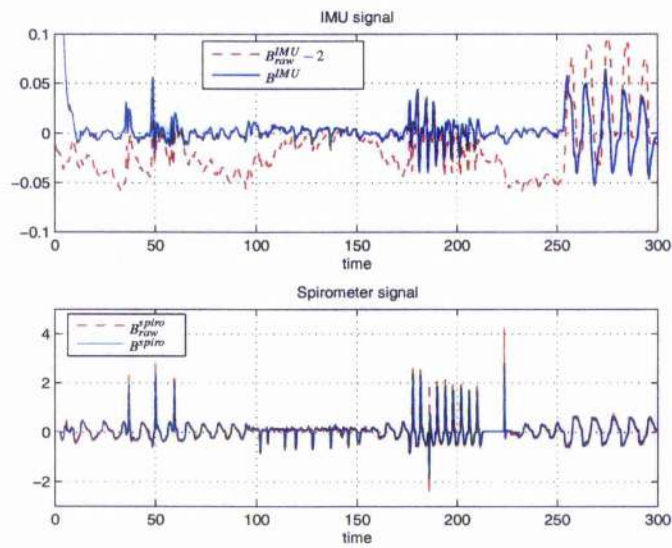


Figure A.17: Original and filtered signal of part ii-1 of the experiment with subject 04.

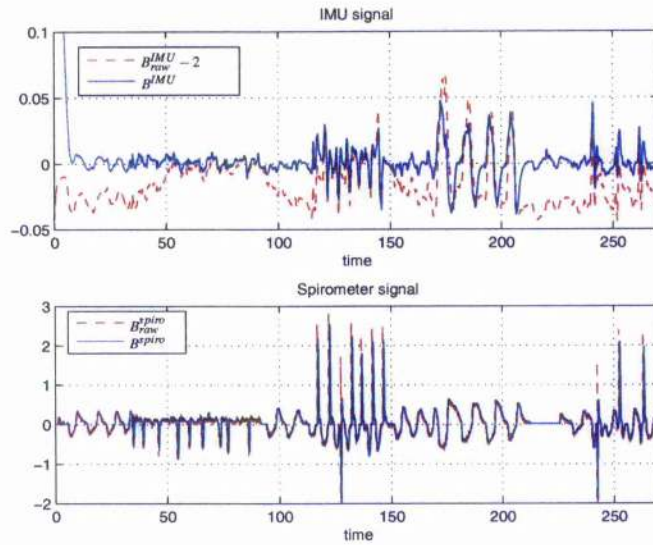


Figure A.18: Original and filtered signal of part ii-2 of the experiment with subject 04.

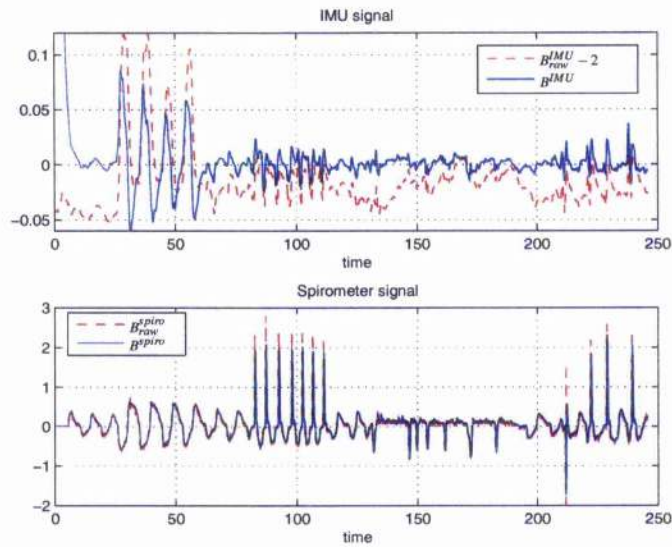


Figure A.19: Original and filtered signal of part ii-3 of the experiment with subject 04.

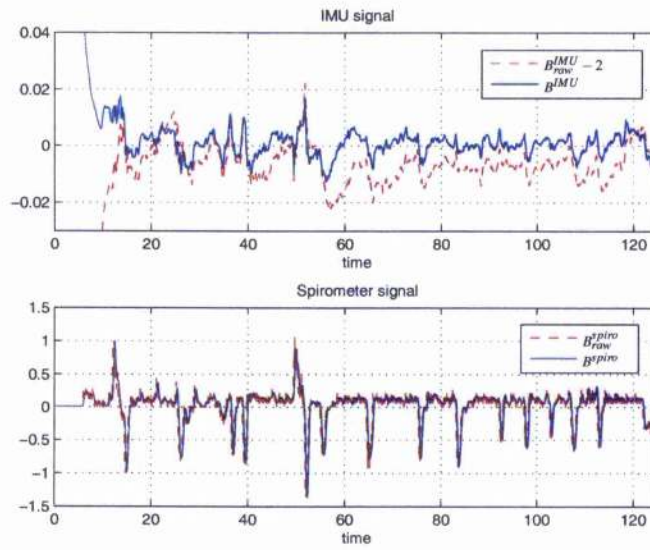


Figure A.20: Original and filtered signal of part iii of the experiment with subject 04.

A.5 Subject 05

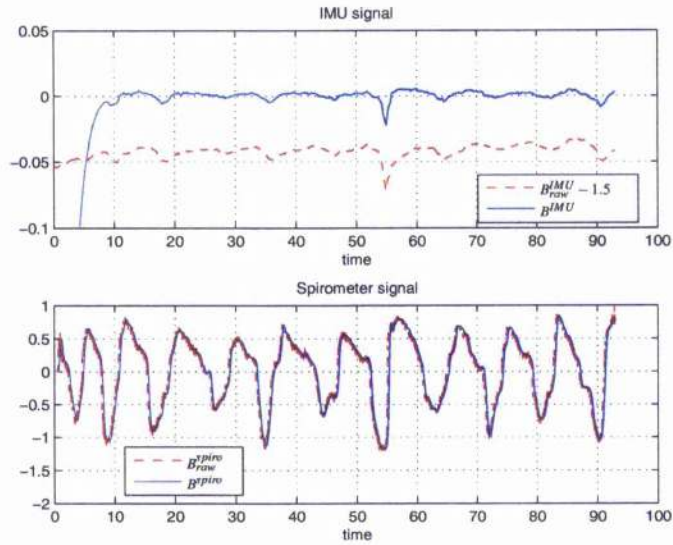


Figure A.21: Original and filtered signal of part i of the experiment with subject 05.

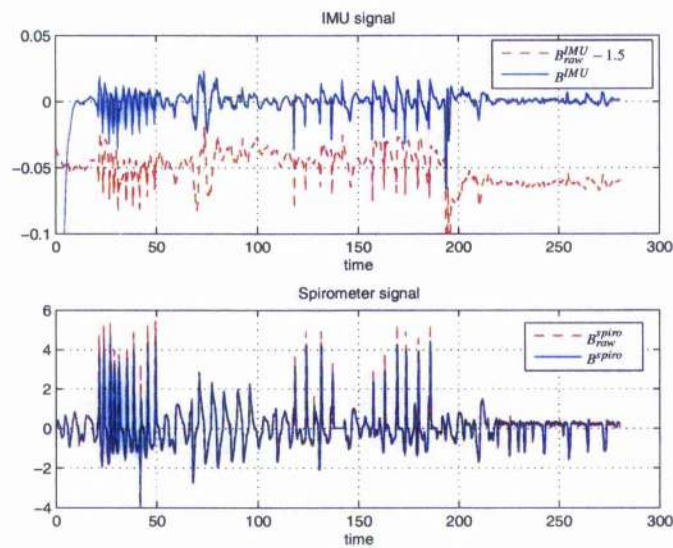


Figure A.22: Original and filtered signal of part ii-1 of the experiment with subject 05.

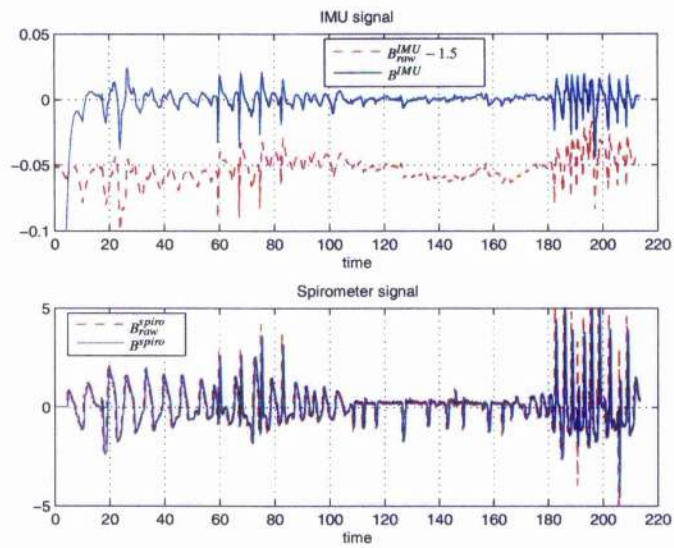


Figure A.23: Original and filtered signal of part ii-2 of the experiment with subject 05.

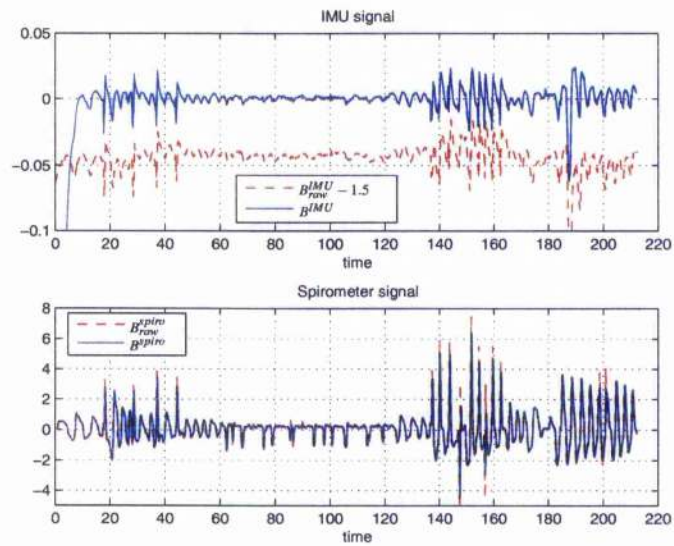


Figure A.24: Original and filtered signal of part ii-3 of the experiment with subject 05.

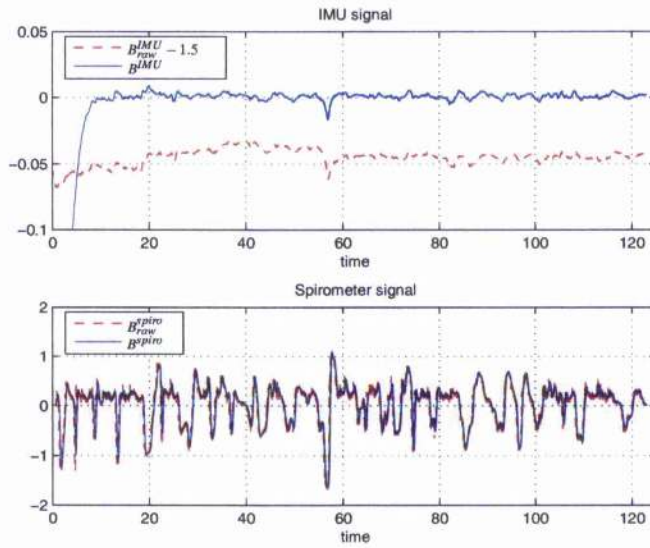


Figure A.25: Original and filtered signal of part iii of the experiment with subject 05.

B Abbreviations

Physiological Terms:

SCI	Spinal Cord Injury
CNS	Central Nervous System
PNS	Peripheral Nervous System

Respiratory Therapies:

MV	Mechanical Ventilation
DP	Diaphragm Pacing
FMS	Functional Magnetic Stimulation
FESAM	Functional Electrical Stimulation of Abdominal Muscles

Breathing Signal Acquisition:

EMG	Electromyography
ENG	Electroneurography
EEG	Electroencephalography
RIP	Respiratory Inductive Plethysmography
EGG	Electroglottography
IMU	Inertial Measurement Unit

Breathing Patterns:

QB	Quiet Breathing
C	Cough
DB	Deep Breathing
SP	Speaking
SC	Single Cough

Data Processing and Analysing:

IQR	Interquartile Range
-----	---------------------

FESAM Control System:

BOS	Basic Control System
MCCS	Multi-characteristic Control System
GUI	Graphical User Interface

Bibliography

- [1] J. Widdicombe and A. Davies, *Respiratory Physiology*. Edward Arnold, 2nd ed., 1991.
- [2] J. B. West, *Respiratory Physiology: The Essentials*. Lippincott Williams & Wilkins, 7th ed., 2005.
- [3] J. E. Cotes, M. R. Miller, J. Reed, D. Chinn, and L. Caplan, *Lung Function: Physiology, Measurement and Application in Medicine*. Blackwell Publishing Professional, 2006.
- [4] J. West, *Ventilation: Blood Flow and Gas Exchange*. Year Book Medical Pub, 1986.
- [5] C. Winslow and J. Rozovsky, "Effect of spinal cord injury on the respiratory system," *American Journal of Physical Medicine & Rehabilitation*, vol. 82, pp. 803–814, 2003.
- [6] M. L. Barr and J. A. Kiernan, *The Human Nervous System: An Anatomical Viewpoint*. J.B. Lippincott Company, 6th ed., 1993.
- [7] I. Bromley, *Tetraplegia and Paraplegia: A Guide for Physiotherapists*. Churchill Livingstone, 5th ed., 1998.
- [8] "Centre for Rehabilitation Engineering at Glasgow University." Website. <http://fesnet.eng.gla.ac.uk/CRE/>.
- [9] "Cleveland FES center." Website. <http://fescenter.case.edu/>.
- [10] J. O. Teeter, C. Kantor, and D. L. Brown, *Functional Electrical Stimulation Resource Guide for Persons with Spinal Cord Injury or Multiple Sclerosis*. FES Information Center, 1995.
- [11] D. J. Ewins, P. N. Taylor, S. E. Crook, R. T. Lipczynski, and I. D. Swain, "Practical low cost stand/sit system for mid-thoracic paraplegics," *J Biomed Eng*, vol. 10, pp. 184–188, Apr 1988.
- [12] R. J. Jaeger, "Design and simulation of closed-loop electrical stimulation orthoses for restoration of quiet standing in paraplegia," *J Biomech*, vol. 19, no. 10, pp. 825–835, 1986.
- [13] A. R. Kralj and T. Bajd, *Functional Electrical Stimulation: Standing and Walking after Spinal Cord Injury*. CRC Press, 1989.
- [14] G. Khang and F. E. Zajac, "Paraplegic standing controlled by functional neuromuscular stimulation: Part ii—computer simulation studies.," *IEEE Trans Biomed Eng*, vol. 36, pp. 885–894, Sep 1989.

- [15] G. Khang and F. E. Zajac, "Paraplegic standing controlled by functional neuromuscular stimulation: Part i—computer model and control-system design.," *IEEE Trans Biomed Eng*, vol. 36, pp. 873–884, Sep 1989.
- [16] K. J. Hunt, H. Gollee, R. Jaime, and N. Donaldson, "Feedback control of unsupported standing.," *Technol Health Care*, vol. 7, no. 6, pp. 443–447, 1999.
- [17] H. Gollee, K. J. Hunt, and D. E. Wood, "New results in feedback control of unsupported standing in paraplegia.," *IEEE Trans Neural Syst Rehabil Eng*, vol. 12, pp. 73–80, Mar 2004.
- [18] D. J. Pons, C. L. Vaughan, and G. G. Jaros, "Cycling device powered by the electrically stimulated muscles of paraplegics.," *Med Biol Eng Comput*, vol. 27, pp. 1–7, Jan 1989.
- [19] T. A. Perkins, N. de N Donaldson, N. A. C. Hatcher, I. D. Swain, and D. E. Wood, "Control of leg-powered paraplegic cycling using stimulation of the lumbo-sacral anterior spinal nerve roots.," *IEEE Trans Neural Syst Rehabil Eng*, vol. 10, pp. 158–164, Sep 2002.
- [20] K. J. Hunt, B. Stone, N.-O. Negrd, T. Schauer, M. H. Fraser, A. J. Cathcart, C. Ferrario, S. A. Ward, and S. Grant, "Control strategies for integration of electric motor assist and functional electrical stimulation in paraplegic cycling: utility for exercise testing and mobile cycling.," *IEEE Trans Neural Syst Rehabil Eng*, vol. 12, pp. 89–101, Mar 2004.
- [21] A. M. Bryden, W. D. Memberg, and P. E. Crago, "Electrically stimulated elbow extension in persons with C5/C6 tetraplegia: a functional and physiological evaluation.," *Arch Phys Med Rehabil*, vol. 81, pp. 80–88, Jan 2000.
- [22] K. J. Hunt, A. N. McLean, S. Coupand, and H. Gollee, "Upper-limb exercise in tetraplegia using functional electrical stimulation.," *Advances in clinical neuroscience and rehabilitation*, vol. 3, pp. 24–25, 2003.
- [23] T. Johnston, R. Betz, B. Smith, B. Benda, M. Mulcahey, R. Davis, T. Houdayer, M. Pontari, A. Barriskill, and G. Creasey, "Implantable FES system for upright mobility and bladder and bowel function for individuals with spinal cord injury.," *Spinal Cord*, vol. 43(12), pp. 713–23, 2005 Dec.
- [24] R. D. Chervin and C. Guilleminault, "Diaphragm pacing for respiratory insufficiency.," *J Clin Neurophysiol*, vol. 14, pp. 369–377, Sep 1997.
- [25] A. F. DiMarco, R. P. Onders, A. Ignagni, and K. E. Kowalski, "Inspiratory muscle pacing in spinal cord injury: case report and clinical commentary.," *J Spinal Cord Med*, vol. 29, no. 2, pp. 95–108, 2006.
- [26] J. A. Elefteriades, J. A. Quin, J. F. Hogan, W. G. Holcomb, G. V. Letsou, W. F. Chlosta, and W. W. W. L. Glenn, "Long-term follow-up of pacing of the conditioned diaphragm in quadriplegia.," *Pacing Clin Electrophysiol*, vol. 25, pp. 897–906, Jun 2002.

- [27] S. H. Linder, "Functional electrical stimulation to enhance cough in quadriplegia," *Chest*, vol. 103, pp. 166–169, 1993.
- [28] J. Šorli, F. Kandare, R. J. Jaeger, and U. Stanič, "Ventilatory assistance using electrical stimulation of abdominal muscles," *IEEE Trans Rehabil Eng*, vol. 4, pp. 1–6, Mar 1996.
- [29] U. Stanič, F. Kandare, R. Jaeger, and J. Šorli, "Functional electrical stimulation of abdominal muscles to augment tidal volume in spinal cord injury," *IEEE Trans Rehab Eng*, vol. 8, pp. 30–34, 2000.
- [30] P. Taylor, A. Tromans, K. Harris, and I. Swain, "Electrical stimulation of abdominal muscles for control of blood pressure and augmentation of cough in a C3/4 level tetraplegic," *Spinal Cord*, vol. 40, pp. 34–36, 2002.
- [31] A. D. Troyer and M. Estenne, "Coordination between rib cage muscles and diaphragm during quiet breathing in humans," *J Appl Physiol*, vol. 57, pp. 899–906, Sep 1984.
- [32] "Common respiratory problems in SCI – what you need to know," tech. rep., Northwest Regional Spinal Cord Injury System (NWRSCIS), 2004.
- [33] M. Estenne and A. D. Troyer, "Relationship between respiratory muscle electromyogram and rib cage motion in tetraplegia," *Am Rev Respir Dis*, vol. 132, pp. 53–59, Jul 1985.
- [34] J. Danon, W. S. Druz, N. B. Goldberg, and J. T. Sharp, "Function of the isolated paced diaphragm and the cervical accessory muscles in C1 quadriplegics," *Am Rev Respir Dis*, vol. 119, pp. 909–919, Jun 1979.
- [35] A. D. Troyer and M. Estenne, "The expiratory muscles in tetraplegia," *Paraplegia*, vol. 29, pp. 359–363, Jul 1991.
- [36] N. Kirby and M. B. A. Siebens, "An evaluation of assisted cough in quadriparetic patients," *Arch Phys Med Rehabil*, vol. 47, pp. 705–710, 1966.
- [37] S. Braum, R. Giovannoni, and M. O'Connor, "Improving the cough in patients with spinal cord injury," *Am J Phys Med*, vol. 63, pp. 1–10, 1984.
- [38] D. J. Stone and H. Keltz, "The effect of respiratory muscle dysfunction on pulmonary function: studies in patients with spinal cord injuries," *Am Rev Respir Dis*, vol. 88, pp. 621–629, Nov 1963.
- [39] A. D. Troyer and A. Heilporn, "Respiratory mechanics in quadriplegia. the respiratory function of the intercostal muscles," *Am Rev Respir Dis*, vol. 122, pp. 591–600, Oct 1980.
- [40] A. D. Troyer, M. Esterne, and A. Heilporn, "Mechanism of active expiration in tetraplegic subjects," *Clinical Biomechanics*, vol. 2, p. 58, 1987.

- [41] M. Estenne and M. Gorini, "Action of the diaphragm during cough in tetraplegic subjects.," *J Appl Physiol*, vol. 72, pp. 1074–1080, Mar 1992.
- [42] M. Estenne and A. D. Troyer, "Cough in tetraplegic subjects: an active process," *Annals of Internal Medicine*, vol. 112, pp. 22–28, 1990.
- [43] M. J. Tobin, *Principle and Practice of Mechanical Ventilation*. McGraw-Hill Professional, 2nd ed., 2006.
- [44] S. Slutsky, "Mechanical ventilation," *Chest*, vol. 104, pp. 1833–59, 1993.
- [45] A. F. DiMarco, R. P. Onders, A. Ignagni, K. E. Kowalski, and J. T. Mortimer, "Phrenic nerve pacing via intramuscular diaphragm electrodes in tetraplegic subjects," *Chest*, vol. 127, pp. 671–678, Feb 2005.
- [46] A. F. DiMarco, R. P. Onders, K. E. Kowalski, M. E. Miller, S. Ferck, and J. T. Mortimer, "Phrenic nerve pacing in a tetraplegic patient via intramuscular diaphragm electrodes," *Am J Respir Crit Care Med*, vol. 166, pp. 1604–1606, Dec 2002.
- [47] V. W. Lin, C. Hsieh, I. N. Hsiao, and J. Canfield, "Functional magnetic stimulation of expiratory muscles: a noninvasive and new method for restoring cough," vol. 84, pp. 1144–1150, Apr 1998.
- [48] V. W. Lin, H. Singh, R. K. Chitkara, and I. Perikash, "Functional magnetic stimulation for restoring cough in patients with tetraplegia," vol. 79, pp. 517–522, May 1998.
- [49] M. I. Polkey, Y. Luo, R. Guleria, C.-H. H. Ard, M. Green, and J. Moxham, "Functional magnetic stimulation of the abdominal muscles in humans," *Am. J. Respir. Crit. Care Med.*, vol. 160, pp. 513–522, Aug. 1999.
- [50] H. Singh, M. Magruder, T. Bushnik, and V. W. Lin, "Expiratory muscle activation by functional magnetic stimulation of thoracic and lumbar spinal nerves.," *Crit Care Med*, vol. 27, pp. 2201–2205, Oct 1999.
- [51] V. W. Lin, I. N. Hsiao, E. Zhu, and I. Perikash, "Functional magnetic stimulation for conditioning of expiratory muscles in patients with spinal cord injury.," *Arch Phys Med Rehabil*, vol. 82, pp. 162–166, Feb 2001.
- [52] I. Hsiao and V. Weh-Hau Lin, "Improved coil design for functional magnetic stimulation of expiratory muscles," *IEEE Transactions on Biomedical Engineering*, vol. 48, no. 6, pp. 684–694, 2001.
- [53] H. Gollee, K. Ilunt, D. Allan, M. Fraser, and A. McLean, "A control system for automatic electrical stimulation of abdominal muscles to assist respiratory function in tetraplegia," *Medical Engineering and Physics*, vol. 29, pp. 799–807, 2006.

- [54] R. J. Jaeger, R. M. Turba, G. M. Yarkony, and E. J. Roth, "Cough in spinal cord injured patients: comparison of three methods to produce cough.," *Arch Phys Med Rehabil*, vol. 74, pp. 1358–1361, Dec 1993.
- [55] A. Zupan, R. Savrin, T. Erjave, A. Kralj, T. Karenik, T. Skorjanc, H. Benko, and P. Obreza, "Effects of respiratory muscle training and electrical stimulation of abdominal muscles on respiratory capabilities in tetraplegic patients," *Spinal Cord*, vol. 35, pp. 540–545, 1997.
- [56] W. E. Langbein, C. Maloney, F. Kandare, U. Stanič, B. Nemchausky, and R. J. Jaeger, "Pulmonary function testing in spinal cord injury: effects of abdominal muscle stimulation," *Journal of Rehabilitation Research and Development*, vol. 38, pp. 591–597, 2001.
- [57] F. Kandare, G. Exner, J. Jeraj, A. Aliverti, R. Dellacá, Uroš, Stanič, A. Pedotti, and R. Jaeger, "Breathing induced by abdominal muscle stimulation in individuals without spontaneous ventilation," *Neuromodulation*, vol. 5, pp. 180–185, 2002.
- [58] "Micro medical." Website. <http://www.micromedical.co.uk>.
- [59] T. Sinkjaer, M. Haugland, A. Inmann, M. Hansen, and K. D. Nielsen, "Biopotentials as command and feedback signals in functional electrical stimulation systems," *Medical Engineering & Physics*, vol. 25, pp. 29–40, Jan. 2003.
- [60] S. L. Pullman, D. S. Goodin, A. I. Marquinez, S. Tabbal, and M. Rubin, "Clinical utility of surface EMG: report of the therapeutics and technology assessment subcommittee of the american academy of neurology," *Neurology*, vol. 55, pp. 171–177, Jul 2000.
- [61] T. R. Scott, P. H. Peckham, and K. L. Kilgore, "Tri-state myoelectric control of bilateral upper extremity neuroprostheses for tetraplegic individuals.," *IEEE Trans Rehabil Eng*, vol. 4, pp. 251–263, Dec 1996.
- [62] G. Lyons, T. Sinkjaer, J. Burridge, and D. Wilcox, "A review of portable FES-based neural orthoses for the correction of drop foot," *IEEE Trans Neural Syst Rehabil Eng*, vol. 10(4), pp. 260–79, 2002 Dec.
- [63] A. Inmann, *Natural sensory feedback for FES controlled hand grasp*. PhD thesis, Center for Sensory-Motor Interaction, Aalborg University, Denmark, 2002.
- [64] C. Frigo, M. Ferrarin, W. Frasson, E. Pavan, and R. Thorsen, "Emg signals detection and processing for on-line control of functional electrical stimulation," *Journal of Electromyography and Kinesiology*, vol. 10, pp. 351–360, Oct. 2000.
- [65] S. Sennels, F. Biering-Srensen, O. T. Andersen, and S. D. Hansen, "Functional neuromuscular stimulation controlled by surface electromyographic signals produced by volitional activation

- of the same muscle: adaptive removal of the muscle response from the recorded EMG-signal," *IEEE Trans Rehabil Eng*, vol. 5, pp. 195–206, Jun 1997.
- [66] R. Thorsen, M. Ferrarin, R. Spadone, and C. Frigo, "Functional control of the hand in tetraplegics based on residual synergistic EMG activity," *Artificial Organs*, vol. 23(5), pp. 470–3, 1999.
- [67] J. R. Wolpaw, N. Birbaumer, W. J. Heetderks, D. J. McFarland, P. H. Peckham, G. Schalk, E. Donchin, L. A. Quatrano, C. J. Robinson, and T. M. Vaughan, "Brain-computer interface technology: a review of the first international meeting.," *IEEE Trans Rehabil Eng*, vol. 8, pp. 164–173, Jun 2000.
- [68] R. T. Lauer, P. H. Peckham, and K. L. Kilgore, "EEG-based control of a hand grasp neuroprosthesis," *Neuroreport*, vol. 10, pp. 1767–1771, Jun 1999.
- [69] K. F. Whyte, M. Guggen, G. A. Gould, J. Molloy, P. K. Wraith, and N. J. Douglas, "Accuracy of respiratory inductive plethysmograph in measuring tidal volume during sleep," *J Appl Physiol*, vol. 71, pp. 1866–1871, Nov. 1991.
- [70] J. D. Witt, J. R. Fisher, J. A. Guenette, K. A. Cheong, B. J. Wilson, and A. W. Sheel, "Measurement of exercise ventilation by a portable respiratory inductive plethysmograph," *Respiratory Physiology & Neurobiology*, vol. 154, pp. 389–395, December 2006.
- [71] C. F. Clarenbach, O. Senn, T. Brack, M. Kohler, and K. E. Bloch, "Monitoring of ventilation during exercise by a portable respiratory inductive plethysmograph," *Chest*, vol. 128, pp. 1282–1290, September 2005.
- [72] VivoMetrics. Website. <http://www.vivometrics.com>.
- [73] R. J. Baken, "Electroglottography," *Journal of Voice*, vol. 6, no. 2, pp. 98–110, 1992.
- [74] H. Luinge, P. Veltink, and C. Baten, "Estimating orientation with gyroscopes and accelerometers," *Technology and Health Care*, vol. 7, pp. 455–459, 1999.
- [75] H. Luinge and P. Veltink, "Measuring orientation of human body segments using miniature gyroscopes and accelerometers," *Medical & Biological Engineering & Computing*, vol. 43, pp. 273–282, 2005.
- [76] D. Roetenberg, H. J. Luinge, C. T. M. Baten, and P. H. Veltink, "Compensation of magnetic disturbances improves inertial and magnetic sensing of human body segment orientation," *IEEE Transactions on Neural systems and rehabilitation engineering*, vol. 13, pp. 395–405, 2005.
- [77] "Xsens motion technologie." Website. <http://www.xsens.com>.

- [78] R. E. Mayagoitia, A. V. Nene, and P. H. Veltink, "Accelerometer and rate gyroscope measurement of kinematics: an inexpensive alternative to optical motion analysis systems," *Journal of Biomechanics*, vol. 35, pp. 537-542, Apr. 2002.
- [79] J. C. Moreno, E. R. de Lima, A. F. Ruiz, F. J. Brunetti, and J. L. Pons, "Design and implementation of an inertial measurement unit for control of artificial limbs: Application on leg orthoses," *Sensors and Actuators B: Chemical*, vol. 118, pp. 333-337, Oct. 2006.
- [80] "Tians Rudolph inc." Website. <http://www.rudolphkc.com>.
- [81] "Mathworks." Website. <http://www.mathworks.com>.
- [82] "Simulink S-function overview." Website. <http://www.mathworks.com/access/helpdesk/help/toolbox/simulink/>.
- [83] J. G. Martin and A. De Troyer, "The behaviour of the abdominal muscles during inspiratory mechanical loading," *Respiration Physiology*, vol. 50, pp. 63-73, Oct. 1982.

